



HAL
open science

Dielectric study of biodegradable and/or bio-based polymeric materials

Vikas Hegde

► **To cite this version:**

Vikas Hegde. Dielectric study of biodegradable and/or bio-based polymeric materials. Materials. Université Grenoble Alpes, 2017. English. NNT : 2017GREAT031 . tel-01689886

HAL Id: tel-01689886

<https://theses.hal.science/tel-01689886>

Submitted on 22 Jan 2018

HAL is a multi-disciplinary open access archive for the deposit and dissemination of scientific research documents, whether they are published or not. The documents may come from teaching and research institutions in France or abroad, or from public or private research centers.

L'archive ouverte pluridisciplinaire **HAL**, est destinée au dépôt et à la diffusion de documents scientifiques de niveau recherche, publiés ou non, émanant des établissements d'enseignement et de recherche français ou étrangers, des laboratoires publics ou privés.

THÈSE

Pour obtenir le grade de

DOCTEUR DE L'UNIVERSITÉ GRENOBLE ALPES

Spécialité : GENIE ELECTRIQUE

Arrêté ministériel : 25 mai 2016

Présentée par

Vikas Jayaprakash HEGDE

Thèse dirigée par **Olivier GALLOT-LAVALLÉE**, **Pascal RAIN** et **Laurent HEUX**

préparée au sein du **Laboratoire de Génie Électrique et Centre de recherches sur les macromolécules végétales** dans l'**École Doctorale Electronique, Electrotechnique, Automatique et Traitement du Signal (EEATS)**

Études diélectriques des matériaux polymères biodégradables et/ou bio-sourcés

Dielectric study of biodegradable and/or bio-based polymeric materials

Thèse soutenue publiquement le **13 Juillet 2017**, devant le jury composé de :

M. François BURET

Professeur, École Centrale de Lyon, Président

M. Juan MARTINEZ-VEGA

Professeur, Université de Toulouse, Rapporteur

M. Sébastien PRUVOST

Maître de conférences, INSA Lyon, Rapporteur

M. Christophe GUILLERMIN

Ingénieur, Schneider Electric, Examineur

M. Pascal RAIN

Professeur, Université Grenoble Alpes, Directeur de thèse

M. Laurent HEUX

Directeur de Recherche, CNRS, Co-Directeur de thèse

M. Olivier GALLOT-LAVALLÉE

Maître de conférences, Université Grenoble Alpes, Co-Directeur de thèse



ACKNOWLEDGEMENT

This thesis work is a collaborative project between G2Elab and CERMAV funded by French Ministry of Education. The work was carried out in MDE (Matériaux Diélectriques et Electrostatique) team in G2Elab and ‘Structure et Propriétés des Glycomatériaux’ team in CERMAV. I first thank all my supervisors for their guidance.

It is a pleasure for me to thank all my colleagues of both the teams in G2Elab and in CERMAV for their assistance of all forms during my Ph.D. work.

I am grateful to Pierre Sailler of CERMAV who offered me a helping hand in polymer processing and Sébastien Flury of G2Elab for his contribution in building the apparatus for electrical experiments. I received generous support from Julien Bamberger, Jean-Paul Baroux and Christophe Pollet for which I want to thank them.

I want to thank Priscillia, Clara, Florian, Antoine, Maximin, Joko, Saber, Raphael, Lauric for their support, warm encouragement and for all the good moments spent together during these years.

I would like to express my gratitude to Nelly and Rachelle for scientific discussion, feedbacks and comments offered by them.

Most of all, I thank my family and friends spread around the globe for their good wishes and support.

Lastly and most importantly, I owe my deepest gratitude to Laure for her uncountable contribution, her encouragement, her confidence in me. I want to thank her very much.

General Introduction.....	8
I. Overview on thermal and dielectric properties of biodegradable polymers .	12
I.1. Introduction.....	12
I.2. Polymers studied	12
I.2.1. Biodegradation	12
I.2.2. Polymer-name	14
I.2.3. Chemical formula.....	14
I.2.4. Origin of biodegradable polymers	16
I.2.1. Polymer-cost.....	17
I.3. Results from the census of publications	17
I.3.1. Publication so far	17
I.3.2. Contribution from different countries.....	18
I.3.3. Academic vs Industrial contribution	18
I.3.4. Editors and Journals	19
I.3.5. Biomaterials and biodegradable polymers studied for dielectric properties	20
I.3.6. Type of dielectric properties studied.....	21
I.4. Investigated properties:.....	21
I.4.1. Differential scanning calorimetry (DSC)	22
I.4.2. Dielectric spectroscopy (DS)	22
I.4.3. Current measurements	25
I.4.4. Electrical breakdown (E_{bd})	26
I.5. Physical properties of the polymers	27
I.5.1. Thermal properties: T_g and T_m	27
I.6. Dielectric and electrical properties of the polymers	28
I.6.1. Relative Permittivity: ϵ_r	28
I.6.2. Dissipation factor or dielectric loss tangent: $\tan\delta$	29
I.6.3. Apparent Conductivity.....	29
I.6.4. Electrical breakdown	30
I.7. Conclusion	31
I.8. Goal of the thesis	32
II. Polymer-film-processing	34
II.1. Introduction.....	34
II.2. Hot-pressing and other processing methods	34
II.3. Mold	35
II.3.1. Calibration of the circular mold.....	36
a) For processing PHB, PHBV, PLA, PP, PLA based composite	36
b) For processing PCL.....	37
II.3.2. Polymers-processed	38
a) PHB	38
b) PHBV, PCL, PLA, PP	39
c) PET, CA.....	40
II.3.3. Preparation of PLA-MFC nanocomposite and its processing	40
II.3.4. Thickness measurement of a film.....	42
II.3.5. Sample-conditioning and preparation.....	43
a) Sample-conditioning.....	43

b) Metalization.....	43
III. Optical microscopy, Drying and Water uptake.....	46
III.1. Introduction.....	46
III.2. Optical microscopy.....	46
III.2.1. Introduction.....	46
III.2.2. Result and Discussion	46
III.3. Drying	47
III.3.1. Introduction.....	47
III.3.2. PHBV	48
III.3.3. PCL	48
III.3.4. PLA	48
III.3.5. PLA (post-treated).....	49
III.3.6. PLA-MFC (post-treated)	50
III.4. Water uptake	50
III.4.1. Introduction	50
III.4.2. Experimental set-up for water uptake study in polymers	51
III.4.3. PHBV	51
III.4.4. PLA	52
IV. Differential scanning calorimetry and Dynamic mechanical thermal analysis	54
IV.1. Differential scanning calorimetry (DSC).....	54
IV.1.1. Introduction.....	54
IV.1.2. Heating cycle and melting temperature of polymers	55
IV.1.3. Cooling cycle and re-crystallization temperature of polymers.....	55
IV.1.4. Non-post-treated and post-treated PHBV studied by DSC	56
IV.2. Dynamic mechanical thermal analysis (DMTA).....	56
IV.2.1. Introduction	56
IV.2.2. T_{α} of polymers.....	57
IV.2.3. Reproducibility in T_{α} with two different films.....	57
IV.2.4. Reproducibility in T_{α} with a same polymer film.....	58
V. Dielectric spectroscopy, Current measurement and Electrical breakdown ...	60
V.1. Introduction.....	60
V.2. Introduction to dielectric spectroscopy.....	60
V.3. Experimental set-up 1	61
V.3.1. Temperature gradient	62
a) Under atmospheric (air) condition	63
b) Under inert (N ₂) gas conditions	63
V.4. Experimental set-up 2	64
V.5. Dielectric spectroscopy: PHBV.....	65
V.5.1. Introduction: Dielectric spectroscopy of PHBV	65
V.5.2. Results: Dielectric spectroscopy of PHBV	66
a) Relative permittivity: ϵ_r'	66
b) Loss factor: ϵ''	67
c) Dissipation factor: $\tan\delta$	68
d) Modulus: M''	69

e)	AC conductivity: σ'	69
V.5.3.	Discussion: Dielectric spectroscopy of PHBV	70
a)	Summary of relaxations and their origin	70
b)	Activation energy.....	73
c)	Reproducibility.....	74
d)	Effect of the temperature cycle on polymer morphology during dielectric spectroscopy measurement.....	75
V.6.	Dielectric spectroscopy: PCL.....	76
V.6.1.	Introduction: Dielectric spectroscopy of PCL	76
V.6.2.	Results: Dielectric spectroscopy of PCL	77
a)	Loss factor: ϵ''	77
b)	Dissipation factor: $\tan\delta$	78
c)	Modulus: M''	79
V.6.3.	Discussion: Dielectric spectroscopy of PCL.....	79
a)	Summary of relaxations and their origin	79
b)	Activation energy.....	82
c)	Reproducibility with a same PCL film	83
d)	Effect of the temperature cycle on polymer morphology during dielectric spectroscopy measurement.....	84
V.7.	Dielectric spectroscopy: PLA	85
V.7.1.	Introduction: Dielectric spectroscopy of PLA	85
V.7.2.	Results: Dielectric spectroscopy of PLA.....	85
a)	Loss factor: ϵ''	85
b)	Modulus: M''	86
V.7.3.	Discussion: Dielectric spectroscopy of PLA.....	87
a)	Summary of relaxations and their origin	87
b)	Activation energy.....	89
c)	Effect of the temperature cycle on polymer morphology during dielectric spectroscopy measurement.....	90
V.8.	Dielectric spectroscopy: PLA-MFC	90
V.8.1.	Result: Dielectric spectroscopy of PLA-MFC.....	91
a)	Relative permittivity: ϵ_r'	91
b)	Loss factor: ϵ''	91
c)	Dissipation factor: $\tan\delta$	92
V.8.2.	Discussion: Dielectric spectroscopy of PLA-MFC.....	92
a)	Summary of relaxations and their origin	92
b)	Activation energy.....	93
V.9.	Comparison of the dielectric properties of PLA and PLA-MFC (post-treated)	94
V.10.	Introduction to current measurement	95
V.11.	Experimental set-up 1	96
V.12.	Experimental set-up 2	97
V.13.	Experimental set-up 3	98
V.14.	Experimental set-up 4	98
V.15.	Experimental set-up 5	99
V.16.	Results: Experimental set-up 1 to Experimental set-up 4	100

V.17. Results: Experimental set-up 5	102
V.17.1. Results: Current measurements of PHBV	102
a) Effect of temperature: PHBV	102
b) Long duration measurement: PHBV	103
c) Effect of post-treatment: PHBV	104
V.17.2. Discussion: Current measurements of PHBV	105
a) Effect of temperature: PHBV	105
b) Comparison of long and short term current measurements in PHBV	106
c) Comparison of current in non-post-treated and post-treated films of PHBV	106
V.17.3. Result: Current measurement of PCL	107
V.17.1. Discussion: Current measurement of PCL.....	108
V.18. Introduction to electrical breakdown	109
V.19. Result: Electrical breakdown of PHBV	110
V.20. Discussion: Electrical breakdown of PHBV	111
V.21. Summary of the contribution to the field of study	112
V.22. Comparison between the biodegradable polymers and conventional polymers	114
Conclusions and perspectives	118
References	120
Annexes	133
Résumé de la thèse en français	135

General Introduction

General Introduction

The extensive use of fossil fuels, enormous increase in wide-spread pollution and emission of green-house gases into the atmosphere has posed a major challenge to the present world. The increasing awareness on this very threat, caused society and industries around the world to practice greener approaches in all facets of life. However, consequences of environment-friendly measures adopted for overturning the present situation will be a factor to watch in time. Nevertheless, in perspective of a better eco-system, it is industries today engaged in research activities for producing more eco-friendly products or in aligning their functioning towards environmental friendly ways.

The declining resources of fossil fuels and difficulties in recycling waste materials are pushing biodegradable polymers into prominence. In addition, International organization for standardization (ISO 26000) and other European directives and regulations such as *REACH* (Registration, Evaluation and Authorization, Restriction of Chemicals, 2007), *DEEE* (déchets d'équipements électriques et électroniques) and *RoHS* (Restriction of Hazardous Substances, 2002) are providing norms and guidelines for industries on environmental friendly approach. These contexts have been the driving force to look for alternatives.

In the domain of electrical engineering, many conventional polymers such as polyethylene (PE), polypropylene (PP), polyethylene terephthalate (PET), polyvinyl chloride (PVC), polyvinylidene fluoride (PVDF), polyphenylene sulfide (PPS), polyamide (PA), polycarbonate (PC) and thermosets (epoxy resin) find applications either in cables, in capacitors and in electrical insulation systems. These polymers are petro-based, not eco-friendly and many of them are not biodegradable. In some cases, recycling is difficult and hence, accumulates in the environment leading towards environmental pollution.

Biodegradable polymers override conventional polymers by virtue of its inherent pro-environment features such as eco-friendly [1]–[11], sustainable materials [3], low-environmental loads, materials that can be broken down by microbes [1], [7], [8], [10]–[12], germs and decomposition enzymes [13], [14] in nature and free of toxic chemicals such as dioxins [13], [14].

With an objective to challenge and replace the use of conventional polymers either partially or completely by biodegradable ones, this thesis work explores the dielectric properties of biodegradable and/or bio-based polymers.

In the first chapter, a detailed study on the current status in the research work on biodegradable polymers in the domain of electrical engineering is presented. This was achieved by carrying out the census of publications on the dielectric properties of biodegradable polymers up-to-date. The results obtained from the statistical study is presented. Thermal properties such as glass transition and melting temperature of both biodegradable and classical polymers are compiled and compared. Similarly, electrical properties such as relative permittivity, dissipation factor, conductivity and electrical

breakdown are compiled and compared. This first chapter is presented in the form of a review work. Based on this review work and other factors, some biodegradable and conventional polymers were chosen to be prepared and/or processed and to be explored for their thermal and electrical properties and the level of water uptake.

In the second chapter named *Polymer-film-processing*, the polymers processed in the laboratory along with their processing conditions are mentioned. The conditions under which different samples were dried and sampled for different characterization techniques are also elaborated.

In the third chapter, optical micrographs and water uptake in polymers are presented and discussed. In the fourth chapter, results from the differential scanning calorimetry and the dynamic mechanical thermal analysis are described.

In the fifth chapter, experimental set-up of dielectric spectroscopy, current measurement and electrical breakdown are shown. The experimental results obtained from the dielectric spectroscopy measurements performed for a wide range of temperature and frequency for different polymer and composite materials are interpreted. Results from the volume resistivity measurements at different temperatures and electrical breakdown measurements at room temperature are explained. The comparison of the thermal and the electrical properties of biodegradable and conventional polymers is carried out at the end of this chapter.

This chapter is followed by *Conclusion and perspectives*.

Chapter 1

Overview on thermal and dielectric properties of biodegradable polymers

I. Overview on thermal and dielectric properties of biodegradable polymers

I.1. Introduction

Today, there are many polymers in use in applications in the domain of electrical engineering. Polymers such as polyethylene (PE), polypropylene (PP), polyethylene terephthalate (PET), polyvinyl chloride (PVC), polyamide (PA), polycarbonate (PC) and epoxy resins find applications either in capacitors, in HVDC cables and in electrical insulation systems. These are not eco-friendly and non-biodegradable polymers. Figure 1 shows products where some of these polymers find use. On the contrary, biodegradable polymers are eco-friendly and biodegradable.



Figure 1. From the left to the right: image of a polypropylene capacitor [15], crosslinked polyethylene (XLPE) insulated power high voltage electrical cables [16] and epoxy termination-board for medium voltage motors or generators [17].

Thus, which are the biodegradable polymers whose dielectric properties have been reported so far and up to what extent, is discussed in this first chapter. This part of the work is presented in the form of a review. To begin with, ten biodegradable polymers, their chemical nature is discussed. This is followed by the results of the statistical study which is obtained by performing the census of publications on dielectric properties of the biodegradable polymers. Thereafter, thermal, dielectric and electrical properties of the biodegradable polymers reported in the literature is extracted and compared with some conventional polymers. The principle of measurement techniques such as differential scanning calorimetry (DSC), dielectric spectroscopy (DS), current measurement and electrical breakdown (E_{bd}) are briefly described.

I.2. Polymers studied

I.2.1. Biodegradation

Biodegradation is a phenomenon in which large chain polymer molecules are broken down into carbon dioxide or methane and water by the action of micro-organisms and enzymes. It can also occur due to combinative action of various parameters such as action of moisture, heat and light. For example, moisture may break down a large chain polymer molecule into smaller one making it accessible for micro-organisms to biodegrade them into carbon dioxide or methane and water.

Biodegradation can be either aerobic or anaerobic. Aerobic biodegradation takes place in presence of oxygen and gives carbon dioxide and water as an end-product. In case of anaerobic biodegradation which takes place in absence of oxygen, methane and water is released [18]. Kijchavengkul and Auras suggested inherent properties of polymers to be responsible for biodegradation [18]. They asserted the role of chemical structure of a polymer in playing a vital role in biodegradation process. Polymers with weak bonds and whose structures partly resemble those of natural polymers are prone to biodegradation. Factors like molecular size also influence the rate of biodegradation. Kale G. *et al.* [19] reported that smaller molecules are more easily biodegraded by the action of enzymes. Moreover, these enzymes also increase the rate of biodegradation process. A study also states that biodegradability could be influenced by presence of additives in polymeric materials [20]. It can either increase or decrease the biodegradability depending on the nature of the additive added. Figure 2 shows a scheme of the biodegradation process of polymers.

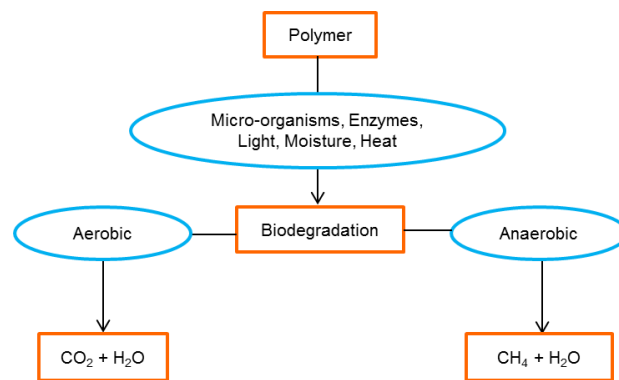


Figure 2. Pathway of biodegradation process of polymers.

Following definitions are made and followed throughout this chapter.

Bio-based polymers are derived from renewable resources. Generally, they are inherently biodegradable. However, there are polymers which can be bio-based and not biodegradable, for example, bio-based polyethylene (PE) which is not biodegradable but bio-based. Bio-based polymers modified by chemistry are also considered as bio-based polymers. For example, cellulose based materials are considered as bio-based as they originate from renewable resources. *Biodegradable polymers* can be either bio-based or of fossil origin and they undergo biodegradation. *Bio-based blend* is a blend in which one of the component of a blend is bio-based. *Bio-based composite* or *bio-composite* is like that of bio-based blend where either matrix or reinforcing material (filler) is of bio-based origin. It cannot be concluded that bio-based blends or bio-composites are completely bio-degradable. A prefix ‘*bio*’ to a ‘*composite*’ and a ‘*blend*’ is in common use even though they may not be completely biodegradable. This prefix usually signifies the presence of a bio-based component in them.

Plasticizers or additives such as antioxidants and flame-retardants are not treated as a component. These are added to ease the processing or for improving thermal or chemical stability of a final material. In this first chapter, bio-based or biopolymers, biodegradable

polymers, bio-based blends and bio-composites are collectively referred to as *biomaterials* which otherwise is specified wherever required.

1.2.2. Polymer-name

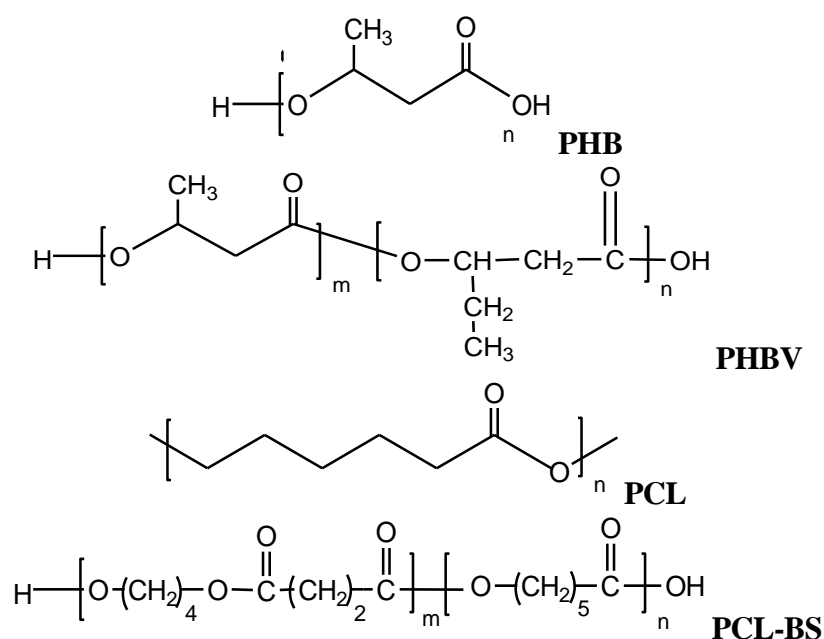
Dielectric properties of ten biodegradable polymers were searched in the literature. Table 1 lists these ten biodegradable polymers.

Table 1. List of biodegradable polymers.

PHB	Polyhydroxybutyrate
PHBV	Poly(3-hydroxybutyrate-co-3-hydroxyvalerate)
PCL	Polycaprolactone
PCL-BS	Polycaprolactone butylene succinate
PBS	Polybutylene succinate
PBSA	Polybutylene succinate adipate
PBAT	Poly(butyleneadipate-co-terephthalate)
PLA	Poly(lactic acid)
PETS	Polyethylene terephthalate succinate
CA	Cellulose acetate

1.2.3. Chemical formula

Figure 3 illustrates the structure of the ten biodegradable polymers listed in the Table 1.



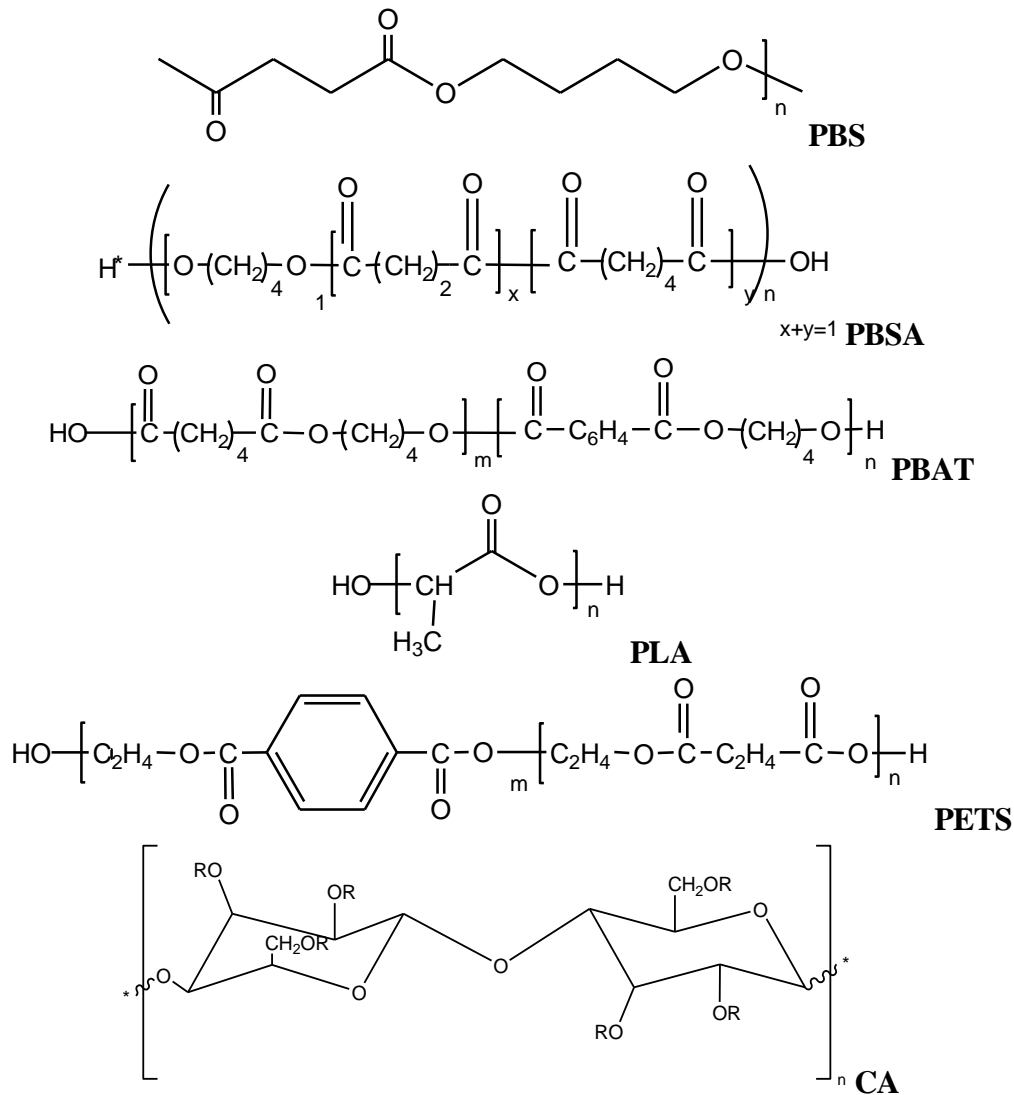


Figure 3. Structure of biodegradable polymers. In the structure of cellulose acetate, R represents Hydrogen or substituent acetyl group depending upon the degree of substitution.

All biodegradable polymers mentioned in the Figure 3 belong to the family of polyesters except cellulose acetate. This is a polysaccharide that has been chemically modified by esterification of cellulose. Chemical groups like hydroxyl (-OH) and carbonyl (>C=O) groups present in the repeating units of these polymers render them polar. All the biodegradable polymers in the Figure 3 are polar in nature unlike PP and PE. In the latter, there is a linear hydrocarbon chain responsible for their non-polar nature.

Copolymers among the ten biodegradable polymers are PHBV, PCL-BS, PBAT, PBSA and PETS. Table 2 shows the list of copolymers and their respective monomers.

Table 2. List of copolymers.

Biodegradable polymer	Monomers
PHBV	hydroxybutyrate, hydroxyvalerate
PCL-BS	caprolactone, butane diol, succinic acid
PBAT	butane diol, adipic acid, dimethyl terephthalate
PBS	butane diol, succinic acid
PBSA	butane diol, succinic acid, adipic acid
PETS	ethylene glycol, terephthalic acid, succinic acid

1.2.4. Origin of biodegradable polymers

Figure 4 illustrates some of the different pathways of obtaining biodegradable polymers both from renewable and non-renewable resources.

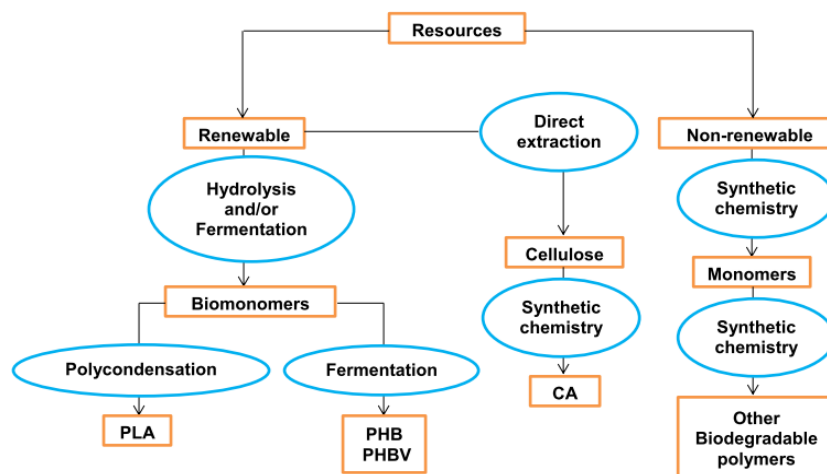


Figure 4. Different methods of obtaining biodegradable polymers.

Certain biodegradable polymers are bio-based while the others are obtained from synthetic chemistry, all of which are classified in the Table 3.

Table 3. Origin of biodegradable polymers.

Biodegradable polymer	Source
PHB	Photosynthetic and non-photosynthetic bacteria [21], Prokaryotic cells [22], Bacteria [23]
PHBV	Prokaryotic cells [22], Fermentation [24]
PLA	Renewable resources like sugarcane and corn
CA	Renewable resources like cellulose
PCL, PCL-BS, PBS, PBSA, PBAT, PETS	Synthetic chemistry

1.2.1. Polymer-cost

Table 4 lists the cost of biodegradable and conventional polymers. Most of the biodegradable polymers are relatively more expensive than the conventional polymers. PHB is the most expensive biodegradable polymer. The lower cost of PE and PP makes it more favored material compared to high-cost biodegradable polymers.

Table 4. Cost of the polymers.

Polymer	Cost (euros/kg)	Cost (in % of cost of PE)
PHB	10.5 [25]	2692
PCL	4 - 7 [26]	1026 - 1795
PBS	3.5 - 4.4 [27]	897 - 1128
PBSA	4.5 - 4.8 [27]	1154 - 1231
PLA	1.37 - 2.75 [26]	351 - 705
CA	0.60 [28]	154
PE	0.39 [28]	-
PP	0.63 [28]	162
epoxy resin	1.8 - 2.2 [27]	462 - 564

1.3. Results from the census of publications

1.3.1. Publication so far

Figure 5 shows the number of publications for each biomaterial per year [1]–[14], [21]–[24], [29]–[143]. The graph demonstrates research interest shown in the field of dielectric properties of biomaterials over past decades. There are very few reports prior to 1980's in this field of research. It is evident from the graph that the peak period of research activity ranged from year 2005 to year 2009 with the year 2007 being the year of highest number of scientific publications communicated. Although it later declined, yet in better phase compared to the situation at the outset.

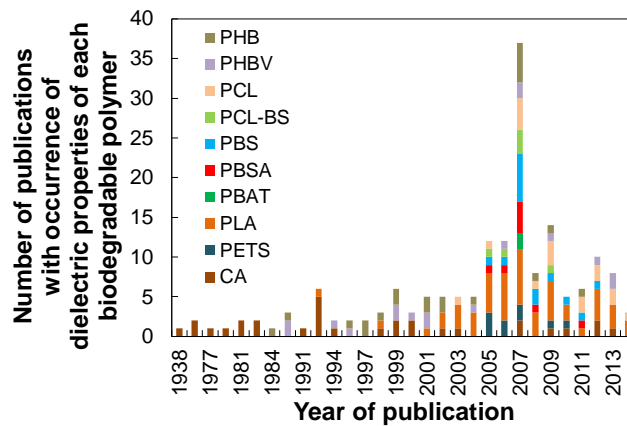


Figure 5. Plot of number of publications with occurrence of dielectric properties of biodegradable polymers for year of publication from 1938 to 2014. Note that the x-axis runs as follows: 1938, ‘64, ‘77, ‘79, ‘81, ‘82, ‘84, ‘86, ‘91, ‘92, ‘94, ‘95 and from 1997 to 2014.

1.3.2. Contribution from different countries

Figure 6 shows the number of publications from each country [1]–[14], [21]–[24], [29]–[143]. The publication made by each laboratory in a country on each biomaterial is counted as a unit while counting the number of publications. The graph shows involvement of laboratories around the world in this research field. Clearly, the laboratories in Japan have made the major contributions to this field of study.

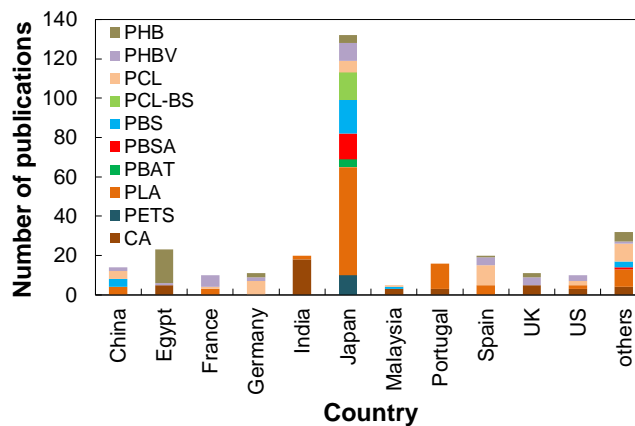


Figure 6. Plot of number of publications from each country which communicated research work on dielectric properties of biomaterials until 2014. Note that the same set of publications was considered in this case as used for the Figure 5. The category ‘others’ in the graph accounts for the publications from laboratories located in 17 countries.

1.3.3. Academic vs Industrial contribution

Figure 7 shows the number of publications communicated by academia, industries and collaborative research groups of both industrial and academic research laboratories [1]–[14], [21]–[24], [29]–[143]. In the Figure 7, number of publications was counted based on the kind of research organization engaged in the scientific work.

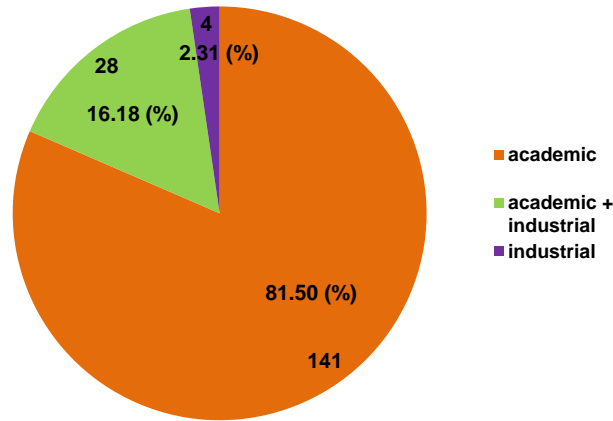


Figure 7. Pie graph representation of both number and percentage of number of publications from different kind of research organization on dielectric properties of biomaterials until 2014.

Scientific reports published by academic research units and collaborative research groups supersede those by industrial projects. This does not reflect the extent of involvement of industrial players in this field of science. Key industrial projects often go un-reported and usually patented thereby leaving much of technical information as confidential. Thus, the number of publications presented here does not form any yardstick for industrial achievements. There are patents reported on application of fluids for dielectrics among which some of them are bio-based and/or biodegradable. Among the ten biodegradable polymers being discussed in this chapter, very few number of patents on them in this domain of electrical engineering is reported. Some of these patents are on CA [144], [145] and PCL [146] as electrically insulating or conducting materials. Figure 8 demonstrates the same information presented in perspective of different biomaterials.

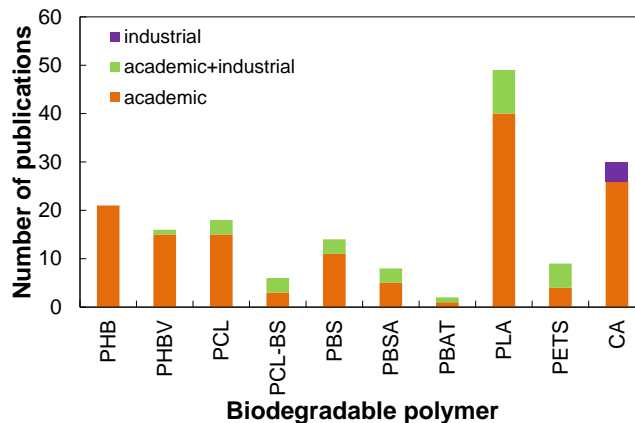


Figure 8. Plot of number of publications on biodegradable polymers examined for their dielectric properties reported by industrial, academic and collaborative research groups until 2014.

1.3.4. Editors and Journals

Figure 9 shows the number of publications on dielectric studies of biomaterials published by different publishers [1]–[14], [21]–[24], [29]–[143]. The IEEE publishers are the leading ones followed by Elsevier and Wiley. IEEE constitutes several streams of journals and the corresponding graph is shown in the Figure 10.

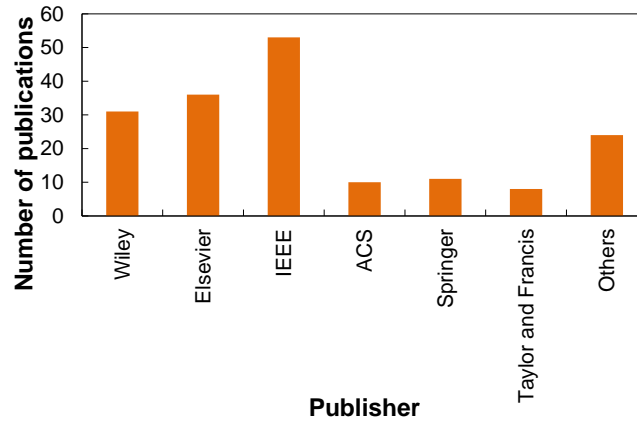


Figure 9. Plot of number of publications published by publishers through scientific journals, conferences and symposiums until 2014. The category ‘others’ in the graph includes many other publishers.

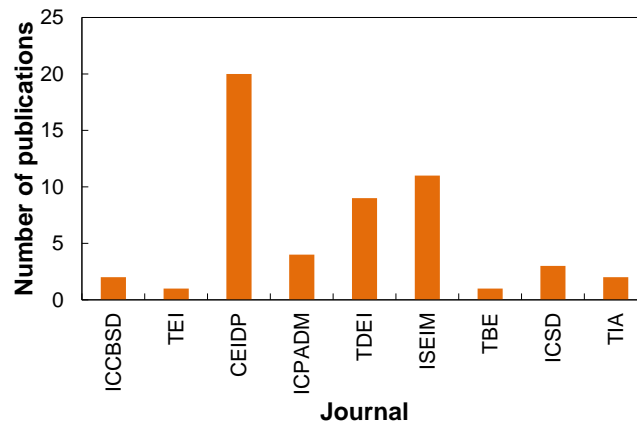


Figure 10. Plot of number of publications published by different journals of IEEE publishers.

1.3.5. Biomaterials and biodegradable polymers studied for dielectric properties

Figure 11 shows the number of publications on each biomaterial [1]–[14], [21]–[24], [29]–[143] and each biodegradable polymer [1]–[14], [21]–[24], [29]–[51], [53], [58], [60]–[86], [88]–[91], [93], [94], [96]–[101], [139]–[142]. A biomaterial is either a bio-based composite or a bio-based blend containing any of the ten biodegradable polymers under consideration in this chapter. They may or may not be biodegradable. A biodegradable polymer means the polymer in its native form without any fillers and additive components.

As biomaterials, the highest number of publications reported are on CA followed by PHB, PCL and PLA. In biodegradable polymers, PLA is the polymer extensively studied for its dielectric properties. The number of publications reported on PHB, PHBV, PETS, PBS and CA are next to and much lesser than PLA. PBAT is the least reported biodegradable polymer for its dielectric properties.

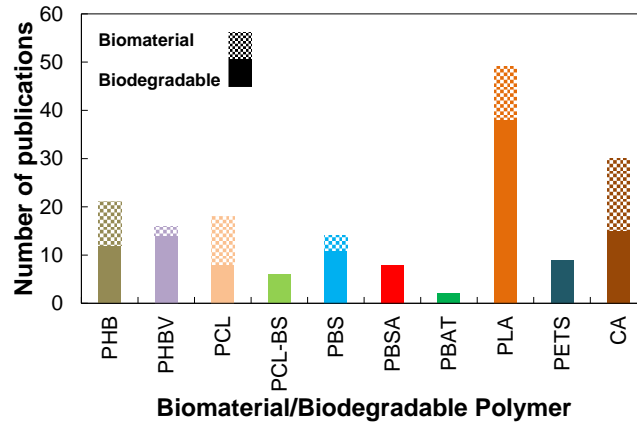


Figure 11. Plot of number of publications of biomaterials and biodegradable polymers studied for dielectric properties until 2014.

1.3.6. Type of dielectric properties studied

Figure 12 shows the number of occurrences of dielectric properties in publications for ten biodegradable polymers [1]–[14], [21]–[24], [29]–[51], [53], [58], [60]–[86], [88]–[91], [93], [94], [96]–[101], [139]–[142]. The dielectric properties those were counted for their occurrence in publications are relative permittivity (ϵ_r'), dissipation factor or dielectric loss tangent ($\tan\delta$), conductivity (σ) and electrical breakdown (E_{bd}). Both relative permittivity and conductivity is reported for all the biodegradable polymers. Electrical breakdown is reported for all polymers except PHB. Dissipation factor is reported for few biodegradable polymers. Relative permittivity is the most occurring dielectric property and dissipation factor is the least one.

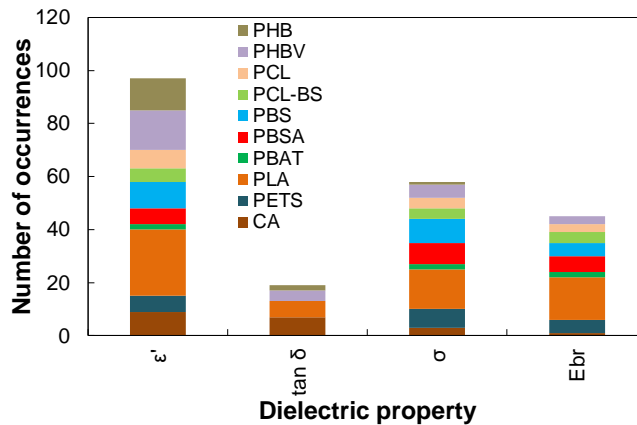


Figure 12. Plot of number of occurrences of dielectric properties in publications for ten biodegradable polymers.

1.4. Investigated properties:

Thermal properties such as glass transition temperature (T_g) and melting temperature (T_m) of biodegradable polymers have been looked for in the literature. These values are usually obtained by differential scanning calorimetry experiments. The dielectric and electric properties investigated are relative permittivity (ϵ_r'), dissipation factor ($\tan\delta$), conductivity (σ) and electrical breakdown (E_{bd}). Thus, the principle of measurement techniques such as

differential scanning calorimetry, dielectric spectroscopy, current measurement and electrical breakdown are introduced.

1.4.1. Differential scanning calorimetry (DSC)

It is an analytical technique to determine the melting temperature (T_m), crystallization temperature (T_c), glass transition temperature (T_g), degree of crystallinity (X_c) of a polymer or a composite material. The principle is to heat a sample and a reference to a constant temperature ramp simultaneously. Any differences in the energy (heat flow) provided to maintain this constant ramp is reflected as a thermal transition occurring in a material. In other words, difference in enthalpy corresponds to thermal transitions taking place in a material.

1.4.2. Dielectric spectroscopy (DS)

A dielectric or a dielectric material comes in form of solids, liquids or gases. In general, dielectric materials are insulators. In this present work, the focus is on solid dielectric materials which are biodegradable thermoplastic polymers. In solid dielectrics, there are many types such as glass, ceramic, polymers (thermoplastics, thermosets) and metal oxides.

When a dielectric material is subjected to an electric field or when a voltage is applied across a dielectric material, it is polarized under the application of an electric field. The extent of polarization of course depends on the nature of the dielectric material. Polarization and conduction must not be confused. Conduction is the flow of current through a material while polarization phenomenon is the orientation of dipole moments in a material in the presence of an electric field. Dielectric materials may be used for capacitors. Figure 13 shows the effect of polarization on real (ϵ') and imaginary (ϵ'') part of complex permittivity (ϵ^*).

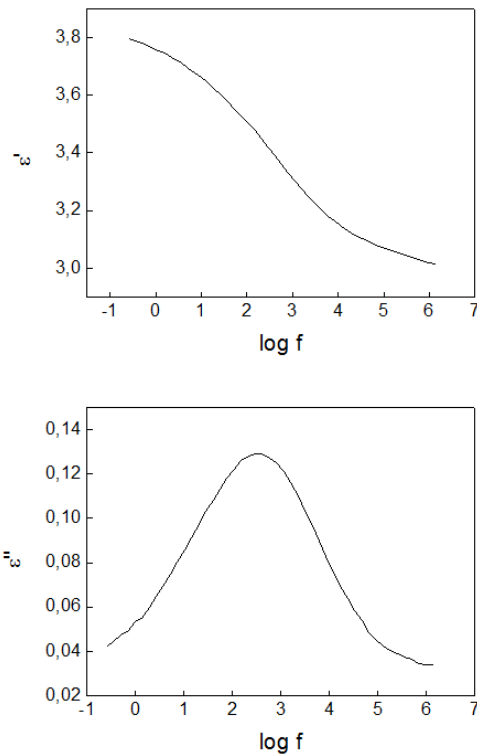


Figure 13. Variation in real and imaginary part of complex permittivity as a function of frequency for PHBV at 20 °C.

A capacitor is an electrical device which consists of two conductive plates separated by a dielectric material with a distance d .

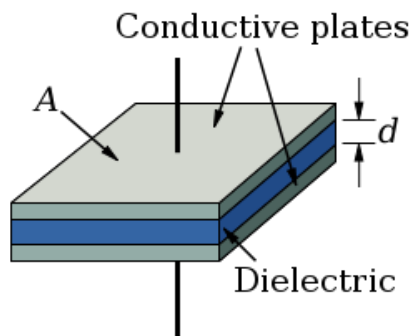


Figure 14. Sketch of a capacitor [147].

In a parallel plate capacitor, capacitance C of a capacitor is given as,

$$C = (\epsilon_r \cdot \epsilon_0 \cdot A) / d,$$

where, ϵ_r is the relative permittivity of a dielectric material, ϵ_0 is the permittivity of free space and its value is $8.854 \cdot 10^{-12}$ F/m and A is the surface area. The relative permittivity (ϵ_r) can be deduced from the measured capacitance (C) as seen in the Equation 1.

Equation 1. $\epsilon_r = (C \cdot d) / (\epsilon_0 \cdot A)$

The ability of a dielectric material to undergo polarization on the application of an electric field is what is quantified in the relative permittivity of a material. In the absence of a dielectric material or in case of free space between the plates of a capacitor, relative permittivity is 1. In the presence of a dielectric material between the plates, relative permittivity is greater than 1. Hence, relative permittivity contributes to the energy stored in a capacitor. It is evident that larger the relative permittivity, larger is the capacitance of a capacitor. The other dielectric properties of a dielectric material are dielectric loss or loss factor (ϵ''), dielectric loss tangent or dissipation factor ($\tan\delta$) and conductivity (σ). These dielectric properties can be measured and studied by dielectric spectroscopy.

Dielectric spectroscopy is an analytic technique where relaxation and conduction phenomena occurring in a dielectric material are studied as a function of frequency ($\omega=2\pi f$) at a given temperature. Dielectric spectroscopy has synonyms such as impedance spectroscopy and broadband dielectric spectroscopy [147],[148]. The principle of measurement is based on the application of a sinusoidal voltage, V^* (of frequency 'f') across a dielectric material resulting in a complex current I^* in the material with a phase shift by a phase angle ϕ as shown in the Figure 15.

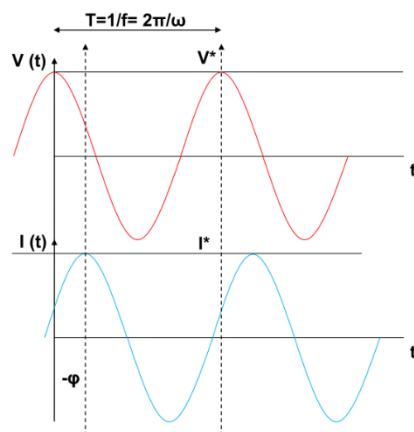


Figure 15. Phase shift by a phase angle ϕ .

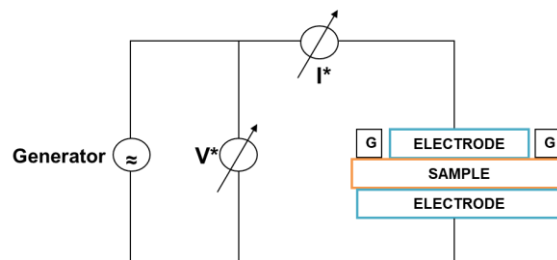


Figure 16. Circuit of dielectric spectroscopy measurement with a capacitor containing two parallel electrodes separated by a dielectric material of thickness 'd' placed in between them. 'G' represents the guard electrode which encircles the electrode on the top of the sample.

The measured impedance of a capacitor is given by [149],

$$Z^* = Z' + i.Z'' = V^*/I^*$$

which is related to complex permittivity as [149],

$$\epsilon^*(\omega) = \epsilon' - i.\epsilon'' = -i/(\omega.Z^*(\omega).C_0)$$

where, C_0 is the capacitance of a capacitor with free space in between parallel plates, ϵ' and ϵ'' are real and imaginary parts of permittivity. Thus from dielectric spectroscopy, complex permittivity is obtained as [148],

$$\epsilon^*(\omega) = \epsilon'(\omega) - i.\epsilon''(\omega) = C^*(\omega)/C_0$$

where, C^* is the capacitor with a dielectric material, ϵ' as already seen is referred to as real part of permittivity or relative permittivity or dielectric constant of a dielectric material. ϵ'' is called the loss factor which is proportional to the energy lost or dissipated per cycle [150]. Subsequently, other dielectric properties such as dielectric loss tangent ($\tan\delta$) and conductivity (σ^*) are related to complex permittivity can be determined as [149],

$$\sigma^* = \sigma' - i.\sigma'' = i.2.\pi.f.\epsilon_0.\epsilon^*$$

$$\tan\delta = \epsilon''/\epsilon'$$

Dielectric loss tangent represents the dissipation of energy.

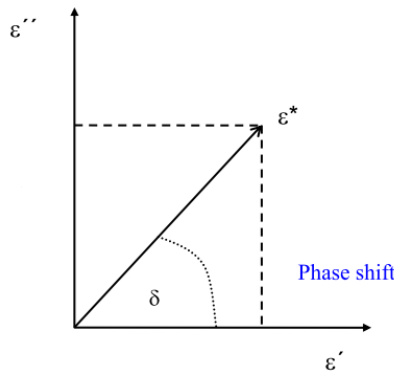


Figure 17. Relationship between relative permittivity, loss factor and dissipation factor in a complex plane. Courtesy : A. Schönhals [151].

1.4.3. Current measurements

When a voltage is applied across a dielectric material, current appears because of polarization and conduction (absorption current). The current may stabilize to give steady or conduction current (I_c). This stage of voltage application is referred to as $Volt_{on}$ (V_{on}). When applied voltage is removed, i.e., $V=0$, known as $Volt_{off}$ (V_{off}), depolarization takes place resulting in depolarization current (desorption current).

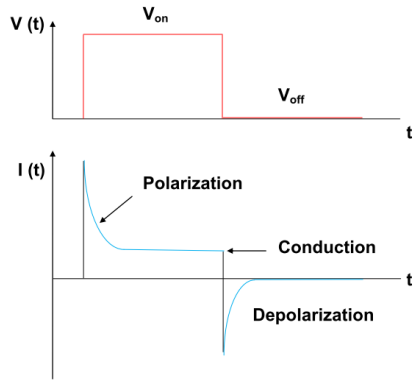


Figure 18. To the above is V_{on} and V_{off} stage as a function of time. To the below is the corresponding current in a dielectric material versus time showing the absorption and the desorption currents.

In general, conduction current can be calculated by adding absorption and desorption currents as shown in the Equation 2,

$$\text{Equation 2. } I_c = I(t) (V_{on}) + I(t) (V_{off})$$

Equation 2 is based on the assumption that currents in V_{on} and V_{off} are symmetric [152]. Another way to arrive at the conduction current from the time-dependent current measurement is to wait until the stabilization. If at all it stabilizes, the time to stabilization may vary depending upon a dielectric material and the conditions of measurement such as temperature, humidity etc. The objective of measuring conduction current is to calculate conductivity or resistivity of a dielectric. Since the conduction is through the bulk or volume of a dielectric, it's called volume resistivity or conductivity. This doesn't consider surface currents and corresponding surface resistivity are not discussed in this work. Volume resistivity (ρ) is calculated by measuring the conduction current (I_c) in a dielectric due to the applied voltage (V). It is given in the Equation 3,

$$\text{Equation 3. } \rho = (A.R)/d$$

where, A is the effective area of the electrode and d is the thickness of a sample.

Since, $V = I.R$,

$$\rho = (A.V)/(d.I_c)$$

The conductivity is the reciprocal of volume resistivity given by the Equation 4,

$$\text{Equation 4. } \sigma = (1/\rho)$$

Since the applied voltage is in *DC*, the conductivity is often referred to as *DC* conductivity.

1.4.4. Electrical breakdown (E_{bd})

It is the phenomenon when a dielectric material cannot further withstand an applied voltage across it resulting in the breakdown of a material. The voltage corresponding to the breakdown is referred to as breakdown voltage. Apart from the nature of a material, the

breakdown process depends on the thickness of a sample, the temperature of measurement, relative humidity, molecular defects [153], structure/shape of electrodes [153] and also the kind of voltage application (AC, DC, impulse). Breakdown field of a dielectric is given by the Equation 5,

$$\text{Equation 5. } E_{bd} = V_{bd}/d$$

where, V_{bd} is the breakdown voltage and d is the thickness of a dielectric material.

Electrical breakdown results are widely analyzed by statistical analysis method such as Weibull distribution. It is given by the Equation 6,

$$\text{Equation 6. } P(x) = 1 - \exp[-(x/\alpha)^\beta]$$

where, $P(x)$ is the cumulative probability, x is a random variable (such as breakdown voltage or breakdown gradient), α is the scale parameter and β is the shape parameter. The scale parameter gives the breakdown strength at which the probability for a breakdown is 63.2 %. On the other hand, the shape parameter describes the distribution range of the electric breakdown field strengths.

1.5. Physical properties of the polymers

1.5.1. Thermal properties: T_g and T_m

A firm understanding of the thermal properties such as glass transition temperature, melting temperature, crystallization temperature and degradation or decomposition temperature of a polymer is needed while studying their dielectric properties. Figure 19 shows the glass transition temperature of biodegradable and conventional polymers [1]–[4], [6]–[9], [13], [14], [22], [31], [71], [72], [88], [154]. The glass transition temperature of epoxy resin is also provided considering it is widely used in insulation applications. Epoxy resin is a thermoset unlike rest of the biodegradable and conventional polymers which are thermoplastics. Figure 20 shows the melting temperature of biodegradable and conventional polymers [1]–[4], [6]–[9], [12]–[14], [29], [31], [36], [88], [155].

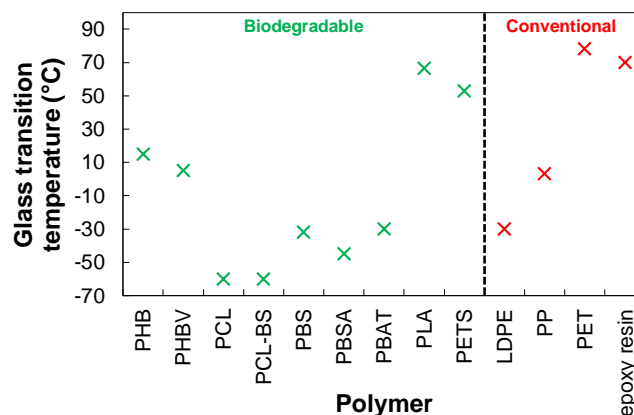


Figure 19. Plot of glass transition temperature of biodegradable and conventional polymers. Epoxy resin is a bisphenol-A epoxy resin with hardener HY956. Cellulose acetate has a degree of substitution of 2.45 and acetyl content of 39.8 %.

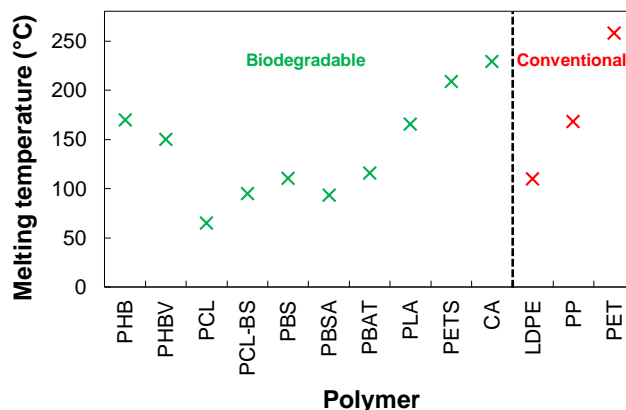


Figure 20. Plot of melting temperature of biodegradable polymers. Cellulose acetate has a degree of substitution of 2.45 and acetyl content of 39.8 %.

A comparison of glass transition and melting temperature of biodegradable and conventional polymers is drawn. The T_g of PLA is the highest followed by PETS. Their T_g is comparable to PET and epoxy resin. The T_g of PHB and PHBV is comparable to PP. The T_g of PBS, PBSA, PBAT is comparable to LDPE.

The T_m of CA is the highest followed by PETS and their T_m is the closest to PET. The T_m of PHB, PHBV and PLA is comparable to PP.

1.6. Dielectric and electrical properties of the polymers

1.6.1. Relative Permittivity: ϵ_r

Figure 21 shows the relative permittivity of biodegradable and conventional polymers [1], [7], [13], [29], [31], [91], [98], [156]–[158]. Higher relative permittivity in biodegradable polymers is due to the presence of polar carbonyl and hydroxyl groups in their structures [1], [8]. Relative permittivity varies with temperature, frequency and polymer-morphology. Various studies on influence of frequency [3], [8], [29], temperature [4], [7], [13], [14] and polymer-crystallinity [3], [61] on relative permittivity are reported.

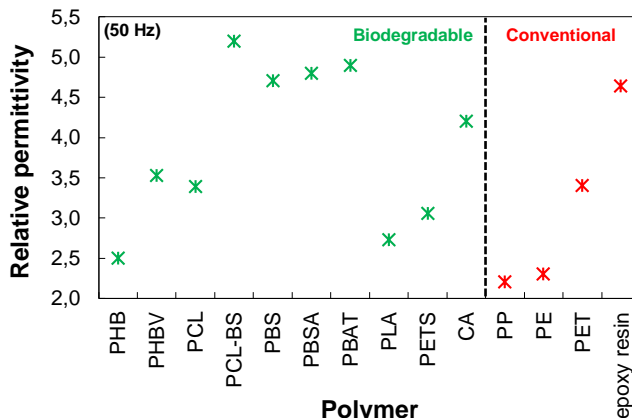


Figure 21. Plot of relative permittivity of biodegradable and conventional polymers at frequency 50 Hz, at room temperature. Epoxy resin is a diglycidyl ether of bisphenol A cured by 4,4'-diaminodiphenylmethane.

1.6.2. Dissipation factor or dielectric loss tangent: $\tan\delta$

Dissipation factor of biodegradable and conventional polymers are shown in the Figure 22 [2], [13], [31], [69], [154], [158] .

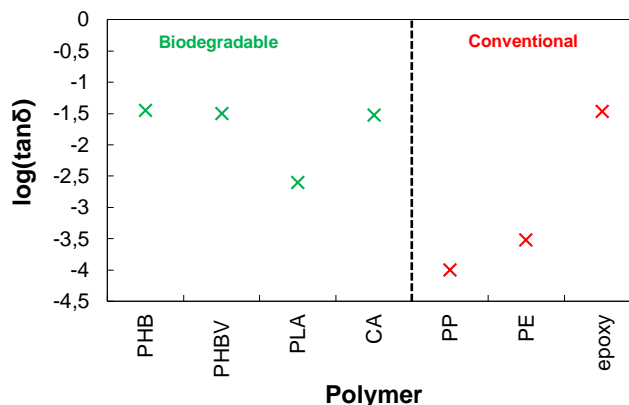


Figure 22. Plot of dielectric loss tangent of biodegradable and conventional polymers at frequency 50 Hz, at room temperature.

Biodegradable polymers show high value of losses. PLA has the lowest level of dissipation factor among the biodegradable polymers.

1.6.3. Apparent Conductivity

Figure 23 shows the apparent conductivity of biodegradable and conventional polymers [1], [8], [29], [159].

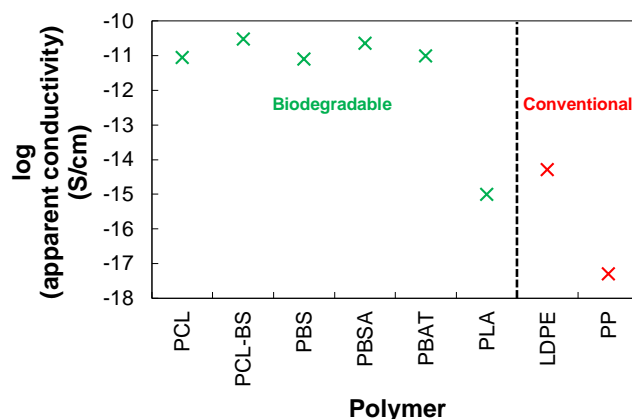


Figure 23. Plot of apparent conductivity of biodegradable and conventional polymers measured at room temperature. The values reported are after 1000 seconds since the beginning of voltage application for all the biodegradable polymers and LDPE. The average electric field is 25 kV/mm. The value of PP is reported as a function of electric field at 25 kV/mm.

Many biodegradable polymers have high apparent conductivity. PLA is the biodegradable polymer with lowest level of apparent conductivity and is comparable to LDPE. PP shows the lowest level of apparent conductivity among all of them.

1.6.4. Electrical breakdown

Figure 24 shows the impulse breakdown strength of biodegradable and conventional polymers as a function of sample thickness at room temperature [1], [7], [8], [60], [63]. Considering both the thickness of a sample and the temperature of measurement, PLA has the highest impulse breakdown strength among biodegradable polymers. It is said that the breakdown strength of a polymer becomes lower when its conductivity is higher [29]. However, in case of impulse breakdown strength, its relation with conductivity is reportedly unclear [1], [7], [8]. Impulse breakdown strength of polymers PLA and PETS as a function of temperature has also been reported earlier [6], [62].

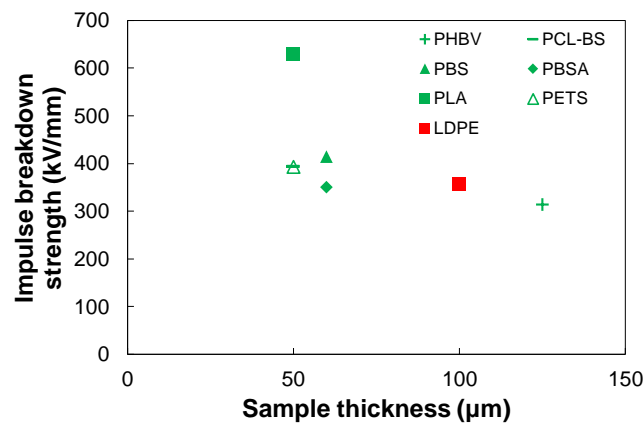


Figure 24. Plot of impulse breakdown strength of biodegradable and conventional polymers as a function of sample thickness at room temperature.

Figure 25 shows the AC breakdown strength of biodegradable and conventional polymers as a function of sample thickness at room temperature [1], [7], [8], [160]. PETS has the highest AC breakdown strength among biodegradable polymers. PLA and LDPE show almost similar AC breakdown strengths.

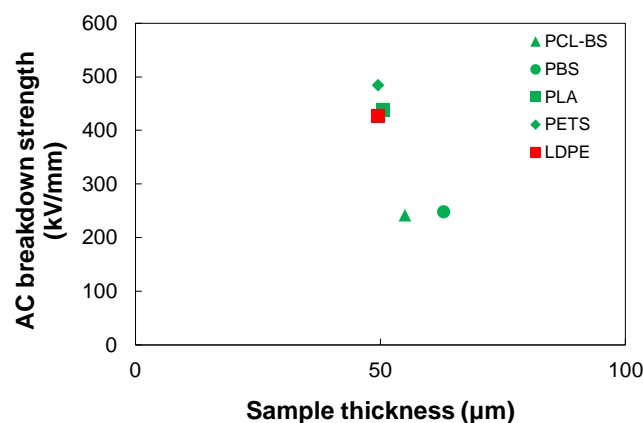


Figure 25. Plot of AC breakdown strength of biodegradable and conventional polymers as a function of sample thickness at room temperature. Voltage (AC) is raised by 1 kV/s for PCL-BS, PBS, PLA, PETS and LDPE.

Figure 26 shows the DC breakdown strength of biodegradable and conventional polymers as a function of sample thickness at room temperature [1], [6]–[8], [160]. Among the biodegradable polymers, PLA has the highest DC breakdown strength followed by PETS.

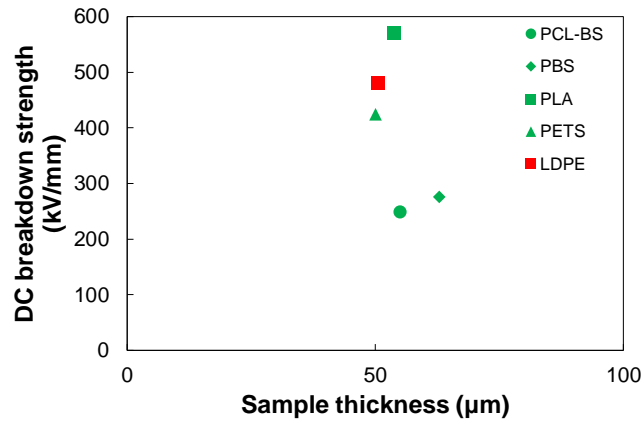


Figure 26. Plot of DC breakdown strength of biodegradable and conventional polymers as a function of sample thickness at room temperature. Voltage (DC) is raised by 1 kV/s for PCL-BS, PBS, PLA, PETS and LDPE.

1.7. Conclusion

The outcome of the census of publications shows PLA is the most studied biodegradable polymer for dielectric properties. Year 2007 is the peak year with maximum number of the research reports communicated. The country with the major contribution is Japan and the major publisher is IEEE. About 81 % of the publications come from academic research institutions. Dielectric properties such as relative permittivity and electrical conductivity are reported for all the ten biodegradable polymers. Electrical breakdown is reported for all except Polyhydroxybutyrate. Dielectric loss tangent is the least discussed limited to only four among the ten biodegradable polymers.

Thermal and electrical properties of the biodegradable polymers and their comparison with some conventional polymers and thermosets were presented. If alone the thermal properties are considered, polymers such as PHB, PHBV, PLA, PETS and CA are comparable with conventional polymers such as PP and PET. In terms of electrical properties such as relative permittivity, PLA shows values (< 3) closer to PE and PP. There are wide range of biodegradable polymers like PCL-BS, PBS, PBSA, PBAT and CA which show relatively higher level of relative permittivity i.e., around 5. This is closer to that of certain type of epoxy resins. PLA has the lowest level of dissipation factor among biodegradable polymers. In terms of apparent conductivity, only PLA could be argued for competing with classical polymers like PE. The rest of the biodegradable polymers shows high level of apparent conductivity and dissipation factor. The electrical breakdown strength of PLA and PETS are interesting when compared with some conventional polymers. Globally, PLA and PETS is found to be the two most promising biodegradable polymers among the ten biodegradable polymers in terms of electric properties. It must be noted that in addition to thermal and electrical properties, there are other crucial factors to be examined when considering a polymer for an application. Some of them are chemical nature, availability, cost, processability, mechanical properties, level and rate of moisture/water uptake in a polymer and ageing. Few of these factors have been addressed in the just concluded review.

1.8. Goal of the thesis

Based on the outcome of the review, PLA and PETS was chosen to be further examined in this Ph.D. work. PETS' raw material had availability issues in the market. Moreover, a possible synthetic chemistry route to prepare PETS in the laboratory was ignored. These reasons led to drop the polymer from further study. Polyhydroxyalkanoates PHB and PHBV is chosen based on their availability even though they possess certain drawbacks. Firstly, it may undergo degradation if heated to about 20 to 30 °C above its melting temperature. This means a narrow processing window for processing these polymers into films. Secondly, they undergo secondary crystallization in time. Finally, there is also the cost factor as seen in the Table 4, they aren't relatively economic. PCL is the fourth polymer chosen owing to its low level of melting temperature. This feature of PCL could be favorable in preparation of blend and composite materials and could also act as a plasticizer. Cellulose acetate is also added to the list on the grounds that it is bio-based and a biodegradable polymer. Thus, biodegradable polymers PHB, PHBV, PCL, PLA, CA were chosen along with conventional polymers PET and PP to allow a comparison.

Undoubtedly, in environmental perspective, biodegradable and/or bio-based polymers have an upper hand over conventional one. It is in this context the thesis originated and the first goal of the thesis is to prepare a database to learn the present status in the research work on the dielectric properties of biodegradable and/or bio-based polymers. This work has been realized and presented in the first chapter. The second objective is to contribute to the database prepared by providing further complementary data on the thermal properties such as glass transition and melting temperature; dielectric and electrical properties such as relative permittivity, level of losses, dielectric relaxation, apparent conductivity and electrical breakdown; and water uptake levels of the biodegradable polymers. During this second phase, several experiments are also planned with an aim to verify the scientific information already reported in the literature. Moreover, the structure-property relationship of biodegradable polymers needs to be explored to study the relaxation phenomena occurring in a polymer due to molecular motions. The third and the final objective is to prepare and process a novel composite material (biomaterial) and examine their thermal and electrical properties. The projected biomaterial is PLA based as it was found to be the most promising biodegradable polymer. Towards the end, comparison of the thermal, dielectric and electrical properties of biodegradable and conventional polymers will be presented using the database prepared and updated during this Ph.D. work.

Chapter 2

Polymer-film-processing

II. Polymer-film-processing

II.1. Introduction

Depending on the different type of processing methods offered by a polymer, its use in an application may vary. Electrical properties of a polymer are predominantly important while considering an application in electrical engineering. However, if a polymer cannot be processed as per the requirements of a specific application, they may not find use. For example, polyethylene can be extruded which is one of the reasons why it can be used in high voltage direct current cables.

Most of the biodegradable polymers being discussed in the first chapter can be processed into films using hot-pressing. Polymers like PLA, PHBV and PCL can be extruded and can be suitable in applications such as cables [161], [162], [142]. The flexibility offered by biodegradable polymers in terms of processing techniques is advantageous in viewpoint of an application.

There are different techniques of processing polymers such as hot-pressing, injection molding, compression molding, extrusion molding and solvent casting to name a few. In most cases in this work, polymers are processed into films by hot-pressing. In this chapter, the hot-pressing apparatus, different type of molds used for hot-pressing, calibration of mold and optimized processing conditions of different polymers into films are described. Once the films are obtained, they are dried and sampled for different experiments. The norms of drying of films and sampling methods for different experiments are also discussed.

II.2. Hot-pressing and other processing methods

The apparatus used for hot-pressing is a *Carver* (Model number: 2629) hot-press (Figure 27). The press comes with two heating plates and a temperature regulation system.

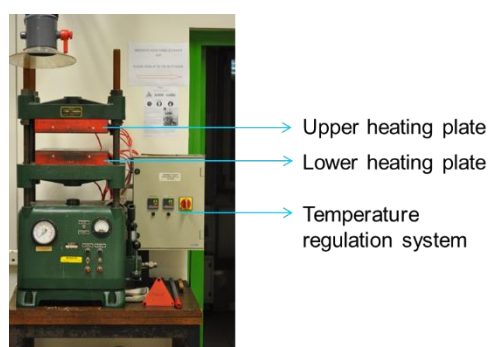


Figure 27. Carver hot-press with heating plates equipped with a temperature regulation system for hot-pressing of polymer and composite materials into films.

In this processing technique, a weighed amount of polymer in form of powder or pellet is sandwiched in between Teflon-discs contained in a mold (Figure 28) and is melted at temperatures higher than the melting temperature of the polymer being processed.

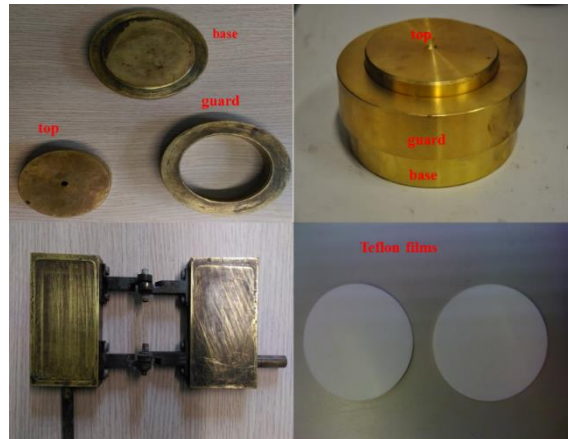


Figure 28. To the top are the circular mold and its components. To the bottom left is a rectangular mold and towards the bottom right is a pair of Teflon-discs.

Once the polymer-melt is formed, it is pressed under pressure and cooled to give films. The time to melting, temperature, pressure at which a polymer melt is pressed and cooling method depends on the polymer being processed.

In certain cases, a combinative method for processing is used. For example, polymer is melted in an internal mixer and then pressed into films in a hot-press. *Brabender* (Model number: FDO 234 H) is the internal mixer apparatus used in this study (Figure 29). It comes with two blades that rotate in opposite directions with different speeds to melt a polymer or to mix two or more different substances. The temperature of the blades is regulated using a temperature control system. As will be seen later, this method is used only for the processing of PHB films and PLA based nanocomposite films.



Figure 29. Brabender internal mixer.

Attempts were made to process polymer films by solvent-casting. Due to the electrical measurement requirements of thinner, homogenous (uniform thickness) films with least defects, this route was discontinued.

II.3. Mold

There are two types of mold used in this study, namely circular mold and rectangular mold. The name of the molds is given based on the circular and rectangular shapes of the mold and the films obtained. Figure 28 shows the circular mold which gives a circular shaped film of 10 cm in diameter. The thickness of a film varies depending up on the amount of the material

used for processing a film. The other is the rectangular mold which gives a rectangular shaped film. Unlike in the circular mold, it gives a film with a fixed thickness of 0.5 mm. The length and breadth of the processed film is 9 cm and 6 cm respectively.

The circular mold has been the most used to prepare polymer films. Figure 30 shows the schematic representation of the circular mold.

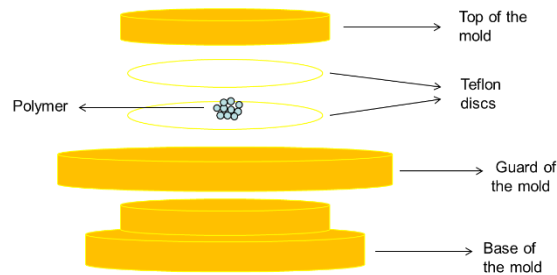


Figure 30. Schematic representation of the constituents of a circular mold for processing of a polymer into its film.

Teflon-discs (Figure 29) were the most used component to contain the polymer raw material along with the circular mold. Teflon-coated-Aluminum-plates (Teflon-coated-Al-plates) were also tried for processing. These Teflon-coated-Aluminum-plates posed limitations in the processing of polymers in the form of pellets. It leads to the non-uniform surfaces in the processed films. The circular mold was calibrated for optimizing the processing conditions of different polymers.

II.3.1. Calibration of the circular mold

The objective of these set of experiments is to study the time taken by the mold to reach the melting temperature of a polymer. The melting temperature of polymers PHB, PHBV, PLA, PP and a PLA based composite is around 160 °C and that of PCL is around 60 °C. Therefore, calibration experiments were performed for two different temperatures. Also, calibration experiments were done with two different mold components: Teflon-discs and Teflon-coated-Aluminum-plates.

a) For processing PHB, PHBV, PLA, PP, PLA based composite

1. Calibration with top and base (without guard) of the mold (Teflon-discs, T = 170 °C)

Apparatus used: *Carver hot-press, Circular mold, Teflon-discs, Temperature sensors*

Figure 31 shows the experimental set-up for calibration of the mold.



Figure 31. Experimental set-up for calibration of the circular mold.

The temperature of the heating plates of the hot-press was set to 170 °C. The mold contained two Teflon-discs with a temperature sensor placed in between them as seen in the Figure 31. The mold was placed on the lower heating plate and raised until the top of the mold came just in contact with the upper heating plate.

Figure 32 shows the temperature variation in the heating plates of the hot-press and in between the Teflon-discs recorded by a temperature sensor. The temperature of 167 °C is attained in 20 minutes and the maximum recorded temperature is 167.9 °C after 25 minutes.

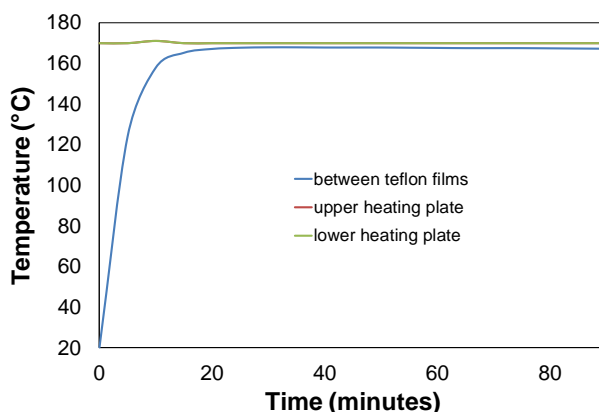


Figure 32. Temperature variation in the heating plates of the hot-press and in between the Teflon-discs.

2. Calibration with top and base (without guard) of the mold (Teflon-coated-Al-plates, T = 190 °C)

Apparatus used: *Carver hot-press, Circular mold, Teflon-coated-Aluminium-plates, Temperature sensors*

Unlike in the previous case, the temperature of the heating plates of hot-press were set to 190 °C and Teflon-coated-Aluminium-plates were used instead of Teflon-discs. It reaches the temperature of 170 °C in around 10 minutes and the maximum recorded temperature of 177 °C in around 22 minutes.

b) For processing PCL

Apparatus used: *Carver hot-press, Circular mold, Teflon-discs, Temperature sensors*

The calibration of the mold for PCL was done only using Teflon-discs. The temperature of the heating plates was set to 70 °C. The temperature reached 60 °C in 5 minutes and the maximum recorded temperature is 69.6 °C in around 13 minutes.

II.3.2. Polymers-processed

The polymer to be processed into films is contained in between two Teflon-discs. These Teflon-discs which contain the polymer are enclosed within the mold. The mold is then placed in between the heating plates of a hot-press where the temperature of the heating plates is well above the melting temperature of the polymer contained in the mold. The polymer in the mold melts, is then pressed under pressure and allowed to cool giving a polymer-film. The method of cooling a polymer-melt varies. Thus, polymers in form of pellets, powder or granules are processed into films.

Following the calibration step, many trials were done by varying experimental parameters such as time, operating temperature, method of cooling and the pressure applied to optimize processing conditions for each kind of polymer. Table 5 shows the mass of polymers to be weighed out for processing it into films of thickness around 0.5 mm (500 μm) with a diameter \approx 10 cm.

Table 5. Mass of the polymers for processing into films.

Polymer	Mass (g)
PHB	4
PHBV	4.5
PCL	4.5
PLA	5
CA	5
PET	6.5
PP	3.6

Following are the polymers processed along with their optimized processing conditions:

a) PHB

1. Hot-press (using circular mold)

Apparatus used: *Carver hot-press, Circular mold, Teflon-discs, Teflon-coated-Aluminum-plates*

A wide range of conditions were tested using hot-pressing technique to process PHB films. The details of the processing conditions aren't discussed here. However, it did not provide a film that would qualify for an electrical measurement. The films showed high degree of crystallinity, brittleness, bubbles and presence of voids.

2. Internal mixer + hot-press (using rectangular mold)

Apparatus used: *Carver hot-press, Brabender internal mixer, Rectangular mold, Teflon-discs*

Approximately 20 g of powder of PHB was melted in an internal mixer at 180 °C for 10 minutes. It was then transferred into a rectangular mold and hot-pressed at 180 °C for 30 seconds and 1 minute respectively providing two different films.

Though plenty of films were produced by the former technique, optical micrographs (discussed later) showed that the films prepared by combinative technique of internal mixer and hot-press are much better than those prepared only using hot-press. Thus, only films processed using combinative method were qualified for performing electrical measurements.

As mentioned earlier, solvent casting did not provide a film suitable for electrical measurements.

b) PHBV, PCL, PLA, PP

Apparatus used: *Carver hot-press, Circular mold, Teflon-discs*

PHBV in powdered form was obtained from Monsanto Europe S.A. (Belgium). It contains 8 % hydroxyvalerate (HV). PHBV films were processed only by hot-pressing. About 4.5 g of PHBV powder sandwiched in between the Teflon-discs contained in a mold was melted at 180 °C and hot-pressed under 1000 psi (i.e., $6.9 \times 10^6 \text{ N/m}^2$) pressure to give a PHBV film. The pellets of PCL were obtained from Sigma-Aldrich. Its number average molecular weight (M_n) is reported to be 45000 g/mol. Pellets of PCL were processed into a film in the same manner as PHBV except the processing conditions which differs. About 4.5 g of PCL is required to obtain a circular film with a thickness of 0.5 mm. Granules of PLA were obtained from Goodfellow [163] which had a nominal size of 3 mm. About 5 grams of PLA was weighed out to obtain a circular film with a thickness of 0.5 mm. The pellets of PP were obtained from *APPRYL*. About 3.6 grams of PP was weighed out to obtain a circular film with a thickness of 0.5 mm. Table 6 shows the optimized processing conditions for PHBV, PCL, PLA and PP.

Table 6. Processing conditions of polymers.

Polymer	Processing temperature (°C)	Processing method	Cooling method
PHBV	180	25 th min. – 1000 psi applied and not released	Turned off heating and cooled the melt in hot-press to R.T.
PCL	80	25 th min. – 1000 psi applied and not released	Turned off heating and cooled the melt in hot-press to R.T.
PLA	200	30 th min. – 1000 psi applied and not released	Turned off heating and cooled the melt in hot-press to R.T.
PP	190	19 th min. – 1000 psi applied and not released	25 th min. – took the films and cooled the melt beneath a weight at R.T.

Processing of polymers into their films came with many challenges. Cooling methods involved cooling the polymer-melt in the hot-press until different temperatures or cooling the polymer-melt out of the hot-press. When cooled out of the hot-press, few trials were also

involved in unmounting the mold and cooling the polymer-melt in between the Teflon-discs at room temperature. In certain cases, some weights were also placed on the Teflon-discs containing the polymer melt to be cooled at room temperature. Quenching methods varied from submerging the mold in liquid nitrogen to water and in many cases, these methods did not yield films or the films obtained weren't suitable for electrical measurements.

c) PET, CA

Polymer PET was obtained in granular form from Sigma-Aldrich. It contained 30 % of glass particles as a reinforcer with a melting temperature of 250 to 255 °C. The operating temperature of the hot-press imposed limitations on processing PET. The maximum working temperature of the hot-press is 260 °C. Another drawback is the Teflon-discs which begins to slightly deform above 200 °C. Thus, PET couldn't be processed.

Cellulose acetate was obtained in powdered form from Sigma-Aldrich. Its M_n is reported to be around 30000. Attempts were made to process CA but without success. It is understood in case of CA, it lacked a plasticizer, unlike in case of cellulose acetate butyrate (CAB) with inherent plasticizing content in its structure. The use of external plasticizer in processing CA was not appreciated as one of the main objectives of preparing these films was to study dielectric relaxation occurring in a polymer. The presence of a plasticizer could pronounce its influence in dielectric spectra. Consequently, processing of CA was dropped.

II.3.3. Preparation of PLA-MFC nanocomposite and its processing

A novel PLA based nanocomposite is prepared by dispersing surfactant-modified micro-fibrillated cellulose (MFC) in the PLA matrix. The micro-fibrillated cellulose is a cellulose-based filler material and it is obtained as described earlier [164]. MFC has one of its dimensions below micrometer range and hence, the name nanocomposite is given. The surface modification of MFC is performed in the laboratory with a surfactant which are kept confidential. The PLA granules used for preparation of nanocomposites' matrix were the same as those used to prepare pure biodegradable PLA films.

The PLA based nanocomposite is referred to as PLA-MFC which represents both the matrix and the filler. Preparation of PLA-MFC nanocomposite is achieved in two stages. In the first stage, surface modification of the MFC is performed with a surfactant. Following this, surfactant-modified MFC is dispersed in the PLA matrix in an internal mixer to give PLA-MFC nanocomposite. The obtained blend is then pressed into films by hot-pressing. The preparation of PLA-MFC is illustrated as follows:

Stage 1: surfactant based surface modification of MFC

Stage 2: mixing of PLA with surfactant-modified MFC in an internal mixer

About 16.4 g of PLA is mixed with 3.6 g of surfactant-modified MFC in an internal mixer at 180 °C for 10 minutes to give a blend of PLA-MFC nanocomposite. This blend is then

pressed in a hot-press at 200 °C to give films. Figure 33 shows the image of the surfactant-modified MFC and the PLA-MFC blend.



Figure 33. To the left is the image of surfactant-modified MFC and to the right is the blend of PLA-MFC obtained from internal mixer.

Earlier studies of dispersion of cellulose whiskers in isotactic polypropylene matrix using bare, grafted and surfactant modified whiskers has been reported [165]. Their focus was on improving the mechanical properties of polypropylene by incorporation of cellulose whiskers as reinforcing elements in its matrix. In their case, the dispersion of hydrophilic cellulose whiskers in hydrophobic polypropylene was enhanced due to the surface modification of cellulose whiskers with the surfactant. They also reported improvement in the mechanical properties of the composite. In this study, surfactant-modified MFC is dispersed in a hydrophilic, bio-based and biodegradable PLA. For a first time, this type of nanocomposite based on PLA has been prepared and processed. The objective here is to study the dielectric properties of the composite unlike mechanical properties studied in the cellulose whiskers based polypropylene composite.

A wide variety of processing methods and cooling conditions were tried to prepare PLA-MFC films. The large chunk of composite material obtained from an internal mixer was cut into small pieces. The first few trials of processing them into films were performed using the rectangular mold in the hot-press. The small pieces of composites to be processed into films were placed in between two paper sheets instead of Teflon-discs usually used with circular mold. When the melt was cooled very slowly in the hot-press, the films obtained lacked homogeneity and was easily visible to the naked eye. In the cases where the melt was quenched by exposing the melt contained in between the papers to room temperature, the films were deformed and with bubbles. In the trials performed with the circular mold, the slow cooling of the melt in the mold lead to very brittle poor-quality films. The cooling of mold in the water was tried but did not work either.

The small chunk of composite material obtained from an internal mixer was later grinded to obtain the powdered form of composite. Processing in powdered form provided films lesser brittle though with defects such as bubbles. With repeated presence of bubbles with lesser brittle films, the focus was shifted towards the post-treatment of these films. The post-treatment addressed the problem of brittleness and reduced bubbles. With repeated efforts, a post-treated PLA-MFC film suitable for electrical measurements was obtained. The film was obtained by post-treating a prepared PLA-MFC film at 125 °C for 8 minutes and the resulting film was apparently free from bubbles and more homogenous in its thickness. Figure 34 shows the images of few films.

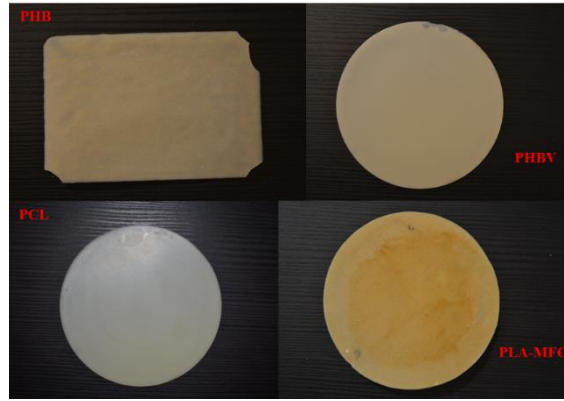


Figure 34. Images of PHB, PHBV, PCL, PLA-MFC films.

II.3.4. Thickness measurement of a film

The polymer/composite films do not show uniform thickness throughout its bulk. Since the thickness could vary significantly, the thickness of a film is reported as an average value of thickness measured at eight different sectors. Figure 35 shows the scheme of a surface of a polymer film and illustrates the eight different sectors for measuring thickness of a film.

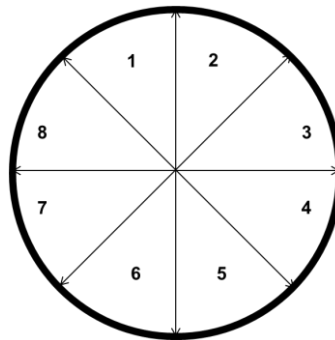


Figure 35. Scheme of the surface of a polymer film of 10 cm in diameter divided into 8 sectors for measuring thickness.

Thickness of a film is measured in each of the 8 sectors at equal distances of the center. Figure 36 shows the thickness of a PHBV film in 8 sectors.

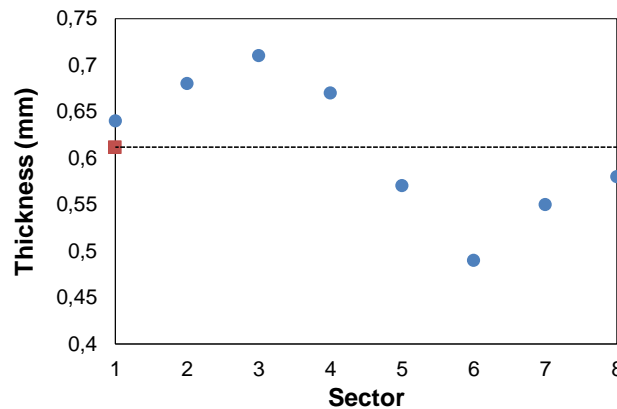


Figure 36. Thickness of a PHBV film in 8 different sectors. The black dotted line represents the average value of thickness.

The hot-pressing was the only processing method available and used to process films in the laboratory. To meet the dimension (surface area) criterium of certain electrical measurements to yield finer results, thinner films were reasonable. However, processing a much thinner film below the thickness of around 0.5 mm wasn't feasible. Using hot-pressing, many attempts were made to process thinner films close to 0.1 mm but without success. These attempts provided films which did not possess enough surface area to be studied for electrical measurements. Also, there were lot of defects such as voids in the films and non-homogenous film thicknesses. Thinner samples of biodegradable polymers are though widely available in the market. Table 7 shows some of the biodegradable polymers with relatively thinner films.

Table 7. Biodegradable polymer films available in the market and their thickness.

Polymer	Thickness (mm)
PHBV	0.01 to 0.05 [163]
CA	0.02 to 0.1, 0.2, 0.5 [163]
PLA	0.05 [163]

II.3.5. Sample-conditioning and preparation

a) Sample-conditioning

Once the polymer/composite films are obtained, they are dried under controlled conditions. This procedure is referred to as *Sample-conditioning* and it is done so to keep a polymer film dry and unaffected by factors such as temperature, humidity and light. The conditions under which a polymer film is stored and dried depends on its thermal properties and morphology. Polymers such as PP, PHB, PHBV films were stored in an oven under vacuum at 60 °C. PLA films and PLA based nanocomposite were also stored in an over under vacuum but at 40 °C as their T_g is around 60 °C. Polymer PCL is stored in a desiccator under vacuum at R.T. Once the samples were dried up to a constant weight, they were used for electrical measurements.

b) Metalization

Prior to electrical measurements such as dielectric spectroscopy and *DC* current of the prepared films, materials were to be metalized for establishing electrical or ohmic contacts. This is achieved by physical vapor deposition (PVD) method where metal particles are sputtered on a polymer film in an inert atmosphere.

For dielectric spectroscopy measurements, films were metalized. In case of *DC* current measurements, depending on the experimental set-up, metalization was done. Some of the sample-cells used for *DC* current measurements do not need a polymer-film to be metallized and can be used as processed. This is mentioned later in each experimental set-up of the *DC* current measurements.

Films are metallized on either side with gold of approximately 45 nm in thickness. *Quorum Q150T ES* is the instrument used for deposition of gold on a polymer film by sputtering

technique. Figure 37 shows the sketch of a metallized sample used for dielectric spectroscopy.

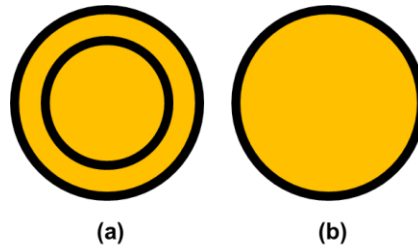


Figure 37. Sketch of a metallized polymer film for DS experiments. Black color represents the un-metallized part and yellow color represent the metallized part of a sample film. (a) obverse side with metallized part for contact with measurement (top) electrode encircled by metallized part for contact with guard electrode, (b) reverse side with metallized part for contact with bottom electrode.

On the obverse side lie the guard and the measurement electrode. The diameter of the measurement electrode is 30 mm and it is encircled by a guard electrode of width 5 mm separated by 1 mm from the measurement electrode. The reverse side consists of an electrode through which a voltage is applied. The diameter of the electrode on the reverse side is 42 mm. The obverse side consists of top and guard electrode and the reverse side is referred to as bottom electrode.

Chapter 3

Optical microscopy, Drying and Water uptake

III. Optical microscopy, Drying and Water uptake

III.1. Introduction

In this chapter, optical micrographs of polymer and composite films are presented. Also, the time taken for drying of these films are reported. A film dried until constant weight is studied for water uptake up to saturation. The conditions of both drying and water uptake and the results are described in this chapter.

III.2. Optical microscopy

III.2.1. Introduction

Optical microscopy was performed using an optical microscope *Zeiss Axiophot II*. It is a classical light microscope equipped with a SIS CCD camera *ColorView 12*. Experiments such as dielectric spectroscopy, current measurement and electrical breakdown are very sensitive to defects in a polymer/composite film. The polymer and composite films prepared were thus analyzed for defects if any due to the presence of bubbles, moisture, impurities and cracks.

III.2.2. Result and Discussion

Figure 38 shows the optical micrograph of PHB film prepared by hot-pressing. It shows many cracks and is probably due to extensive crystallization or thermal degradation. The processing at temperature beyond 180 °C might have led to thermal degradation. This kind of films with defects weren't suitable for experiments.

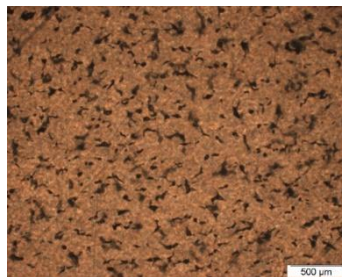


Figure 38. Optical micrograph of PHB film prepared by hot-pressing.

The PHB films prepared by another method, melting in an internal mixer and pressing the polymer melt in a hot-press did not show defects as observed earlier as in the Figure 38. Figure 39 shows the optical micrograph of PHB film prepared by a combination of internal mixer and hot-pressing. These films were more suitable for electrical measurements.

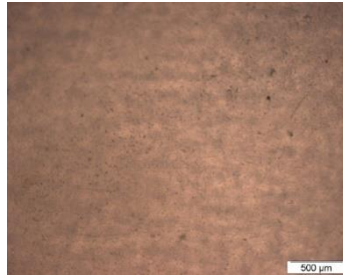


Figure 39. Optical micrograph of PHB film prepared by combination of internal mixer and hot-press.

PHBV just like PHB also belongs to the family of polyhydroxyalkanoates. In PHBV, the *HV* content acts as a plasticizer and scales down the occurrence of crystallization. Figure 40 shows a PHBV film with and without defects. The polymer-melt of PHBV which was cooled out of the mold showed bubbles and the one gradually cooled in the mold shows no defects.

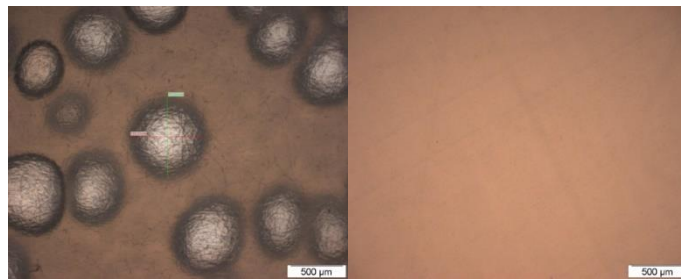


Figure 40. Optical micrograph of PHBV film with defects (towards the left) and without defects (towards the right).

Figure 41 shows the optical micrographs of PCL, PLA, PP and PLA-MFC films. These films are homogenous and apparently free of defects as seen in their micrographs.

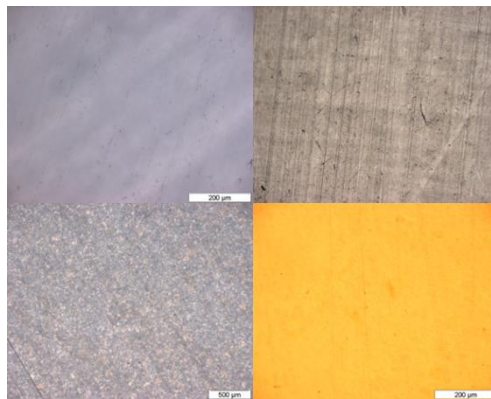


Figure 41. In clockwise direction from the top-left are the optical micrograph of PCL, PLA, PLA-MFC and PP.

III.3. Drying

III.3.1. Introduction

The prepared films were either dried in a desiccator under vacuum or in an oven at a temperature T under vacuum. They were dried under the conditions specific to each polymer or composite material. The mass loss in a polymer film and time for drying are described in this section.

III.3.2. PHBV

Figure 42 shows the loss in mass in a PHBV film during drying. The drying condition was 60 °C in an oven under vacuum. Under these conditions, the mass stabilizes within 2 days of time with a mass loss of 1.6 %.

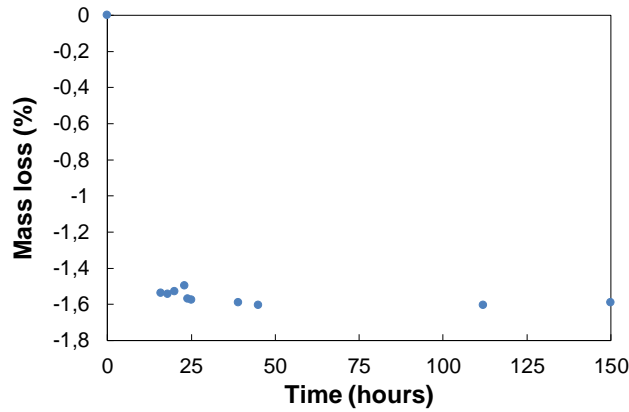


Figure 42. Loss in mass in time in a PHBV film during drying.

III.3.3. PCL

Figure 43 shows the loss in mass in a PCL film during drying at room temperature in a desiccator under vacuum. The mass loss is negligible and the stability in mass is reached rapidly in less than a day with a mass loss of only 0.08 %.

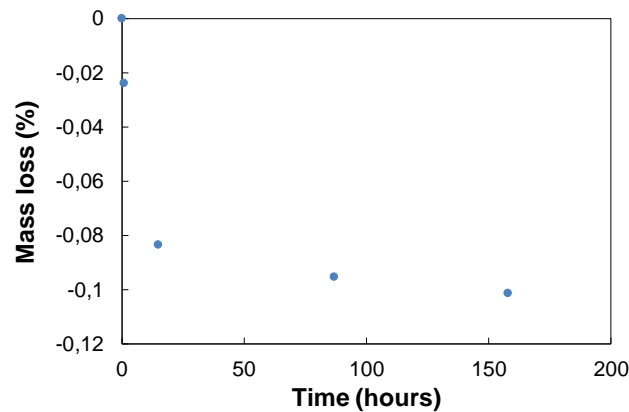


Figure 43. Mass loss in time in a PCL film during drying.

III.3.4. PLA

Figure 44 shows the loss in mass in a PLA film during drying at 40 °C in an oven under vacuum.

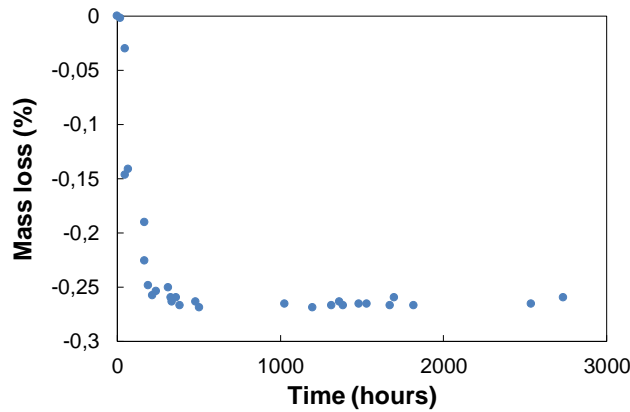


Figure 44. Loss in mass in time in a PLA film during drying.

The mass loss is apparently negligible in the first 48 hours of drying. The mass stabilizes in around 215 hours with a small mass loss of 0.25 %. Weighing of the film was continued for 114 days during which the mass remained almost constant.

III.3.5. PLA (post-treated)

A post-treated PLA film was studied for drying time until a constant weight. A prepared PLA film was post-treated at 125 °C for 8 minutes in a hot-press to obtain a post-treated PLA film. The condition of drying was 40 °C in an oven under vacuum. Figure 45 shows the loss in mass in a post-treated PLA film during drying.

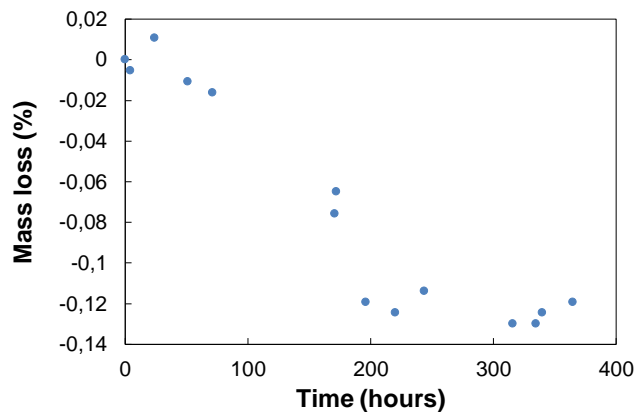


Figure 45. Loss in mass in time in a post-treated PLA film during drying.

As observed in PLA, the mass loss is negligible in the first 48 hours of drying. This observation is consistent with analysis performed on other post-treated PLA films. The mass of the film stabilizes in around 196 hours with a lower mass loss of 0.12 %.

In both PLA and post-treated PLA films, the rate of drying is much slower compared to PHBV. This could be attributed to the glassy state of PLA at the drying temperature which may decelerate the release of water molecules from the polymer matrix.

III.3.6. PLA-MFC (post-treated)

A prepared PLA-MFC film was post-treated at 125 °C for 8 minutes in a hot-press to obtain a post-treated PLA-MFC film. The drying conditions were 40 °C in an oven under vacuum. Figure 46 shows the loss in mass in a post-treated PLA-MFC film during drying.

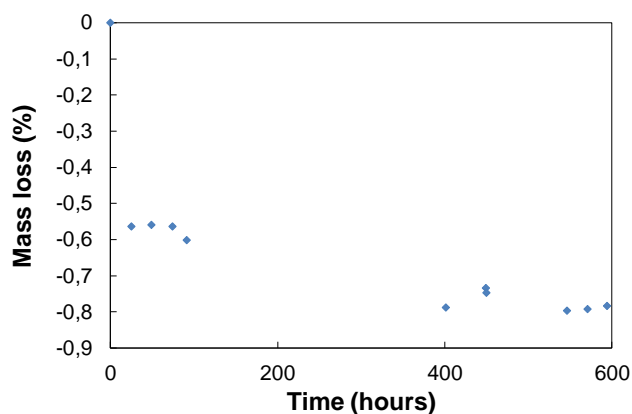


Figure 46. Loss in mass in time in a post-treated PLA-MFC film during drying.

Drying of these films is a gradual process with a total mass loss of 0.8 % with a mass loss of 0.6 % occurring in the first 48 hours of drying.

III.4. Water uptake

III.4.1. Introduction

The presence of water molecules in a polymer matrix can influence its mechanical, thermal and electrical properties. To understand the diffusion of water vapor in a biodegradable polymer, dynamics of water absorption and percentage of mass uptake at saturation are determined. These quantities are influenced by the experimental conditions such as relative humidity and temperature. The nature of a polymer, its morphology, i.e., crystalline or amorphous may influence the diffusion coefficient of water molecules in a polymer. Few reports are communicated on mass uptake (in %) at saturation of the biodegradable polymers. Dynamic aspect such as diffusion coefficient of some biodegradable polymers have been discussed earlier [166], [167].

The polymer/composite material if used in an application is usually in contact with the environment. Hence, the humidity in the air can influence the material's morphology and may contribute towards the degradation of a polymer/composite material. Since biodegradable polymers are more prone to humidity in air, water uptake in polymer/composite material is studied. In this section, water uptake in PHBV and PLA is presented.

III.4.2. Experimental set-up for water uptake study in polymers

A dried polymer film is kept in Vötsch climatic test chamber (type VC 0018) at 40 °C and 80 % relative humidity (RH) to study amount of water uptake. Figure 47 shows the climatic test chamber.



Figure 47. Towards the left is the Vötsch climatic test chamber and towards the right is the enlarged image of the display (touch) screen.

The amount of water uptake is measured by weighing a polymer film as a function of time until a constant weight is reached. The water uptake in a polymer's film in mass percentage is given as,

$$M_g (\%) = [(M_t - M_0)/(M_0)].100$$

where, M_0 is the initial mass, M_t is the mass measured at time t , M_g is the mass gain in percentage corresponding to M_t . *OUHAS Explorer* is the instrument used for weighing samples with a resolution of 0.1 mg.

III.4.3. PHBV

Figure 48 shows the mass gain in a PHBV film during water uptake.

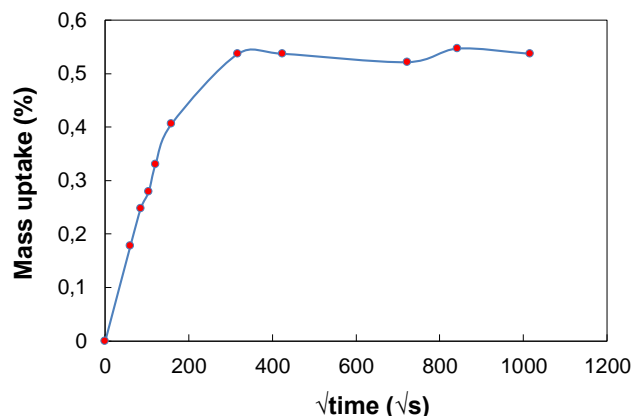


Figure 48. Mass gain in time in a PHBV film during water uptake. Conditions of measurement: 40 °C, 80 % RH.

The dried PHBV film takes around a day for mass uptake up to saturation. There was an observed mass loss of 1.6 % during drying (seen earlier in Figure 42) and 0.5 % mass gain during water uptake respectively.

III.4.4. PLA

Figure 49 shows the mass gain in PLA during water uptake measurement.

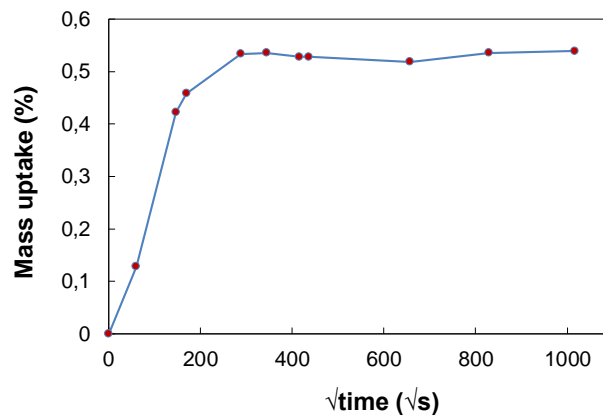


Figure 49. Mass gain in time in a PLA film during water uptake. Conditions of measurement: 40 °C, 80 % RH.

It has been clear from the drying time measurements of PLA (Figure 44, Figure 45) that the film takes considerable time for drying. The corresponding mass loss (%) during drying is lower compared to PHBV. Contrary to the rate of drying, the rate of mass uptake to saturation in PLA is a very rapid process. It takes around a day for mass uptake up to saturation with 0.5 % mass gain during water uptake. Table 8 shows the mass of water uptake (%) and diffusion coefficient of biodegradable polymers PHBV and PLA.

Table 8. Mass of water uptake (%) and diffusion coefficient of PHBV and PLA.

Polymer	Measurement conditions	Thickness of the film (mm)	Diffusion coefficient (m ² /s)	Mass uptake (%)
PHBV	40 °C, 80 % RH	0.598	6.3E-13	0.5
PLA	40 °C, 80 % RH	0.518	1.06E-13	0.5

Chapter 4

Differential scanning calorimetry and Dynamic mechanical thermal analysis

IV. Differential scanning calorimetry and Dynamic mechanical thermal analysis

IV.1. Differential scanning calorimetry (DSC)

IV.1.1. Introduction

In this section, the results obtained from the differential scanning calorimetry measurements are described and discussed. *DSC Q200 V23.5 Build 72* is the instrument used for DSC analysis. *TA Instruments Universal Analysis 2000* is the software used to analyze DSC thermograms. The sample cell is an aluminum pan in which few milligrams (between 6 mg to 10 mg) of a polymeric material is placed. The reference cell is an empty aluminum pan. Both sample and reference cell is heated with a constant heating rate (in most cases in this study, it is 10 K/min.). Difference occurring in enthalpy meant thermal transitions taking place in the material. Figure 50 shows the sample-chamber and the enlarged image of sample and reference cells placed on a sample base.

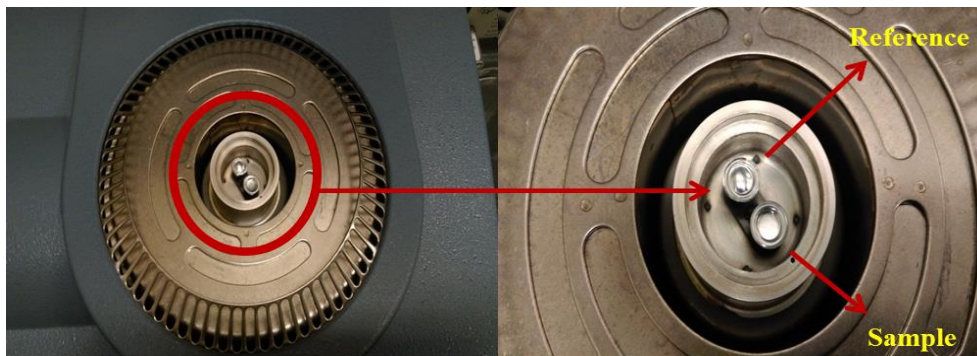


Figure 50. Sample and reference cells in DSC Q200.

The sample base is connected to a thermocouple and heater. Degree of crystallinity of a polymer is calculated as given in the Equation 7,

$$\text{Equation 7. } X_c (\%) = (\Delta H_m / \Delta H_m^\circ) \cdot 100$$

where, ΔH_m is the heat of melting of the polymer studied and ΔH_m° is the heat of melting of the respective polymer which is totally (100 %) crystalline. The Table 9 below shows the heat of melting of 100 % crystalline polymer for different polymers.

Table 9. Heat of melting of 100 % crystalline polymer (ΔH_m°).

Polymer	(ΔH_m°) (J/g)
PHB	146
PHBV	146
PCL	139.5
PLA	93
CA	58.8
PP	207.1
PET	140.1

IV.1.2. Heating cycle and melting temperature of polymers

The *heating cycle* of the polymers in DSC allows to study the thermal history and the polymer morphology by determining their melting temperature and degree of crystallinity. In a *heating cycle*, a polymer is heated to its melt. During this cycle, glass transition temperature, melting temperature and in case of certain polymers, cold-crystallization process is also observed. On the contrary, in a *cooling cycle*, a polymer melt is cooled back to its glassy state. This cycle often shows the occurrence of re-crystallization of the polymer-melt. Table 10 summarizes the glass-transition, melting, crystallization temperatures and degree of crystallinity of many polymers analyzed during their heating cycles. The crystallization temperature corresponds to cold-crystallization processes occurring in PET and PLA. The melting temperatures found in this study is in agreement for PHB [58], PHBV [142], PCL [29], PLA [45], PET [168] and PP [169].

Table 10. Thermal properties and degree of crystallinity of polymers during heating cycle.

Polymer	Heating rate (°C/min)	T _g (°C)	T _c (°C)	T _m (°C)	X _c (%)
PHB	10	-	-	177	56
PHBV	10	-	-	163	48
PCL	10	-	-	64	51
PLA	10	≈ 60	120 (8 %)*	155	11
PET	10	≈ 75	115 (2 %)*	258	19
PP	10	-	-	168	39

*indicates the degree of crystallinity for the cold-crystallization process.

IV.1.3. Cooling cycle and re-crystallization temperature of polymers

Table 11 shows the crystallization temperature and the corresponding degree of crystallinity in the *cooling cycle* of several polymers. Cooling cycle usually involves the crystallization of the polymer melt at crystallization temperature.

Table 11. Crystallization temperature and degree of crystallinity of polymers during cooling cycle.

Polymer	Cooling rate (°C/min)	T _g (°C)	T _c (°C)	X _c (%)
PHB	10	-	69	39
PHBV	10	-	112	43
PCL	10	-	26	46
PLA	10	≈ 50	-	-
PET	10	-	218	25
PP	10	-	112	44

IV.1.4. Non-post-treated and post-treated PHBV studied by DSC

A PHBV film was prepared by melting powdered polymer for 30 minutes at 180 °C in a hot-press and hot-pressed by applying 1500 psi pressure. Another PHBV film with same processing conditions was prepared and post-treated to give a post-treated PHBV film. The post-treated PHBV film was obtained by post treating the prepared PHBV film at 120 °C for 10 minutes. The post-treatment resulted in an increase in the degree of crystallinity. Table 12 shows the thickness, melting temperature and degree of crystallinity of post- and non-post-treated PHBV films.

Table 12. Thickness and DSC results of post- and non-post-treated PHBV films.

PHBV film type	Thickness (cm)	X _c (%)	T _m (°C)
non-post-treated	0.06	44	166
post-treated	0.062	46	161

IV.2. Dynamic mechanical thermal analysis (DMTA)

IV.2.1. Introduction

In this section, the results obtained from the dynamic mechanical thermal analysis are described and discussed. The glass transition temperature can be directly estimated by *DSC* measurements as seen earlier. However, using the dynamic mechanical-thermal analysis, the T_g can be estimated. The principle of the measurement is to subject a material in form of a strip to an oscillatory force (or stress) at a set frequency and study its response as a function of temperature. The applied stress leads to strain which arise causing deformation and damping in a material and corresponding ratio (stress to strain) gives modulus of elasticity. The degree of deformation depends up on the stiffness of the material which is referred to as modulus and is represented by E . Damping is measured as $\tan\delta$. The maximum of the peak of $\tan\delta$ corresponds to α transition and the corresponding temperature corresponds to T_α . This transition reflects the relaxations occurring in a polymer due to molecular motions and may be related to the glass transition phenomenon. Note that though this is a method to evaluate T_g , the T_g determined directly in *DSC* and T_α obtained in *DMTA* may differ slightly as *DMTA* is measured as a function of frequency [170].

Rheometrics RSA 2 is the name of the instrument used for *DMTA* analysis. Polymer to be examined is in form of a strip and its geometry is defined by its length, width and thickness. The sample is placed vertically in a sample holder inside the sample-chamber as shown in the Figure 51. The temperature in the sample-chamber is maintained by air or liquid nitrogen depending upon the experimental conditions. A constant heating rate of 3 °C/minute and frequency of 1Hz was maintained for all the measurements. The temperature range was chosen depending on the polymer under study. *DMTA* analysis of PHB, PHBV, PCL and PP were performed.

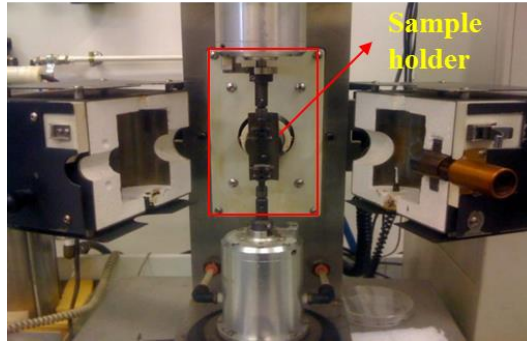


Figure 51. Sample-chamber in Rheometrics RSA 2.

IV.2.2. T_α of polymers

Figure 52 shows the T_α of the following polymers: PHB, PHBV and PCL.

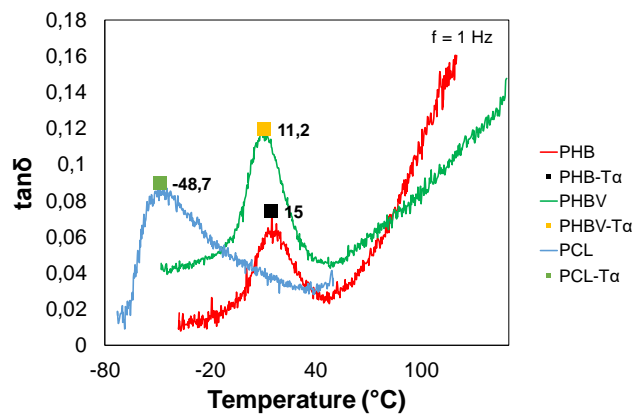
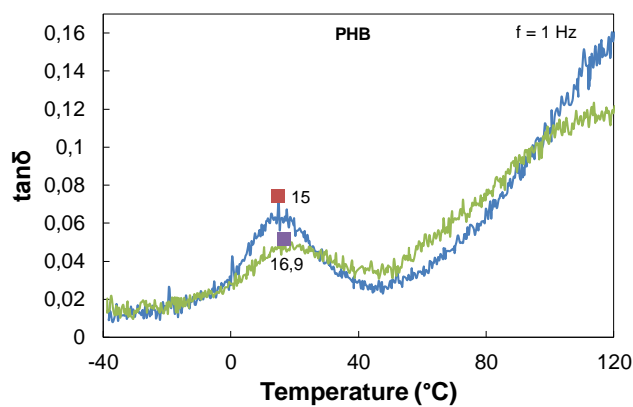


Figure 52. $\text{Tan}\delta$ plots of PHB, PHBV and PCL.

IV.2.3. Reproducibility in T_α with two different films

Figure 53 shows the $\text{tan}\delta$ plots of two different films of PHB and PCL demonstrating the reproducibility in T_α .



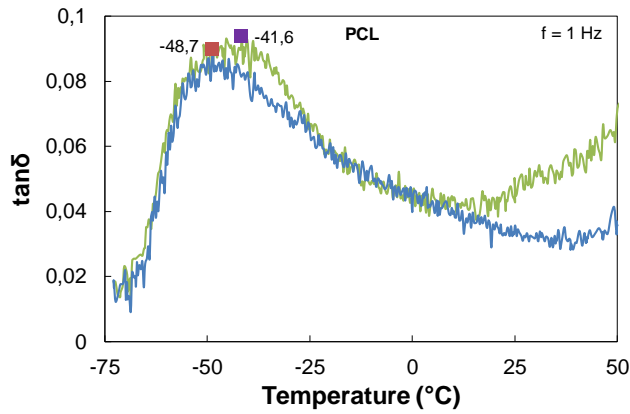


Figure 53. $\tan\delta$ plots of two films of PHB and PCL.

IV.2.4. Reproducibility in T_α with a same polymer film

Figure 54 shows the $\tan\delta$ plots for the two DMTA measurements made on the same film of PP where T_α are in good agreement with each other.

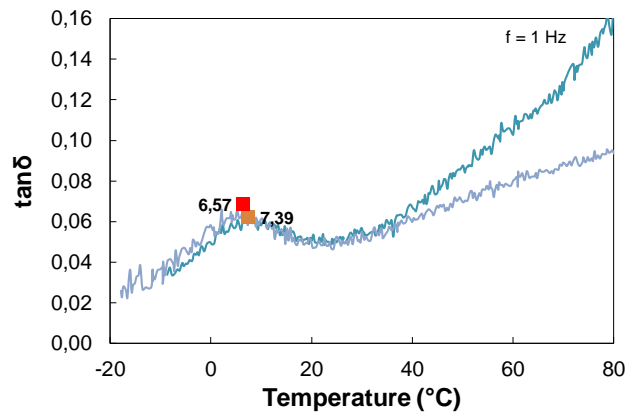


Figure 54. $\tan\delta$ plots for the same film of PP.

Chapter 5

Dielectric spectroscopy, Current
measurement and Electrical breakdown

V. Dielectric spectroscopy, Current measurement and Electrical breakdown

V.1. Introduction

These are the three types of electrical measurements performed in this work. In this section, one or many experimental set-ups of dielectric spectroscopy, current measurement and electrical breakdown are presented and explained. The results from the dielectric spectroscopy of PHBV, PCL, PLA and PLA-MFC are described using dielectric spectra and interpreted. The current measured in PHBV, post-treated PHBV and PCL at room and different temperatures and the electrical breakdown of PHBV at room temperature are also explained. Towards the end, the electrical properties of biodegradable polymers are compared with conventional polymers.

V.2. Introduction to dielectric spectroscopy

Novocontrol Alpha-A High Performance Frequency Analyzer is used for dielectric spectroscopy. A metallized film is placed between flat-disc type metallic electrodes on a sample-base housed in a sample-chamber. An AC voltage (V_{out}) of 1 V ($=1 V_{\text{rms}}$) is applied across the sample which in this study is a polymer or a composite. As explained by F. Kremer and A. Schönhals [148], the principle of measurement of dielectric spectroscopy is based on the application of a sinusoidal voltage as a function of frequency across a sample. The current response of the sample is analyzed with respect to their amplitudes and phase shift. This data is used to calculate the complex impedance from which rest of the physical quantities are derived. These include complex capacitance (C^*), complex permittivity (ϵ^*), dissipation factor ($\tan\delta$), complex modulus (M^*) and complex conductivity (σ^*).

Figure 55 shows the schematic diagram of dielectric spectroscopy experimental set-up. The sample-cell is enclosed in a sample-chamber isolated from the surroundings by vacuum. Heating or cooling of a sample is achieved by flushing nitrogen gas and the temperature is regulated by a temperature controlling device.

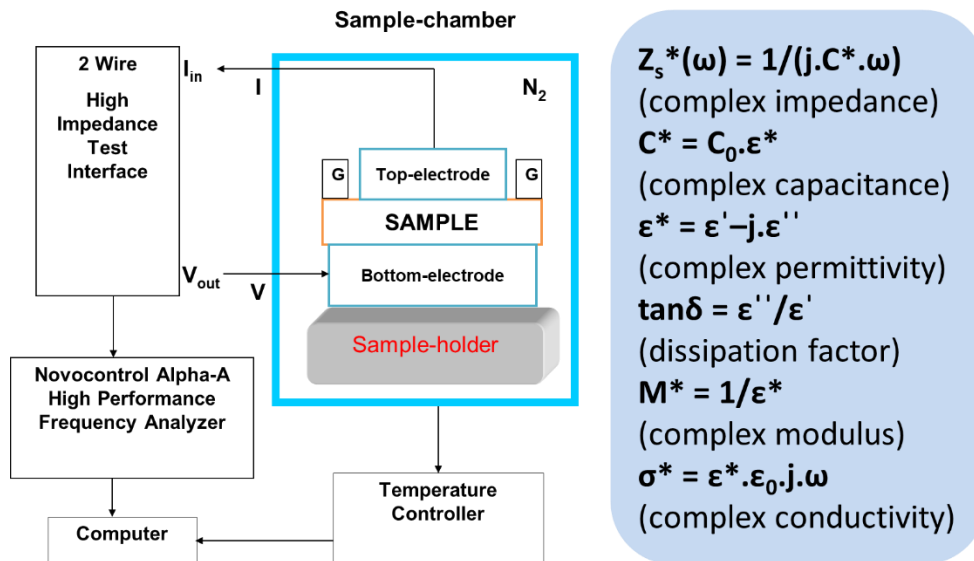


Figure 55. Schematic diagram of the dielectric spectroscopy analysis. ‘G’ represents the guard electrode which encircles the electrode on the top (top-electrode) of the sample.

V.3. Experimental set-up 1

Characteristics of the experimental set-up 1:

Spectroscopy analyzer: *Novocontrol Alpha-A High Performance Frequency Analyzer;*

Sample-chamber: *cylindrical;* Temperature regulation system: *Linkam TMS 94;*

Acquisition software: *WinDETA;* Electrodes: *large-sized*

A large cylindrical sample-chamber houses the sample under study and electrodes, all of which are mounted on a sample-holder. The electrodes are made of brass. Figure 56 shows the set-up and the enlarged image of a sample and the electrodes.

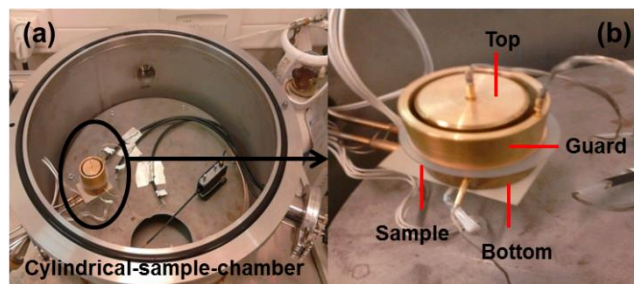


Figure 56. (a) Cylindrical sample-chamber for dielectric spectroscopy; (b) enlarged image of a sample and the electrodes.

The electrical connections for V_{in} , I_{out} and guard are established after placing a sample and the electrodes in the sample-chamber. The vacuum is generated inside the chamber and subsequently filled with nitrogen creating an inert environment for performing dielectric spectroscopy measurements.

Linkam TMS 94 is used for temperature control. For temperatures above *RT*, sample-base is electrically heated. Cooling is done by circulating liquid nitrogen. The desired temperature is set manually using *Linkam TMS 94*. *Novocontrol Alpha-A High Performance Frequency-*

Analyzer and *Linkam TMS 94* are not controlled by a single software. The analyzer is controlled by the *WinDETA* acquisition software while the temperature control is manually set as already described. Dielectric spectroscopy can be performed over a wide frequency range of 3 μ Hz to 10 MHz. Applied voltage (V_{rms}) can be varied from 10 mV to 3 V.

Based on this experimental set-up, dielectric spectroscopy measurements were conducted for two polymers, PHBV and PP. Measurements were done for temperature ranges -30 $^{\circ}$ C to 110 $^{\circ}$ C and -20 $^{\circ}$ C to 110 $^{\circ}$ C for PHBV and PP respectively in steps of 10 $^{\circ}$ C. Twenty minutes interval was maintained between measurement at each temperature. This time was for an increment/decrement of 10 $^{\circ}$ C step and for achieving temperature stabilization.

The diameter and the height of the cylindrical sample-chamber is 40 cm and 17 cm respectively. This is a large volume compared to the volume occupied together by a sample and the electrodes. For instance, diameter of the guard electrode is 3.9 cm and height of a sample, top and bottom electrode altogether sums up to \approx 4 cm.

This experimental set-up showed temperature gradient along the electrodes. This is one of the main reason for which this experimental set-up was abandoned for further spectroscopy measurements throughout the study and a new sample-chamber was designed. This new sample-chamber is discussed later in the experimental set-up 2. The temperature gradient was studied by monitoring temperature in the top and the bottom electrode. As seen in the Figure 56, Figure 57, the sample is placed between the top and the bottom electrode. The guard electrode encircles the top electrode.

V.3.1. Temperature gradient

The objective of this experiment is to examine the temperature gradient in the electrodes. A thermocouple each was attached to the top and the bottom electrode. This allowed studying the real temperature in these electrodes against the temperature shown by the *Linkam TMS-94*.

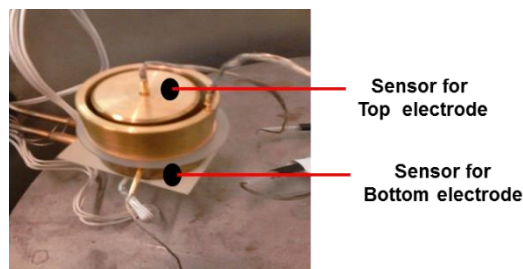


Figure 57. Experimental set-up for studying the temperature gradient in the electrodes.

The temperature gradient in the electrodes was studied under two different conditions:

- Under atmospheric (air) condition
- Under inert (N_2) gas condition

a) Under atmospheric (air) condition

Table 13 shows the protocol of a measurement to study the temperature gradient under atmospheric conditions. The same measurement protocol is applied for studying the temperature gradient under inert gas conditions.

Table 13. Protocol for measuring the temperature gradient along the electrodes.

Time (s)	0	1	3601	3602	14402	14403	18003	18004	28804	28805	32405
T _{set} (°C)	36	46	46	100	100	110	110	-100	-100	-110	-110

Figure 58 shows the temperature gradients under atmospheric conditions.

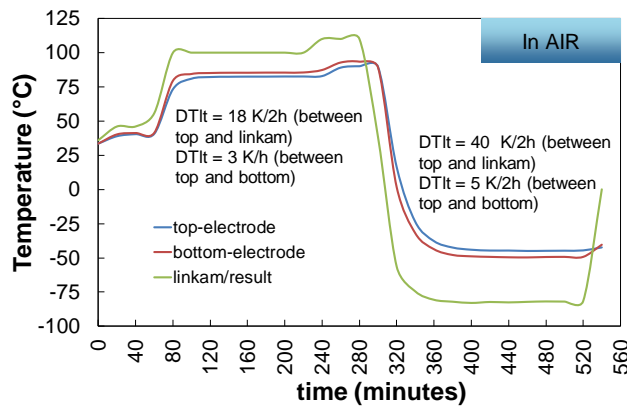


Figure 58. Temperature profile of top electrode, bottom electrode and Linkam TMS 94 corresponding to the protocol in Table 13 under atmospheric conditions. The temperature gradient between the top electrode and the Linkam TMS 94, the top electrode and the bottom electrode are mentioned.

b) Under inert (N₂) gas conditions

Figure 59 shows the temperature gradients under inert gas conditions.

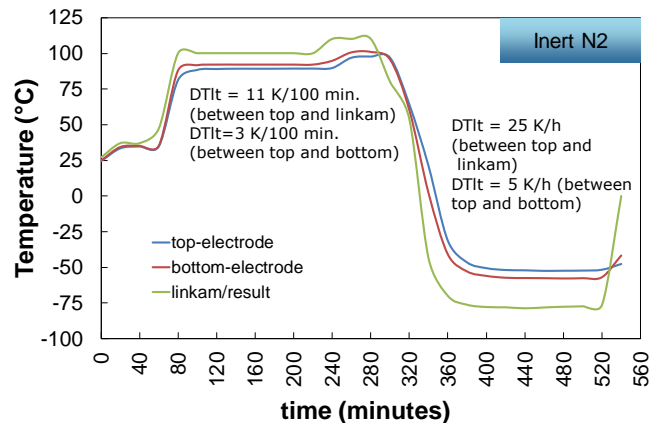


Figure 59. Temperature profile of top electrode, bottom electrode and Linkam TMS 94 corresponding to the protocol in Table 13 under inert conditions. The temperature gradient between the top electrode and the Linkam TMS 94, the top electrode and the bottom electrode are mentioned.

Table 14 shows the gradient observed under both air and inert conditions. The gradient demonstrates a significant difference in the temperature between those shown by the temperature regulation system *Linkam TMS 94* and the real temperature of the electrodes. The sample placed in between the electrodes therefore is at much different temperature than appeared in *Linkam TMS 94*.

Table 14. Gradient among the electrodes and the electrodes and temperature regulation system.

	ΔT (K) while increasing temperature	ΔT (K) while decreasing temperature
Between top and bottom (air)	3 K/h	5 K/2 h
Between top and bottom (N ₂)	3 K/100 min.	5 K/h
Between top and Linkam TMS 94 (air)	18 K/2 h	40 K/2 h
Between top and Linkam TMS 94 (N ₂)	11 K/100 min.	25 K/h

The result confirms a significant degree of gradient between the electrodes and between the electrodes and *Linkam TMS 94*. This problem in the gradient resulted in the experimental set-up 2.

V.4. Experimental set-up 2

Characteristics of the experimental set-up 2:

Spectroscopy analyzer: *Novocontrol Alpha-A High Performance Frequency Analyzer*;
 Sample-chamber: *Cryostat*; Temperature regulation system: *TDK Lambda*; Acquisition-software: *WinDETA*; Electrodes: *small-sized*

Figure 60 shows the schematic diagram of small sized electrodes.

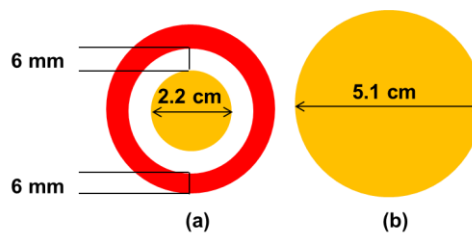


Figure 60. Schematic diagram of the small sized electrodes. Towards the left is the top electrode (in yellow) encircled by guard electrode (in red). Towards the right is the bottom electrode. The thickness of the top, the guard and the bottom electrodes is 2 mm compared to the large-sized electrodes which are few centimeters.

This experimental set-up was built during this work. In this set-up, cylindrical-sample-chamber is replaced by cryostat which is isolated from surroundings by vacuum. The sample-cell which consists of a sample and the electrodes is enclosed in the cryostat. The volume of the cryostat is significantly less compared to the cylindrical-sample-chamber. The electrodes are much thinner disc types compared to the one used in experimental set-up 1. The heating unit is changed from *Linkam TMS 94* to much sophisticated temperature regulation system: *TDK Lambda*. The temperature is well controlled with a maximum variation of less than 1 °C

from the measurement temperature. Heating or cooling of the sample placed in the sample cell housed in the cryostat is achieved by flushing nitrogen gas.

Figure 61 shows the experimental set-up of the dielectric spectroscopy. Here the temperature control system *TDK Lambda* is integrated with *WinDETA* software. The temperature regulation can be programmed and is automatic unlike in the previous case where the temperature regulation system and *WinDETA* software functioned independently. Thus, *Novocontrol Alpha-A High Performance Frequency Analyzer* and *TDK Lambda* are both controlled by *WinDETA*.



Figure 61. Towards the left is the experimental set-up of dielectric spectroscopy and towards the right is the Cryostat.

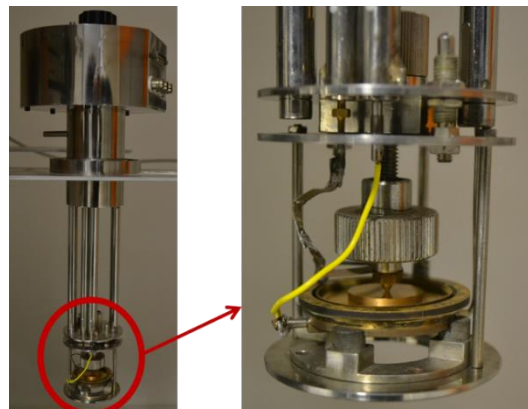


Figure 62. Image of the sample-cell for dielectric spectroscopy used in the experimental set-up 2. The enlarged image shows a metallized polymer film placed in between the electrodes in the sample-cell.

V.5. Dielectric spectroscopy: PHBV

V.5.1. Introduction: Dielectric spectroscopy of PHBV

PHBV is a bio-based, biodegradable polymer. It belongs to the family called polyhydroxyalkanoates. It is a copolymer made up of two monomers: hydroxybutyrate and hydroxyvalerate. It can be synthesized by photosynthetic and non-photosynthetic bacteria [21]. It is extracted as a white powder and is a semi-crystalline polymer with a high degree of crystallinity [39]. The highly crystalline morphology of this polymer is attributed to its repeating unit which in turn depends on the bacterial strains used and the fermentation conditions [39],[171]. Figure 3 shows the structure of PHBV polymer. The structure consists

of polar carbonyl and hydroxyl groups which renders the polymer polar. PHBV possess better mechanical properties over its homopolymer counterpart poly(3-hydroxybutyrate) (PHB) which has several mechanical drawbacks due to its physical ageing process [172]. It undergoes crystallization upon storage at room temperatures leading to embrittlement of the material [172], [173]. Additionally, PHB also shows poor thermal properties [58]. Heating around 20 °C above its melting point causes a significant change in its molecular weight which in turn manifests in its mechanical properties [174].

Many studies on the dielectric properties of PHBV have been reported so far. Shanming Ke *et al.* showed PHBV exhibits nearly constant dielectric (NCL) loss in high frequency range above 1 kHz [37]. PHBV is believed to undergo secondary crystallization on ageing and the ageing phenomenon of PHBV was studied by dielectric studies [53]. The isothermal crystallization process of PHBV was studied by dielectric spectroscopy and it deduced that mechanical properties of PHBV can be improved by increasing hydroxyvalerate (HV) content [40]. It has been reported that below the threshold of 22 % of HV units in PHBV, phenomenon such as secondary crystallization or physical ageing like effects causing embrittlement can be seen [175]. Also, dielectric relaxations of PHBV with different percentage of HV content was studied by dielectric spectroscopy and difference in their relaxation spectra was discussed [58]. In addition to piezoelectric relaxation, dielectric relaxation around glass transition temperature was reported for PHBV with 25 % HV content [38]. Relaxations α , β and relaxation due to Maxwell-Wagner-Sillars (MWS) polarization were reported for PHBV with 24 % HV content [39], [36]. These dielectric relaxation phenomena were confirmed by another study [31]. Compression molded and extruded PHBV films' properties were studied by dielectric spectroscopy. It was shown that the processing technique has a consequence on the resultant polymer morphology especially the rigid amorphous phase [142]. They reported MWS polarization for higher temperatures above T_g at lower frequency region [142]. Real-time isothermal crystallization of PHBV with different HV contents was studied by dielectric measurements [175]. Several studies showed dielectric spectroscopy were used as an analytical tool to study the polymer-morphology of PHBV [40], [53], [58], [83], [142].

In the following section, dielectric spectra of PHBV over a frequency range of 252 mHz to 1.3 MHz for temperatures ranging from -150 °C to 140 °C for every 10 °C is described. Using the dielectric spectra, dielectric relaxation phenomena are explained.

V.5.2. Results: Dielectric spectroscopy of PHBV

a) Relative permittivity: ϵ_r

Figure 63 shows the relative permittivity spectra of PHBV for the temperatures -150 °C to 50 °C. The relative permittivity stays between 2.9 to 3.9 as the temperature shifts from -150 °C to 50 °C throughout the measured frequency range. A phenomenon of polarization is observed from 30 °C to 50 °C. It is named as *Relaxation 1*.

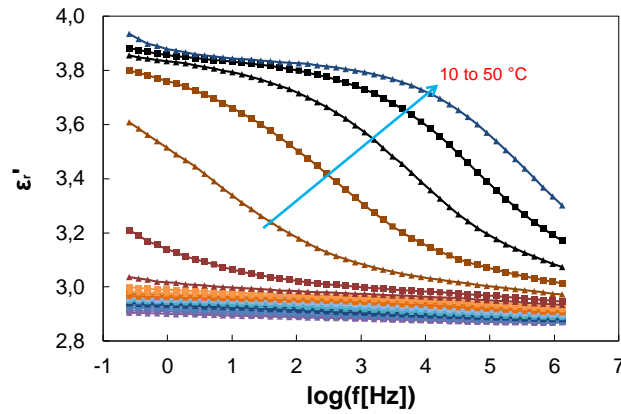


Figure 63. Relative permittivity spectra for temperature scale -150 °C to 50 °C for every 10 °C.

Figure 64 shows the relative permittivity spectra of PHBV for temperatures 60 °C to 140 °C. Beyond 60 °C, another polarization is observed, which leads to a significant increase in relative permittivity as seen for the temperatures 80 °C to 140 °C towards the lower frequency end. It is named as *Relaxation 2*. At 20 °C, relative permittivity of PHBV at 50 Hz and 1 kHz is 3.6 and 3.3 respectively.

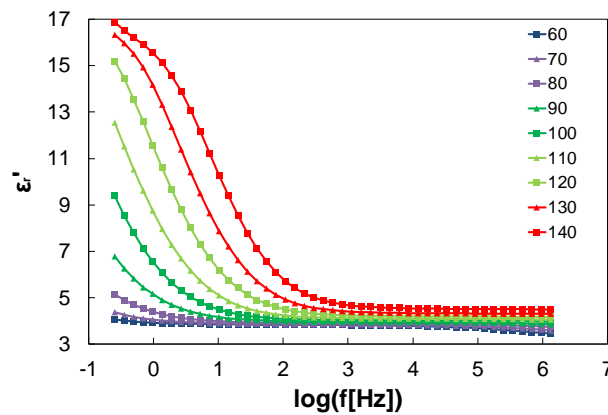


Figure 64. Relative permittivity spectra for temperature scale 60 °C to 140 °C for every 10 °C.

b) Loss factor: ϵ''

Figure 65 and Figure 66 shows the loss factor spectra for the temperatures -150 °C to 50 °C and 60 °C to 140 °C respectively. Figure 65 shows the set of peaks from 10 °C to 50 °C signifying the occurrence of polarization. The peaks shift towards higher frequency with increasing temperature. This observation corresponds to *Relaxation 1* in the relative permittivity spectrum (Figure 63). Figure 66 shows the continuous increase of the losses towards lower frequencies. This observation corresponds to *Relaxation 2*.

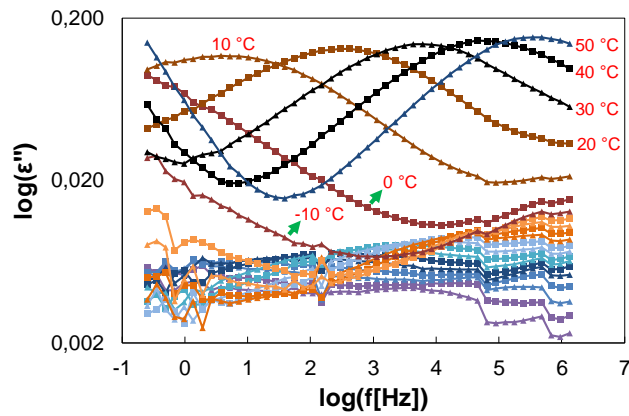


Figure 65. Loss factor spectra for temperature scale -150 °C to 50 °C for every 10 °C.

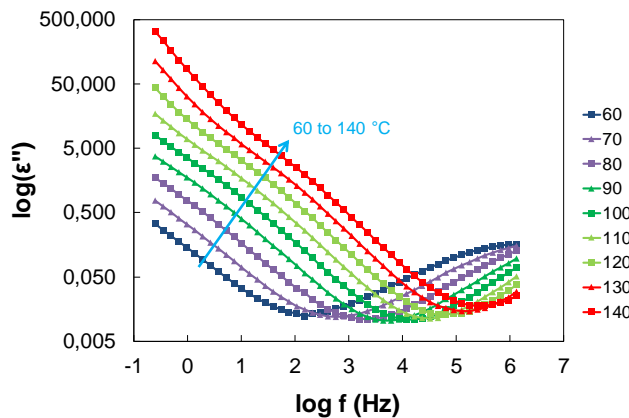


Figure 66. Loss factor spectra for temperature scale 60 °C to 140 °C for every 10 °C.

c) Dissipation factor: $\tan\delta$

Figure 67 shows the dissipation factor spectra for the temperatures -150 °C to 50 °C. A set of polarization peaks corresponding to *Relaxation 1* is observed.

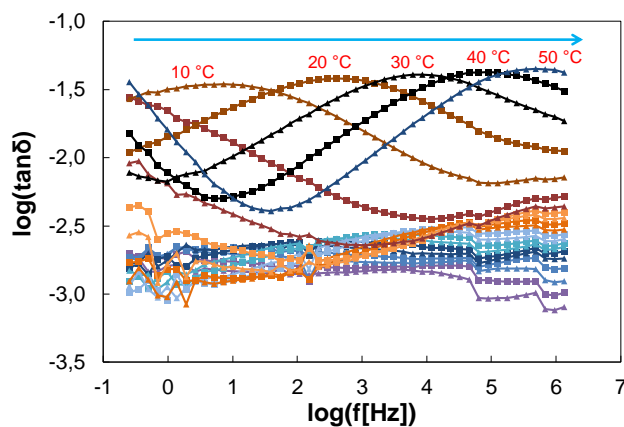


Figure 67. Dissipation factor spectra for temperature scale -150 °C to 50 °C for every 10°C.

For temperatures 60 °C to 140 °C, *Relaxation 2* can also be observed towards lower frequency region in the dissipation factor curves in the Figure 68. This observation is consistent with relative permittivity curves (Figure 64) and loss factor curves (Figure 66). At 20 °C, dissipation factor of PHBV at 50 Hz and 1 kHz is 0.032 and 0.037 respectively.

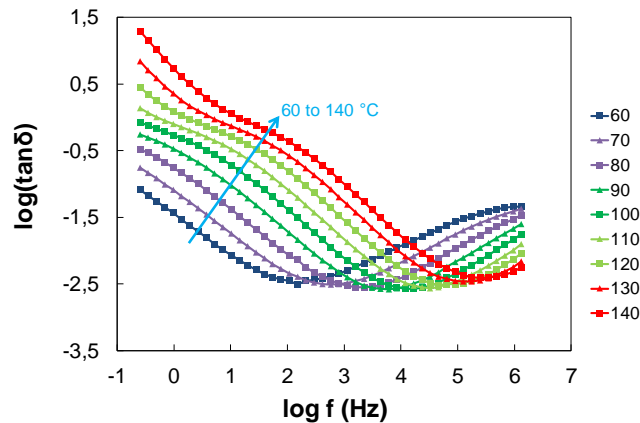


Figure 68. Dissipation factor spectra for temperature scale 60 °C to 140 °C for every 10 °C.

d) Modulus: M''

Figure 69 shows the M'' spectra. Two main set of relaxation peaks are observed. Peaks corresponding to *Relaxation 1* occur for temperatures 10 °C to 60 °C (seen in the inlet of the Figure 69). Peaks corresponding to *Relaxation 2* are seen for temperatures 90 °C to 140 °C. In both cases, relaxation peaks drift towards higher frequency with increase in temperature.

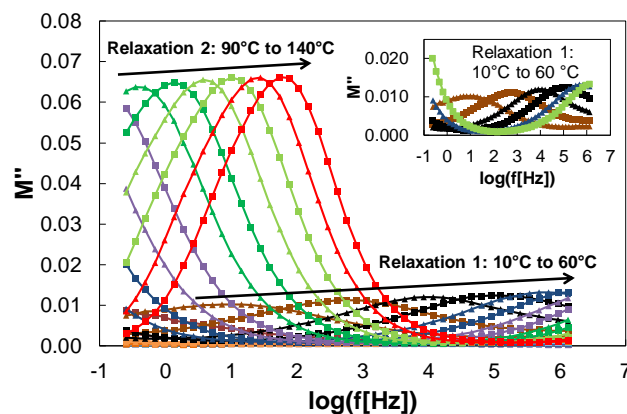


Figure 69. M'' spectra for temperature scale -150 °C to 140 °C for every 10 °C. The inlet in the figure highlights the set of peaks for Relaxation 1 for temperatures 10 °C to 60 °C.

e) AC conductivity: σ'

Figure 70 shows the AC conductivity spectra of PHBV. Three distinct regions are observed and marked as *linear*, *dispersive* and *flat* region respectively. An apparent linear relationship between AC conductivity and the frequency appears for all the measured temperatures in higher frequency region (above 0.1 MHz). While moving towards the lower frequency region, around 1 kHz, deviation from apparent linear behavior is seen for the temperatures 60 °C to 140 °C. This corresponds to the dispersive region. Below 1 kHz, AC conductivity curves for temperatures 60 °C to 140 °C appears to be approaching a steady state. However, this apparent approach towards steady state becomes more prominent with the increasing temperature especially beyond 120 °C.

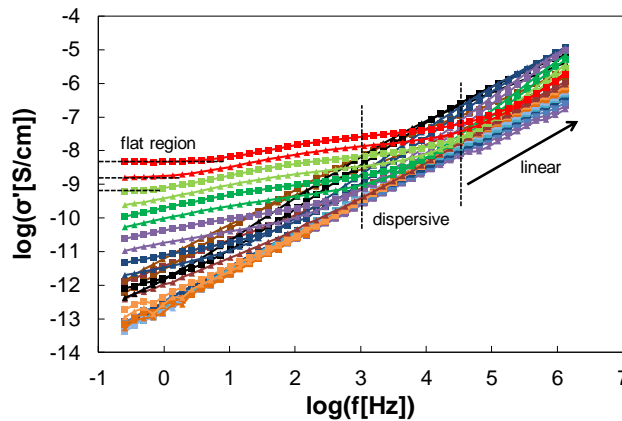


Figure 70. AC conductivity spectra for temperature scale -150 °C to 140 °C every 10 °C.

Furthermore, as seen in the Figure 71, AC conductivity curves are apparently independent of temperature until -20 °C. Above this temperature, the curves show an increase in AC conductivity which continues with rise in temperature as seen in the Figure 70.

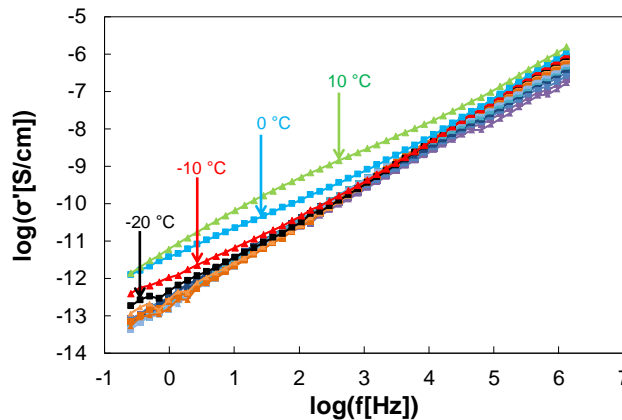


Figure 71. AC conductivity spectra for temperature scale -150 °C to 10 °C for every 10 °C.

V.5.3. Discussion: Dielectric spectroscopy of PHBV

a) Summary of relaxations and their origin

The values obtained from the frequency plots of relative permittivity of PHBV at 20 °C for 50 Hz and 1 kHz is from a dried PHBV film with 8 % HV content. Very few reports on relative permittivity of PHBV under such conditions is reported in the literature. Mansour *et al.* reported the relative permittivity of PHBV with 7 % HV content at 20 °C to be around 4.5 at 1 kHz [58]. Shanming Ke *et al.* reported the relative permittivity values only for the temperatures from 40 °C and above [37]. Daly *et al.* studied the relative permittivity of aged and rejuvenated PHBV at 30 °C [53]. Another study reported the relative permittivity of PHBV with 22 % HV content at 35 °C [40]. In another case, relative permittivity can be deduced from contour maps of temperature-frequency variation but for PHBV with 24 % HV content [39]. Thus, the results were left to be compared with [31] where the relative permittivity values at 20 °C is reported for PHBV with 8 % HV at 50 Hz and 1 kHz. However, in their study, the experiments were performed using the experimental set-up 1 of dielectric spectroscopy. The error caused by the temperature gradients in the electrodes used

haven't been addressed then. In this study, such problems were addressed and the values are mostly free from such errors.

Two different phenomena were observed from the frequency plots of relative permittivity. One is the phenomenon of polarization beginning to occur around 10 °C known as *Relaxation 1*. The other is the significant increase in the relative permittivity towards the lower frequency region for the curves beyond 60 °C. Similar observations were deduced from the loss factor and the dissipation factor spectra.

The *Relaxation 1* is widely recognized as α transition and the corresponding temperature is referred to as T_α . As observed in the case of *DMTA* measurements, α transition occurs due to certain molecular motions occurring in a polymer and this transition is dependent on frequency. The transition signifies the micro-Brownian motions of polymer chains and is related to glass transition phenomenon. The T_α at $f \approx 1$ Hz compared among *DMTA* and *DS* is consistent as seen in the Figure 72.

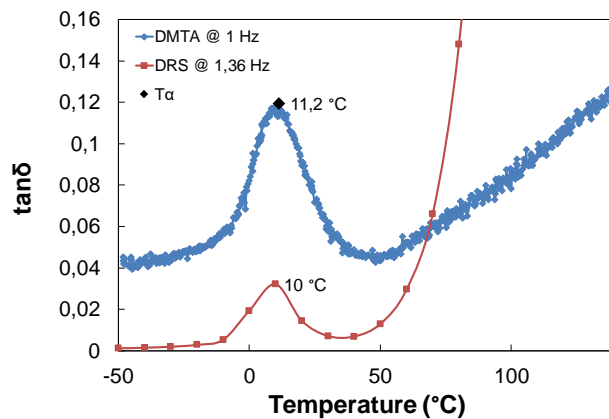


Figure 72. DS and DMTA plots of dissipation factor as a function of temperature.

The strong increase in loss factor in the lower frequency region signifies conduction behavior and corresponds to the law closely to $1/f$ [73]. This also manifests as *DC* conductivity observed at the higher temperatures and lower frequency as seen in the Figure 70. The slope of these curves is closer to -1 as seen in the Figure 73. Based on earlier dielectric spectroscopy reports [37], [142], *Relaxation 2* can be concluded due to Maxwell-Wagner-Sillars (MWS) polarization occurring in the lower frequency region for higher temperatures. This polarization arises due to the accumulation of charges at the interface of two separate phases. The PHBV film is prepared from pure PHBV powder and constitutes no other chemical substances like fillers or additives in them. It can be assumed that it is free of impurities and is a single component system. The semi-crystalline nature of the PHBV creates an interphase between crystalline and amorphous phase within the material. The other interphase appears between the PHBV material and the electrode which could be a second probable reason for interfacial polarization. Based on earlier reports, *MWS* polarization occurring at crystalline-amorphous interface is confirmed [39].

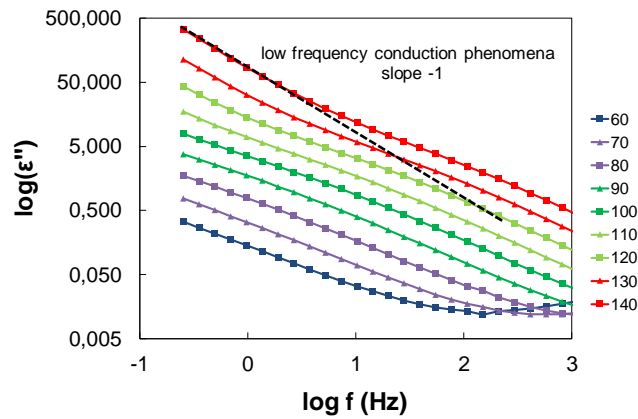


Figure 73. Loss factor spectra for temperatures 60 °C to 140 °C for every 10 °C. The black line represents the slope -1.

Apparently, two relaxation phenomena seem to occur in PHBV from dielectric spectra: α transition and *MWS* polarization. In the Figure 74, in the temperature plot of dissipation factor, a third relaxation phenomenon can be noticed in addition to the existing two.

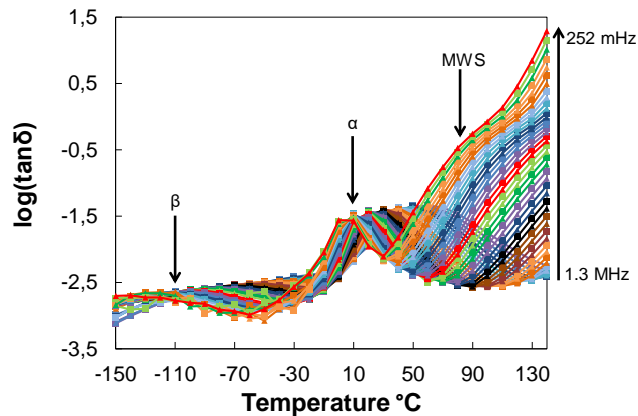


Figure 74. Plot of $\tan\delta$ as a function of temperature for frequency scale 252 mHz to 1.3 MHz.

The lately noticed relaxation shows a peak at around -110 °C and is attributed to β relaxation. Unlike the α relaxation, where the polymer chains swing into motion, here the motions of certain groups in a monomer are responsible for the relaxation. The β relaxation arises due to the cooperative motions of methyl and ester groups inherent in the polymer structure [39]. The temperature plot of modulus (Figure 75) confirms the three relaxational peaks: β , α and *MWS* in the order of increasing temperature.

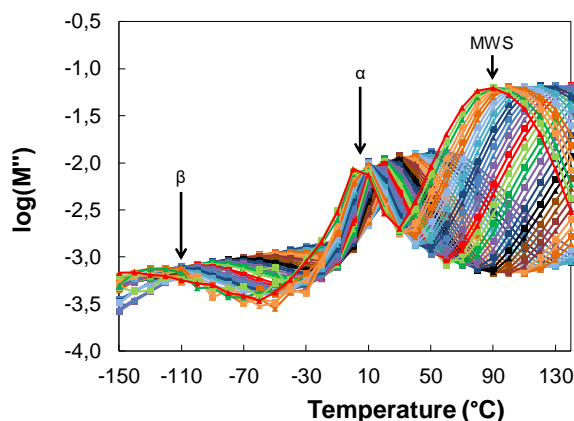


Figure 75. Plot of M'' as a function of temperature for frequency scale 252 mHz to 1.3 MHz.

The flat region in the AC conductivity spectra (Figure 70) signifies the reaching of σ_{ac} towards σ_{dc} . It is at these low frequencies and elevated temperatures that the DC behavior is seen. In the Figure 71, sudden increase between 0 °C to 10 °C is seen in AC conductivity. This temperature zone corresponds to the α transition in PHBV. Hence, this transition results in the increase in AC conductivity which is consistent with a previous report [37].

Thus, three relaxation phenomenon has been reported in this study against four as reported in [31], [36], [39]. The fourth relaxation absent in this study and discussed in others is due to the presence of impurities.

b) Activation energy

Relaxation α abides by Vogel-Fulcher-Tamann (VFT) law and relaxation due to MWS polarization is governed by Arrhenius law since it is based on conduction phenomenon. These fittings are realized in the Figure 76 where a graph of characteristic frequency (f_c) corresponding to these relaxation processes and conductivity at 252 mHz against inverse of temperature is shown.

Apparent conduction is observed from 120 °C to 140 °C (Figure 70) and MWS polarization from 90 °C to 140 °C (Figure 69). They both obey Arrhenius law and the calculated activation energy of charge carriers is 1.4 eV (135 kJ/mol) and 1.3 eV (125 kJ/mol) for conduction phenomenon and MWS polarization respectively. It is attributed to charge carriers of ionic type. It must be noted that the activation energy corresponding to conduction is based on the AC conductivity spectra. These currents are appearing to be but not stable at the lowest frequency for temperatures 120 °C and 130 °C. The f_c derived from M'' and $\tan\delta$ plots for α transition relaxation follows VFT law. The activation energy due to conduction behavior and MWS polarization has not been reported earlier.

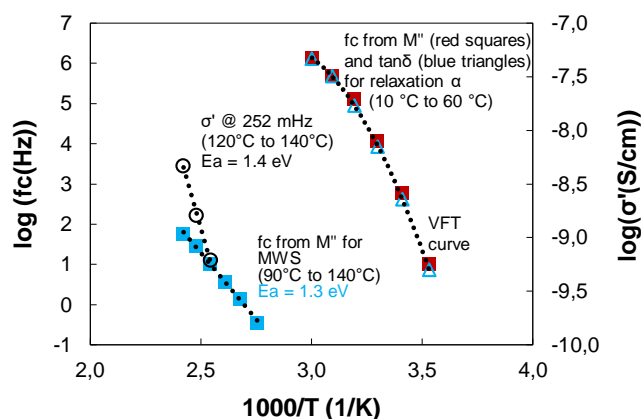


Figure 76. Plot of f_c of α relaxation from M'' and $\tan\delta$ spectra and MWS polarization from M'' spectra as a function of temperature (primary axis). Plot of σ' at 0.25 Hz as a function of temperature (secondary axis).

c) Reproducibility

The objective of this experiment is to verify if two polymer films of PHBV processed and stored under identical conditions gives identical dielectric spectra. The obtained films were named as PHBV1 and PHBV2. Table 15 shows their degree of crystallinity, melting temperature and thickness.

Table 15. Thickness and DSC results of PHBV1 and PHBV2 films.

Film	Mean thickness (mm)	X_c (%)	T_m (°C)
PHBV1	0.611	46	164
PHBV2	0.603	48	162

The variation in the degree of crystallinity among the two PHBV films is 2 % and 2 °C in melting temperature. Figure 77 shows the relative permittivity spectra of PHBV1 and PHBV2 for temperatures -110 °C and -50 °C.

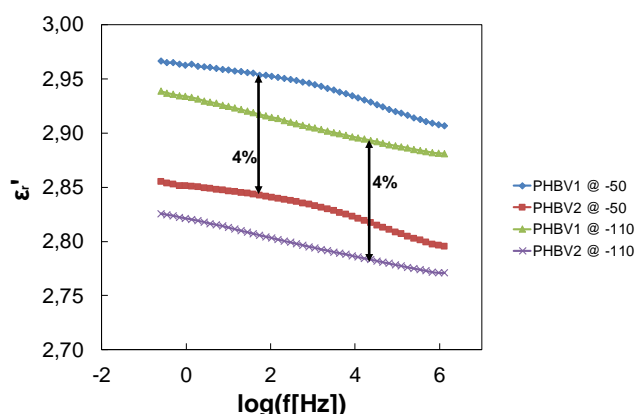


Figure 77. ϵ_r spectra of PHBV1 and PHBV2 at temperatures -110 °C and -50 °C.

Figure 78 shows the relative permittivity spectra of PHBV1 and PHBV2 for temperatures 20 °C and 90 °C.

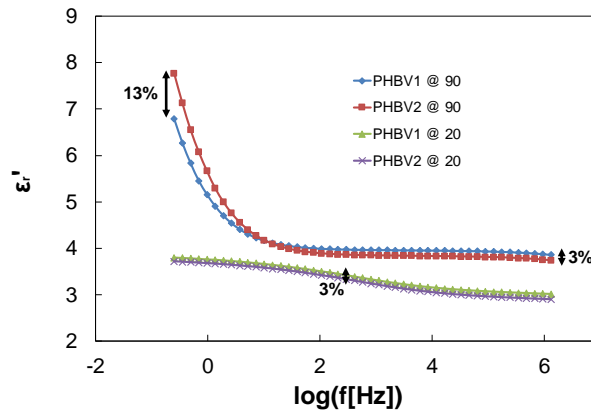


Figure 78. ϵ_r spectra of PHBV1 and PHBV2 at temperatures 20 °C and 90 °C.

The variation in the relative permittivity among PHBV1 and PHBV2 at -110 °C, -50 °C and 20 °C is up to 4 %. At 90 °C, above 10 Hz, the variation remains within 3 %. It rises to 13 % at the lowest frequency. The variation in the dissipation factor among PHBV1 and PHBV2 at -50 °C and -110 °C is \approx 1%. Figure 79 shows the dissipation factor spectra of PHBV1 and PHBV2 at 20 °C and 90 °C. The variation at 20 °C remains within 5 % to 7 % depending on the frequency range. At 90 °C, the variation increases from 1 % to 11 % while moving from high frequency towards lower frequencies.

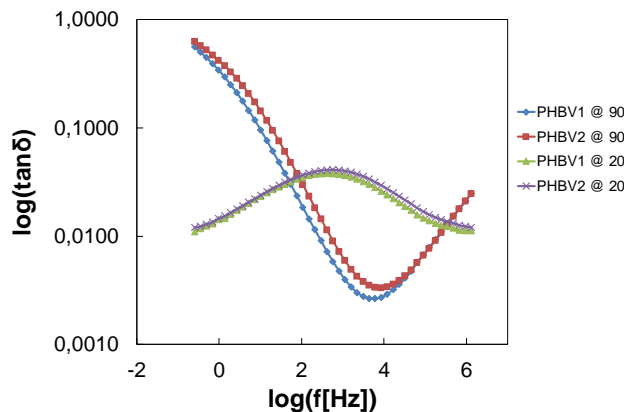


Figure 79. Dissipation factor spectra of PHBV1 and PHBV2 at 20 °C and 90 °C.

The degree of crystallinity and the melting temperature of the two PHBV appears to be identical. The difference in relative permittivity may be explained by geometrical (thickness of a film) and measurement errors. The variation in dissipation factor may be due to the difference in a polymer response towards the applied electric field.

d) Effect of the temperature cycle on polymer morphology during dielectric spectroscopy measurement

Figure 80 shows the dissipation factor spectra of PHBV at 20 °C on four different instances during the dielectric spectroscopy measurement. The *cycle 1* is the first dielectric spectroscopy measurement which is performed at 20 °C. The polymer was then heated to 60 °C and measured by dielectric spectroscopy. It was then cooled down to 20 °C and measured

which is represented as *cycle 2*. The sample was then cooled to -160 °C and dielectric spectroscopy measurements were carried out for -160 °C to 140 °C in steps of 10 °C. The *cycle 3* is referred to the spectroscopy measurement performed at 20 °C during this measurement sequence. After the dielectric spectroscopy measurement at 140 °C, the sample was cooled down to 20 °C and measured again. This measurement at 20 °C is termed as *cycle 4*. Figure 80 shows the dissipation factor spectra at 20 °C during all the four cycles.

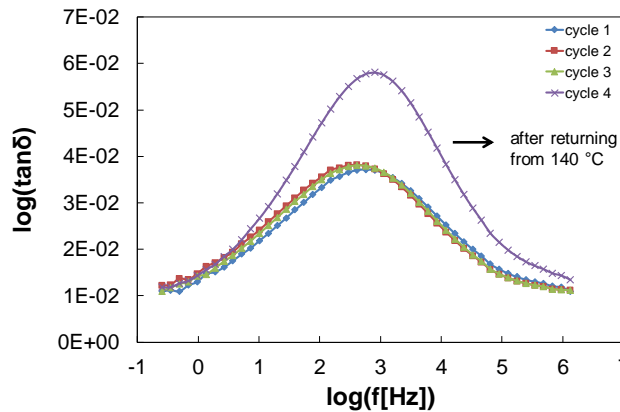


Figure 80. Dissipation factor spectra of PHBV at 20 °C during different cycle of measurement.

The change brought in the polymer morphology after being heated up to 140 °C is manifested as a difference in physical quantities. The amplitude of dissipation factor peak increased significantly after the polymer has been heated until 140 °C. The thermal history of the polymer is thus replaced by a new one after dielectric spectroscopy measurement at temperature close to the melting point of the polymer.

V.6. Dielectric spectroscopy: PCL

V.6.1. Introduction: Dielectric spectroscopy of PCL

Figure 3 shows the structure of PCL polymer. It is an aliphatic, synthetic, biodegradable polyester. It is a nontoxic polymer, semi-crystalline in nature with a glass transition temperature around -60 °C and melting temperature around 60 °C [176], [177]. This polymer is known to be an easy to blend component and therefore, many research work has been focused in this perspective [177].

It is a type A-B-polymer and therefore polarization takes place both perpendicular and parallel to the main chain [176]. Limited studies on the electrical properties of PCL have been reported so far when compared to its thermal or mechanical properties. Thermally stimulated depolarization current studied by Vanderschueren *et al.* showed local mode β relaxation, α relaxation and high temperature MWS polarization due to ionic motions [178]. M. Grimau *et al.* analyzed dielectric spectroscopy by ϵ^* formalism observing local modes γ , β and segmental mode relaxation α [176]. A. Bello *et al.* analyzed dielectric spectra of PCL using M^* formalism highlighting the high temperature-low frequency MWS polarization in addition to local modes γ , β and segmental mode α relaxation [67]. Nemoto *et al.* studied dielectric

spectroscopy of PCL over frequency range of 10 mHz to 10 kHz for temperatures 20 °C to 50 °C [30]. Dielectric spectroscopy of PCL was also used as an analytical tool to study polymer-morphology [70], [84], [85]. Hirai *et al.* [8], [29] reported permittivity spectrum of PCL at room temperature and time dependent conductivity in the order of 10^{-11} S/m with low AC breakdown strength. Nemoto *et al.* also studied time dependent conductivity and AC breakdown strength of PCL [30].

In the following section, dielectric spectra of PCL over a frequency range of 12 mHz to 2.6 MHz for temperatures ranging from -160 °C to 40 °C for every 10 °C is described.

V.6.2. Results: Dielectric spectroscopy of PCL

a) Loss factor: ϵ''

Figure 81 shows the dielectric loss factor spectra for temperatures -160 °C to -30 °C. These loss factor curves show the occurrence of polarization when the temperature raises from -130 °C to -30 °C. The peaks shift towards higher frequency with increasing temperature. This set of peaks is named as *Relaxation 1* occurring frequency above 10 Hz.

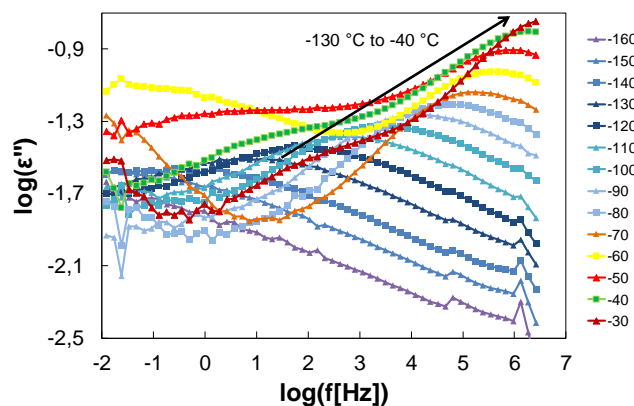


Figure 81. Loss factor spectra for temperature scale -160 °C to -30 °C for every 10 °C.

Figure 82 shows the loss factor spectra for temperatures -20 °C to 40 °C. These higher temperature curves show continuous increase of the loss factor towards low frequencies. This indicates a relaxation phenomenon and is named as *Relaxation 2*.

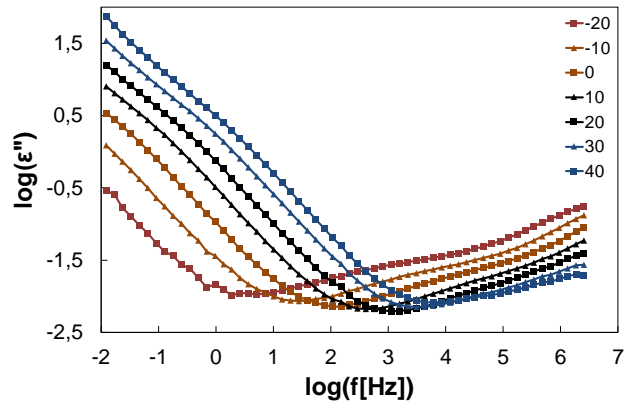


Figure 82. Loss factor spectra for temperature scale -20 °C to 40 °C for every 10 °C.

b) Dissipation factor: $\tan\delta$

Figure 83 shows the dissipation factor spectra representing *Relaxation 1*.

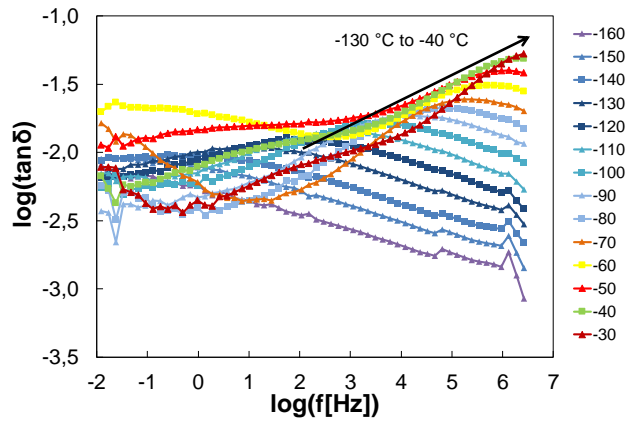


Figure 83. Dissipation factor spectra for temperature scale -130 °C to -30 °C for every 10 °C.

For temperatures -20 °C to 40 °C, *Relaxation 2* can be observed towards the lower frequency region in the dissipation factor spectra as seen in the Figure 84.

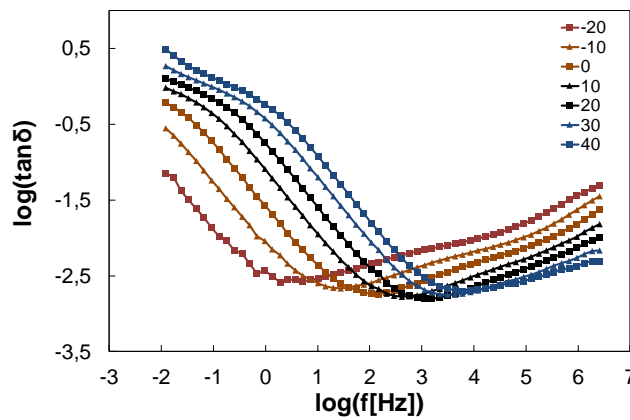


Figure 84. Dissipation factor spectra for temperature scale -20 °C to 40 °C for every 10 °C.

Thus, the observations made from the dielectric loss tangent spectra is in coherence with loss factor spectra for similar frequency and temperature ranges. At 20 °C, dissipation factor of PCL at 1 kHz and 50 Hz is 0.002 and 0.006 respectively.

c) Modulus: M''

The M'' spectra are shown in the Figure 85 and the Figure 86. Two main set of peaks are observed: *Relaxation 1* and *Relaxation 2*.

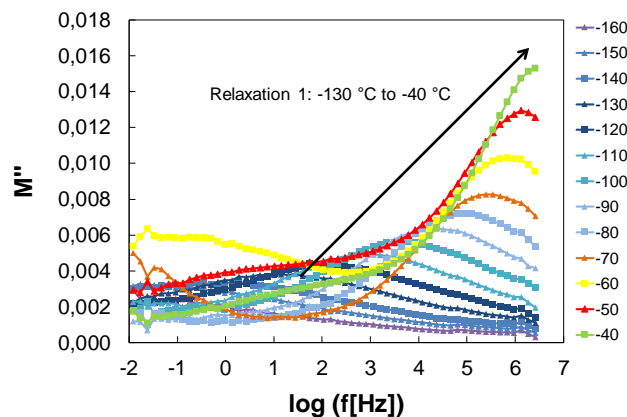


Figure 85. M'' spectra for temperature scale -160 °C to -40 °C for every 10 °C.

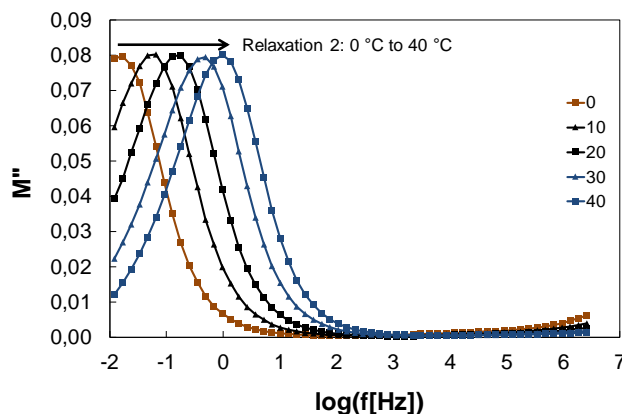


Figure 86. M'' spectra for temperature scale 0 °C to 40 °C for every 10 °C.

V.6.3. Discussion: Dielectric spectroscopy of PCL

a) Summary of relaxations and their origin

At 20 °C, relative permittivity of PCL at 50 Hz and 1 kHz is measured to be 3.9. This is lower by about 20 % reported by Y. Ohki *et al.* [8], [29]. They lacked details on the degree of crystallinity of PCL, conditions of drying and the temperature of measurement. Nemoto *et al.* reported the relative permittivity of PCL at 20 °C to be around 3 [30]. They have reported relative permittivity of PCL until 50 °C. On the contrary, in this study, the relative permittivity has been studied for a wide range of temperatures and frequency not reported earlier.

Two different phenomena were observed from the frequency spectra. The high frequency relaxation (Relaxation 1) corresponds to the β relaxation. In general, in a spectra α relaxation occurs towards the lower frequency end and the β relaxation towards the higher frequency as seen in the dielectric spectra of PCL. This is because the time needed for the polarization corresponding to α is higher than β relaxation which involves only mobility of certain groups in a polymer. The significant increase in the loss factor spectra towards lower frequency end is classical of conduction behavior and is attributed to *MWS* polarization. Thus, *Relaxation 2* corresponds to relaxation due to *MWS* polarization. Thus, from the frequency plots of dielectric spectra, two relaxation phenomena are confirmed. However, in the temperature plot of dissipation factor (Figure 87), four relaxation peaks are seen against the two noticed so far.

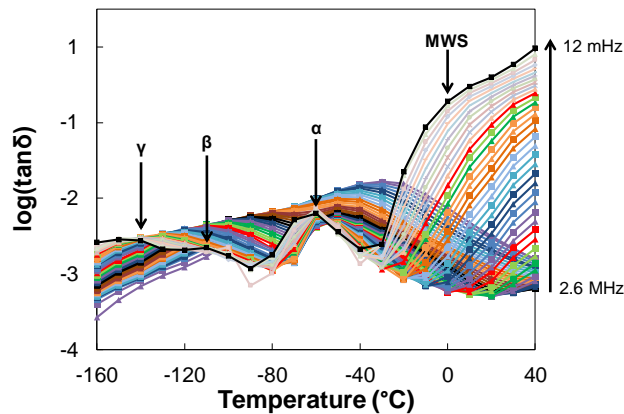


Figure 87. Plot of dissipation factor as a function of temperature from -160 °C to 40 °C for frequency scale 12 mHz to 2.6 MHz.

The relaxation due to *MWS* polarization with peaks centered at 0 °C is attributed to ionic motions between crystalline-amorphous interfaces [178],[67]. Peaks at -60 °C represents α transition due to micro-Brownian motions. This agrees with the $\tan\delta$ peak of *DMTA* measurement as shown in the Figure 88.

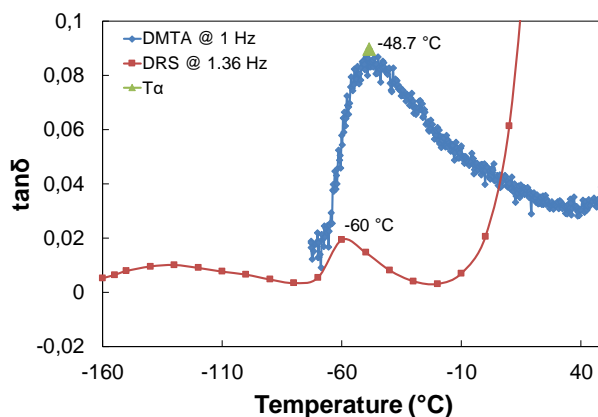


Figure 88. DS and DMTA plots of $\tan\delta$ as a function of temperature.

From the temperature plot of dissipation factor, the two lower temperature peaks are understood to be due to local mode relaxations and are denoted as β and γ with peaks at -110 °C and -150 °C respectively [176]. To better observe all the relaxation phenomena, imaginary

part (M'') of modulus as a function of temperature is shown in the Figure 89. Four relaxation peaks for a single frequency (0.012 Hz) curve can be observed.

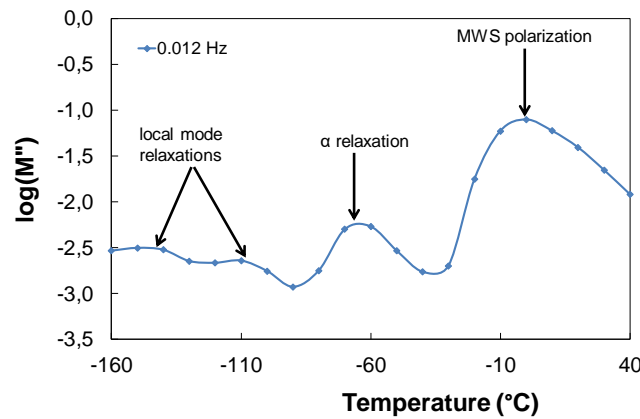


Figure 89. Plot of M'' as a function of temperature for frequency 0.012 Hz.

Figure 90 shows the temperature plot of modulus M'' for 0.97 Hz and Figure 91 shows the temperature plot of modulus for frequencies ≈ 1 kHz, 12 kHz and 126 kHz respectively.

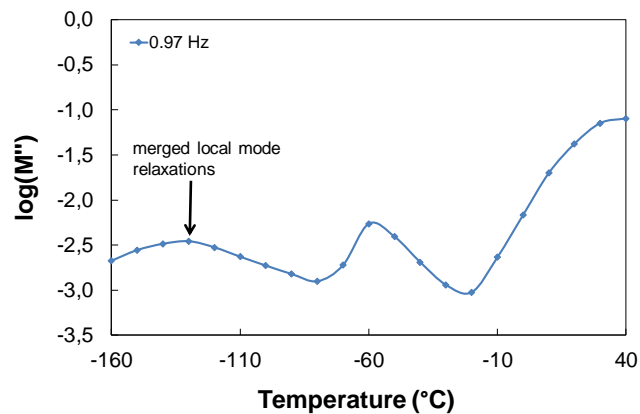


Figure 90. Plot of M'' as a function of temperature for frequency 0.97 Hz.

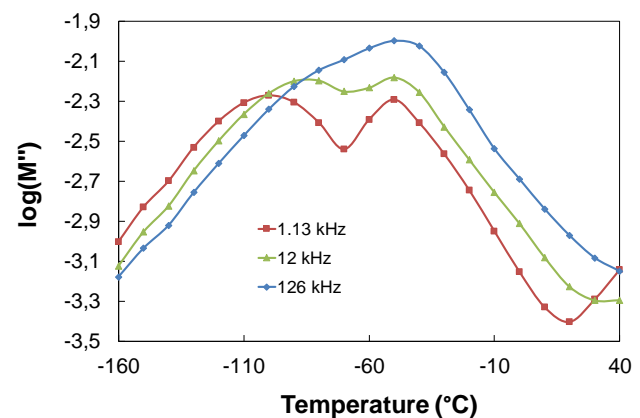


Figure 91. Plot of M'' against temperature for frequencies ≈ 1 kHz, 12 kHz and 126 kHz.

The merging of local mode relaxation peaks takes place around 1 Hz as seen in the Figure 90. The merged local mode of β and γ is denoted as γ - β mode. As the frequency further increases, merging of local mode and α transition takes place as shown in the Figure 91. It must be

noted that this merging of local and α relaxation mode takes place at temperatures higher than its glass transition temperature as reported earlier [176]. Johari and Goldstein reported merging of β mode and α mode [179]. It was unclear for them to reason the influence of molecular mobility on merging behavior. Another study reported similar observation on merging of different relaxation modes with increasing temperature [180]. Grimau *et al.* reported merging of β and α mode in PCL. They also stated that the merged α - β mode influences the intensity of the γ mode and eventually merging of the merged α - β mode with γ mode occurs [176]. In this study, merging of the local modes (γ , β) prior to the merging of α and merged γ - β modes is found. In both the cases, there exists an eventual merging of different relaxation phenomena with increasing frequencies. Based on the experimental observations, Grimau *et al.* justified their remarks by suggesting possible merging of α mode with each of the local modes. The reason for such a merger in any of the cases considering various relaxation phenomena, conduction phenomena and MWS polarization could not be justified straightforward.

b) Activation energy

Figure 92 shows the graph of characteristic frequency (f_c) for relaxation processes and conductivity at 12 mHz against inverse of the temperature. The conduction phenomena are observed for temperatures $-20\text{ }^\circ\text{C}$ to $40\text{ }^\circ\text{C}$ and MWS relaxation from $0\text{ }^\circ\text{C}$ to $40\text{ }^\circ\text{C}$. They both obey Arrhenius law as MWS polarization is said to be governed by Arrhenius law since it's based on conductivity. The calculated activation energy of charge carriers is 0.61 eV (59 kJ/mol) and 0.75 eV (72 kJ/mol) for conduction phenomenon and MWS polarization respectively. The level of the activation energy in both conductivity and MWS indicates carriers of ionic charge as corroborated in [30], [67]. Nemoto *et al.* reported the activation energy for conductivity to be 0.51 eV [30]. In another study by Bello *et al.*, the activation energy of conductivity in PCL is found to be 0.63 eV [67]. This value is much closer to the value reported in this study of 0.61 eV . They also reported activation energy corresponding to MWS polarization to be 0.71 eV against 0.75 eV found in this study.

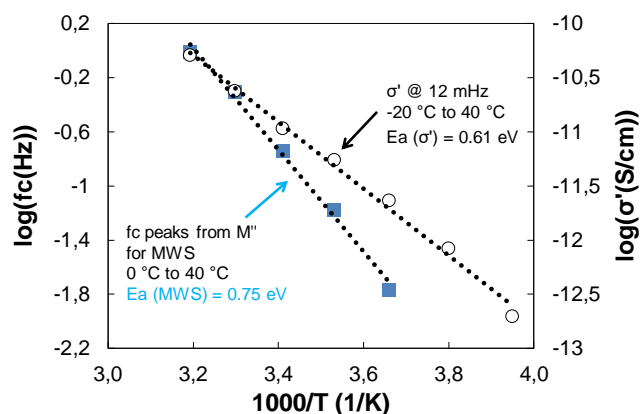


Figure 92. Plot of f_c for MWS polarization from M'' spectra as a function of temperature (primary axis). Plot of conductivity at 12 mHz as a function of temperature (secondary axis).

In the Figure 93, characteristic frequency (f_c) of β relaxation against inverse of the measured temperature is given and the corresponding activation energy is 0.41 eV . Bella *et al.* observed

β relaxation for temperatures around $-130\text{ }^{\circ}\text{C}$ to $-30\text{ }^{\circ}\text{C}$ and their activation energy was found to be 0.6 eV [67].

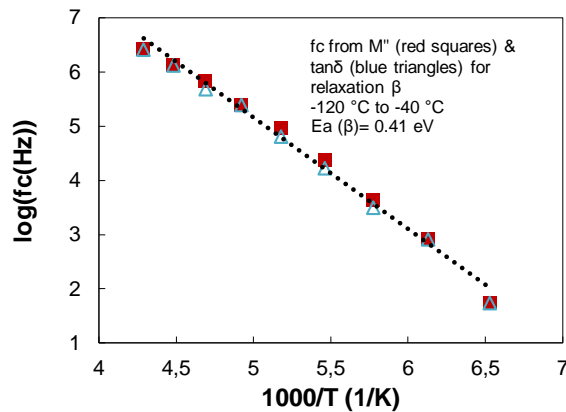


Figure 93. Plot of f_c for β relaxation from M'' and $\tan\delta$ spectra against inverse of the temperature.

c) Reproducibility with a same PCL film

To study the reproducibility in dielectric spectra with a same film, PCL was measured twice for the entire temperature and frequency range of $-140\text{ }^{\circ}\text{C}$ to $20\text{ }^{\circ}\text{C}$ and 12 mHz to 2.6 MHz respectively. The first sequence of spectroscopy measurement was performed for temperature scale $-140\text{ }^{\circ}\text{C}$ to $20\text{ }^{\circ}\text{C}$ for every $10\text{ }^{\circ}\text{C}$. This sequence is named as *Round 1*. The same sequence was repeated for the second time and is named as *Round 2*. Figure 94 and Figure 95 shows the relative permittivity and the dissipation factor spectra at $-140\text{ }^{\circ}\text{C}$, $-50\text{ }^{\circ}\text{C}$ and $20\text{ }^{\circ}\text{C}$ of both the rounds of the dielectric spectroscopy measurement of PCL.

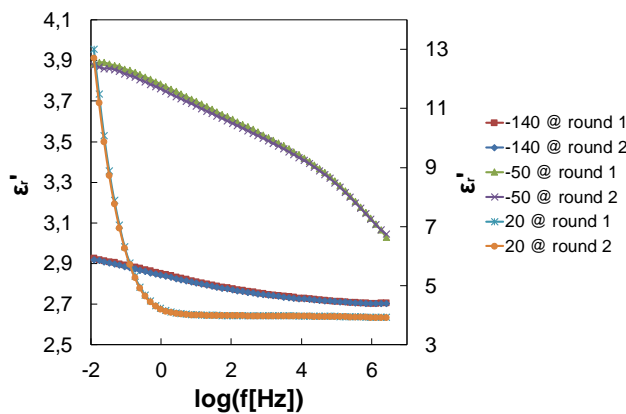


Figure 94. Relative permittivity spectra of PCL at temperatures $-140\text{ }^{\circ}\text{C}$, $-50\text{ }^{\circ}\text{C}$ and $20\text{ }^{\circ}\text{C}$ for round 1 and round 2. The curves at $-140\text{ }^{\circ}\text{C}$ and $-50\text{ }^{\circ}\text{C}$ are represented by primary axis. The curves at $20\text{ }^{\circ}\text{C}$ is represented by secondary axis.

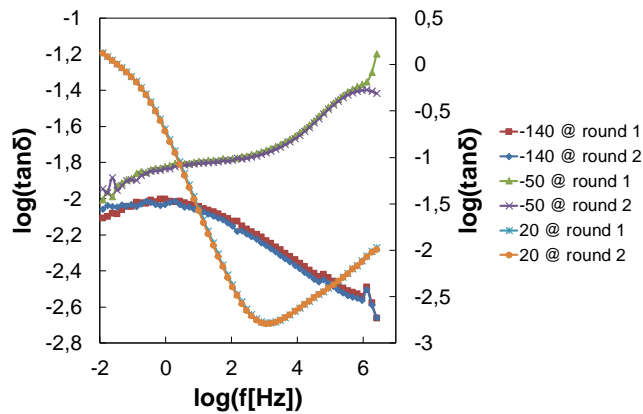


Figure 95. Dissipation factor spectra of PCL at temperatures -140 °C, -50 °C and 20 °C for round 1 and round 2. The curves at -140 °C and -50 °C are represented by primary axis. The curves at 20 °C is represented by secondary axis.

The relative permittivity at the three temperatures shows negligible difference between *Round 1* and *Round 2* with a difference less than 1 %. At 20 °C, towards the lower frequency region, difference reaches up to 2 %. Dissipation factor at the three temperatures for both the rounds show a variation of up to 6 %. Defects occur at higher frequencies (above 1 MHz) and lower frequencies (below 0.1 Hz). Otherwise, a satisfactory level of reproducibility in the dielectric spectra can be obtained with a same PCL film.

d) Effect of the temperature cycle on polymer morphology during dielectric spectroscopy measurement

Figure 96 shows the dissipation factor spectra of PCL at 20 °C on three different instances during the dielectric spectroscopy measurement. The *start point* indicates the first dielectric spectroscopy measurement at 20 °C. The polymer film was then cooled to -160 °C and spectroscopy measurements were performed for -160 °C to 40 °C in steps of 10 °C. During this measurement sequence, spectroscopy measurement performed at 20 °C is referred to as *during run*. After the spectroscopy measurement at 40 °C, the sample was cooled to 20 °C and measured. This dielectric spectroscopy measurement at 20 °C is named as *after 40 °C*.

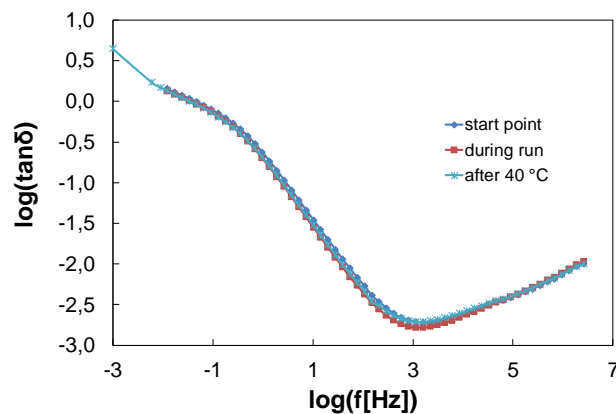


Figure 96. Dissipation spectra of PCL at 20 °C during different sequences of measurement.

The spectra at all the three different instances of dielectric spectroscopy measurement at 20 °C doesn't reflect changes occurring in the polymer morphology. This suggests that the polymer morphology remains unaltered after the dielectric spectroscopy measurements.

V.7. Dielectric spectroscopy: PLA

V.7.1. Introduction: Dielectric spectroscopy of PLA

Figure 3 shows the structure of a PLA polymer. It is a biodegradable, bio-based polyester most commonly obtained from corn starch. The polymer is obtained through condensation polymerization. It is a semi-crystalline polymer like PHBV and PCL. Its glass transition temperature is around 65 °C and the melting temperature around 160 °C. The dipole moment in PLA is both perpendicular and parallel to the polymer backbone [74]. This polymer can undergo degradation due to the presence of hydrolysable hydrophilic groups in their backbone [78]. This polymer is sensitive to moisture which is why it must be dried prior to processing.

PLA is one of the most studied bio-based and biodegradable polymer for its electrical and dielectric properties which includes dielectric spectroscopy, *DC* conductivity and *DC* breakdown strength. It is the biodegradable polymer known to show interesting electrical properties in terms of level of apparent conductivity and *DC* breakdown strength [50]. Y. Ohki *et al.* have reported numerous communications on dielectric and electrical properties of PLA [62], [61], [1], [29]. Dielectric spectroscopy was used as a tool to study the crystallization process in PLA [68], [47] and to study the degradability in PLA [78]. The effect of crystallinity on the molecular motions of PLA is reported [46]. The effect of physical ageing on the properties of PLA is also discussed earlier [45]. In the following section, dielectric spectra of PLA over a frequency range of 10 mHz to 2.6 MHz for temperature scale ranging from -160 °C to 120 °C for every 10 °C is discussed and the dielectric relaxation phenomena are highlighted.

V.7.2. Results: Dielectric spectroscopy of PLA

a) Loss factor: ϵ''

Figure 97 shows the loss factor spectra for the temperatures -110 °C to 50 °C. A set of relaxation peaks is observed and is named as *Relaxation 1*.

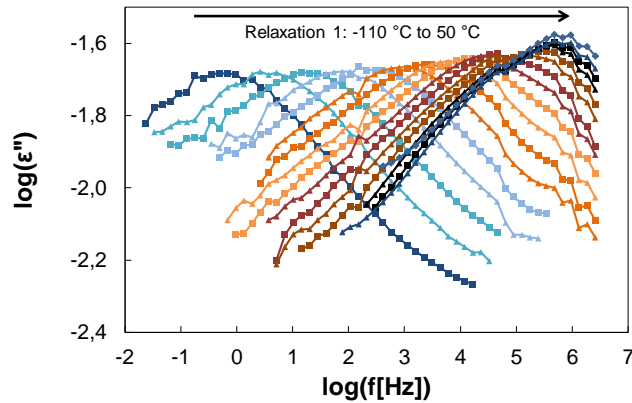


Figure 97. ϵ'' spectra of PLA for temperature scale -110 °C to 50 °C for every 10 °C.

Two relaxation phenomena can be deduced from the loss factor spectra in the Figure 98. A set of peaks of relaxation occurs for temperatures 60 °C to 90 °C and is referred to as *Relaxation 2*. The peaks shift towards higher frequency region with the increase in temperature. The other is the significant increase in imaginary part of permittivity towards the lower frequency end for the temperatures 80 °C to 120 °C. This relaxation is termed as *Relaxation 3*. Dissipation factor spectra shows all the three relaxations (figures not shown).

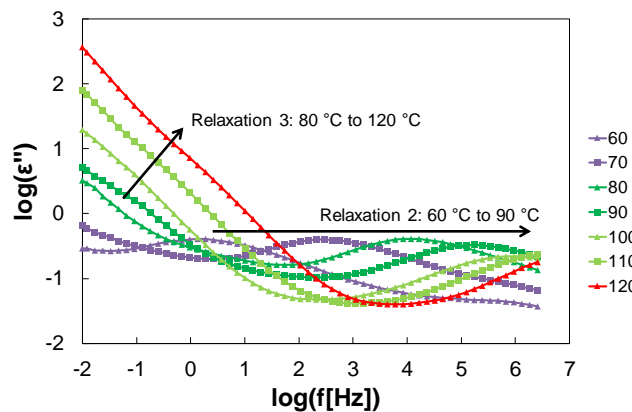


Figure 98. ϵ'' spectra for temperatures 60 °C to 120 °C for every 10 °C.

b) Modulus: M''

Figure 99 and Figure 100 shows the modulus (M'') spectra. Three set of peaks are observed. Peaks for *Relaxation 1* occur for temperatures -110 °C to 50°C. Peaks for *Relaxation 2* occur for temperatures 60 °C to 100 °C. Peaks corresponding to *Relaxation 3* are observed for temperatures 90 °C to 120 °C. The observations deduced from M'' spectra are in coherence with dielectric loss factor and dissipation factor spectra.

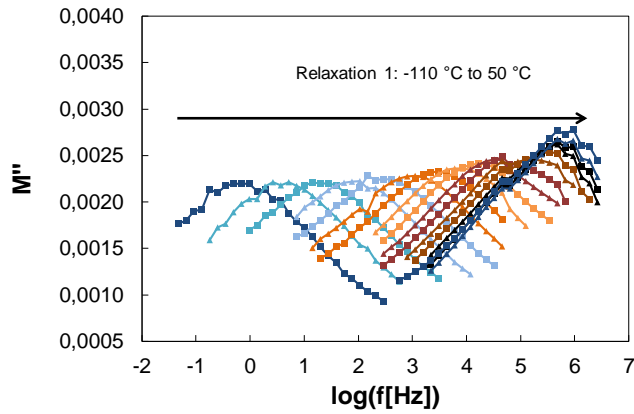


Figure 99. M'' spectra for temperature scale -110 °C to 50 °C for every 10 °C.

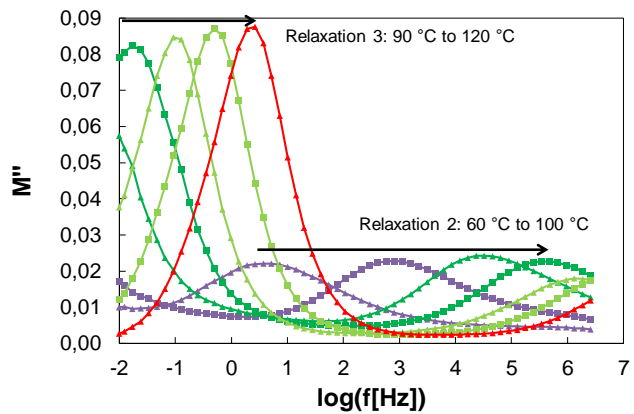


Figure 100. M'' spectra for temperature scale 60 °C to 120 °C for every 10 °C.

V.7.3. Discussion: Dielectric spectroscopy of PLA

a) Summary of relaxations and their origin

At 20 °C, relative permittivity of PLA at 50 Hz and 1 kHz is 3.2. There are many reports on the relative permittivity of PLA in the literature which agree with this study. Table 16 shows few of the reports on relative permittivity.

Table 16. Relative permittivity of PLA extracted from the literature.

Reference	Relative permittivity @ 1 kHz	Relative permittivity @ 50 Hz	Measurement conditions
[29]	2.7	2.7	RT
[13]	2.46 to 2.59	-	27 °C
[7]	2.7	-	RT
[1]	2.7	2.7	RT
[60]	-	3.8	RT
From this study	3.2	3.2	20 °C

Figure 101 shows the relative permittivity spectrum of PLA for temperatures -160 °C to 50 °C. It shows a sudden jump in its value around 50 °C which continues to increase further with temperature. This temperature is close to the glass transition temperature of PLA and this influence can be attributed to such a transition.

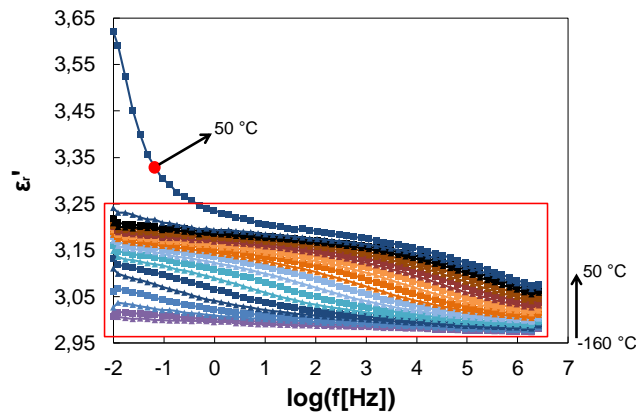


Figure 101. ϵ_r' spectra for temperatures $-160\text{ }^{\circ}\text{C}$ to $50\text{ }^{\circ}\text{C}$. The red colored box represents the relative permittivity curves for temperatures $-160\text{ }^{\circ}\text{C}$ to $40\text{ }^{\circ}\text{C}$.

Figure 98 shows a set of peaks for temperatures $60\text{ }^{\circ}\text{C}$ to $90\text{ }^{\circ}\text{C}$. Based on the previous reports and the measured glass transition temperature of PLA, these set of peaks corresponds to α transition and is attributed to glass transition [181]. Thus, *Relaxation 2* in dielectric loss factor, dissipation factor (figure not shown) and modulus spectra represents α transition.

Relaxation 3 manifests towards lower frequency as a significant increase in both real (figure not shown) and imaginary parts of permittivity in PLA. This is due *MWS* polarization which has been widely reported. This is explained by Y. Ohki *et al.* to be due to the motion of charge carriers which leads to a conduction behavior [73]. Another study also states this huge increase occurring at lower frequencies for temperatures above the glass transition temperature of PLA is due to conduction behavior [181]. Therefore, *Relaxation 3* in the dielectric spectra corresponds to *MWS* polarization.

The *Relaxation 1* occurring for temperature curves from $-110\text{ }^{\circ}\text{C}$ to $50\text{ }^{\circ}\text{C}$ in dielectric loss factor (Figure 97), dissipation factor (figure not shown) and moduli spectra (Figure 99) is attributed to relaxation β due to the twisting motions of the main chain [181], [46]. In the Figure 102, the temperature plot of modulus (M'') shows relaxation α and local mode relaxation β with peaks centered at around $70\text{ }^{\circ}\text{C}$ and $-70\text{ }^{\circ}\text{C}$ respectively.

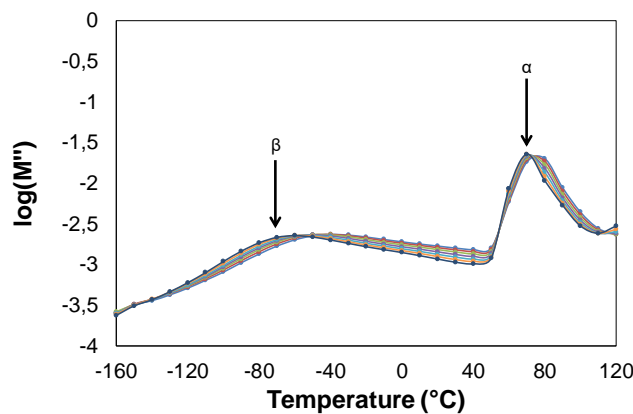


Figure 102. Plot of M'' as a function of temperature for frequencies 810 Hz to 6.1 kHz.

b) Activation energy

The polymer PLA exhibits three relaxation behaviors in addition to conduction phenomena. In Figure 103, both conduction and *MWS* polarization phenomena obeys Arrhenius law. Apparent conduction behavior can be remarked in the frequency plot of AC conductivity (figure not shown) curves for temperatures 90 °C to 120 °C. Similarly, from the frequency plots of modulus, the *MWS* polarization occurs for the same temperature range. The activation energy of charge carriers is 1.76 eV (169 kJ/mol) and 2.1 eV (199 kJ/mol) for conduction phenomenon and *MWS* polarization respectively. The level of the activation energy indicates carriers of ionic charge.

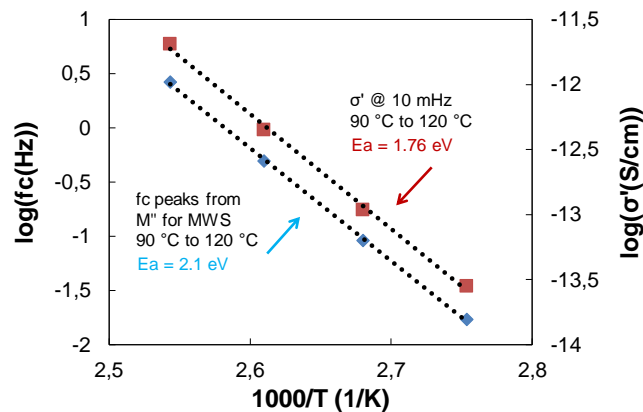


Figure 103. Plot of f_c for *MWS* polarization from M'' spectra as a function of temperature (primary axis). Plot of conductivity at 10 mHz as a function of temperature (secondary axis).

In the Figure 104, characteristic frequency (f_c) of β relaxation against inverse of the measured temperature is shown. A linear plot is obtained for low temperature local mode β relaxation occurring for temperatures -110 °C to 50 °C. This is indicative of an Arrhenius behavior. The activation energy for β relaxation is 0.41 eV (39.5 kJ/mol) which is in agreement with literature [182].

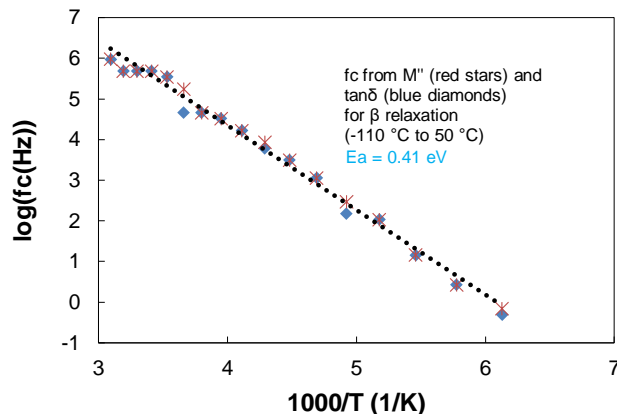


Figure 104. Plot of f_c for β relaxation from M'' and $\tan\delta$ as a function of temperature.

Figure 105 shows the plot of characteristic frequency (f_c) from modulus and dissipation factor spectra for α transition against inverse of temperature. The curve is of non-linear form obeying VFT law confirming the occurrence of glass transition in PLA.

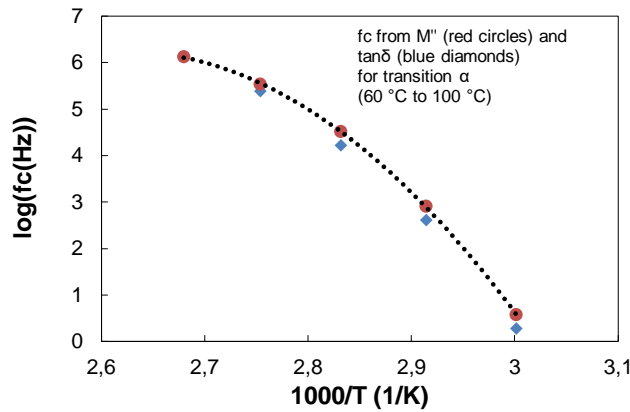


Figure 105. Plot of f_c for α transition from M'' and $\tan\delta$ spectra as a function of temperature.

c) Effect of the temperature cycle on polymer morphology during dielectric spectroscopy measurement

Figure 106 shows the dissipation factor spectra of PLA at 20 °C on three different instances during the dielectric spectroscopy measurement.

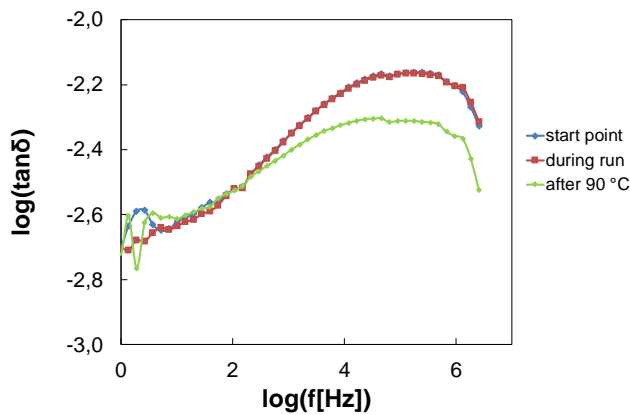


Figure 106. Dissipation factor spectra of PLA at 20 °C during different sequence of measurement.

The *start point* is the first dielectric spectroscopy measurement performed at 20 °C. The polymer was then cooled to -160 °C and spectroscopy measurements were performed for -160 °C to 90 °C in steps of 10 °C. During this measurement sequence, spectroscopy measurement performed at 20 °C is named as *during run*. After the spectroscopy measurement at the highest temperature i.e., 90 °C, the sample was cooled to 20 °C and measured. This last dielectric spectroscopy measurement at 20 °C is termed as *after 90 °C*. A considerable decrease in dissipation factor confirms a change in PLA's morphology.

V.8. Dielectric spectroscopy: PLA-MFC

Dielectric spectroscopy of a post-treated PLA-MFC nanocomposite (PLA-MFC-pt) was performed over a frequency range of 0.35 Hz to 1.3 MHz for temperature scale ranging from -160 °C to 100 °C.

V.8.1. Result: Dielectric spectroscopy of PLA-MFC

a) Relative permittivity: ϵ_r'

Figure 107 shows the relative permittivity spectra for temperatures -160 °C to 0 °C. Towards the lowest extreme frequency of 0.35 Hz, the relative permittivity varies from 3 (at -160 °C) to 3.5 (at 0 °C). At the highest frequency of 1.3 MHz, relative permittivity varies to much lesser extent from 2.97 (at -160 °C) to 3.09 (at 0 °C). The relative permittivity stays between 2.9 to 3.5 throughout the measured frequency for all temperatures.

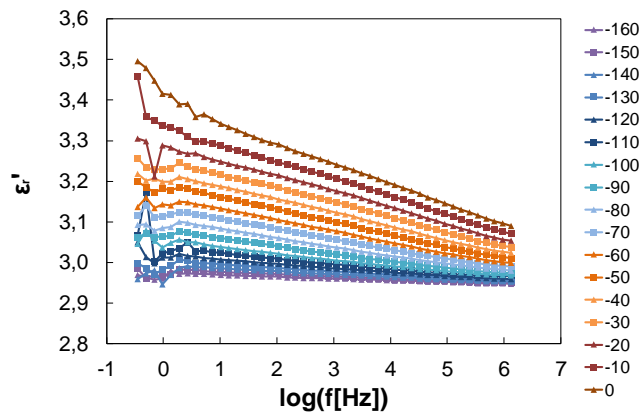


Figure 107. ϵ_r' spectra for temperature scale -160 °C to 0 °C for every 10 °C.

Figure 108 shows a significant increase in relative permittivity for temperatures 10 °C to 100 °C at lower frequency end. This is named as *Relaxation I*.

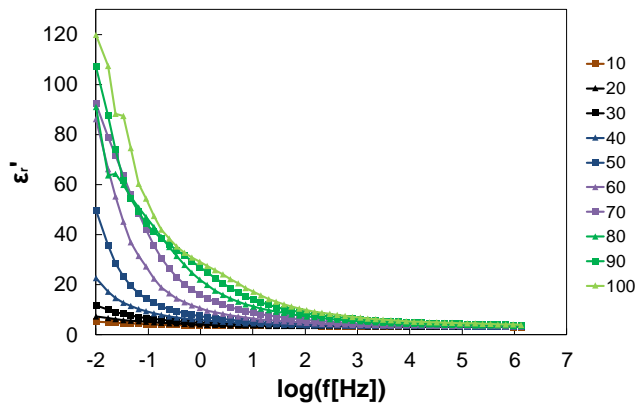


Figure 108. Plot of ϵ_r' as a function of frequency from 10 mHz to 1 MHz for temperature scale 10 °C to 100 °C for every 10 °C.

b) Loss factor: ϵ_r''

Figure 109 shows the loss factor spectra for temperatures 10 °C to 100 °C. The observations made in the relative permittivity spectra is in coherence with the loss factor spectra. *Relaxation I* is observed for the curves for temperatures 10 °C to 100 °C.

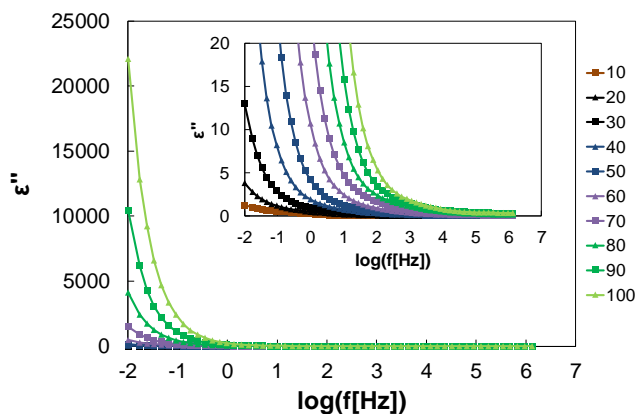


Figure 109. Plot of ϵ'' as a function of frequency from 10 mHz to 1 MHz for temperature scale 10 °C to 100 °C for every 10 °C. The inset in the figure shows the same plot to highlight the overlapped curves of relatively lower values.

c) Dissipation factor: $\tan\delta$

Dissipation factor spectrum is shown for temperatures 10 °C to 100 °C in the Figure 110. *Relaxation 1* is observed for temperatures 10 °C to 100 °C as seen in the permittivity and loss factor spectra.

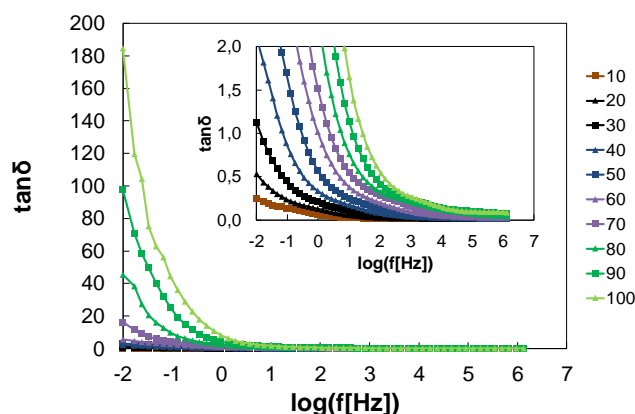


Figure 110. Plot of dissipation factor as a function of frequency from 10 mHz to 1 MHz for temperature scale 10 °C to 100 °C for every 10 °C. The inset in the figure shows the same plot to highlight the overlapped curves of relatively lower values.

V.8.2. Discussion: Dielectric spectroscopy of PLA-MFC

a) Summary of relaxations and their origin

At 20 °C, relative permittivity at 50 Hz and 1 kHz is 3.5 and 3.3 respectively. Dissipation factor at 20 °C for 50 Hz and 1 kHz is found to be 0.03 and 0.016 respectively. From the spectra of permittivity (Figure 108), loss factor (Figure 109) and dissipation factor (Figure 110) of PLA-MFC-pt, only one relaxation known as *Relaxation 1* was observed. Figure 111 represents the modulus spectrum for the temperature range of *Relaxation 1*. A set of peaks corresponding to *Relaxation 1* can be seen. This phenomenon appears to be due to conduction phenomenon. A small shoulder in the peak can be observed for the curves beginning from 10 °C. The peak becomes broader with increase in temperature from 30 °C to 100 °C. With-

increase in temperature, the shoulder becomes more pronounced into a peak beginning around 70 °C. This temperature is after the T_g (≈ 60 °C) of the matrix (PLA) of the composite. This could have lead to a coupled response of already existing conduction phenomenon as well as α transition.

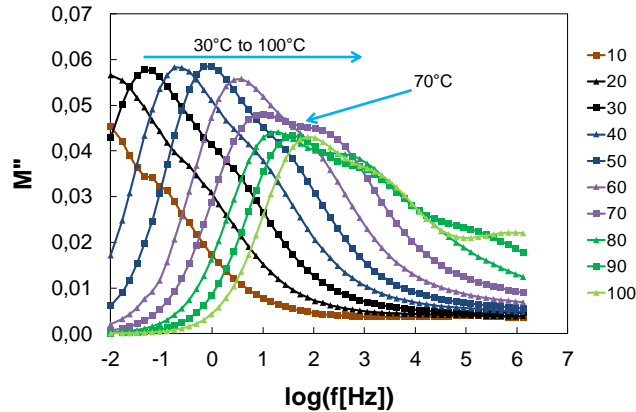


Figure 111. Plot of M'' as a function of frequency from 10 mHz to 1 MHz for temperature scale 10 °C to 100 °C for every 10 °C.

Figure 112 shows the AC conductivity spectra of PLA-MFC-pt nanocomposite. The AC conductivity approaches the steady state DC behavior at lower frequencies for temperatures 60 °C and above. Figure 112 shows the DC behavior at the lowest measured frequencies for these temperatures.

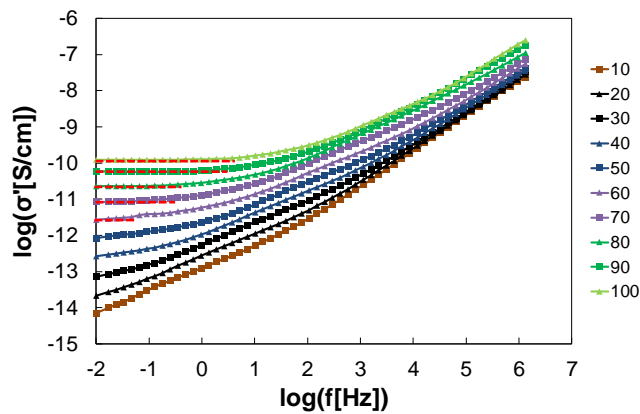


Figure 112. Plot of σ' as a function of frequency from 10 mHz to 1 MHz for temperature scale 10 °C to 100 °C for every 10 °C. The dotted red lines indicate DC behavior.

b) Activation energy

Figure 113 shows the plot of characteristic frequency (f_c) from modulus spectra for MWS polarization and conductivity at 10 mHz against inverse of temperature. The calculated activation energy for conduction phenomenon and MWS polarization is 1.03 eV and 1.29 eV respectively. These values are reported for the first time for such a nanocomposite and hence, no comparison is available in the literature.

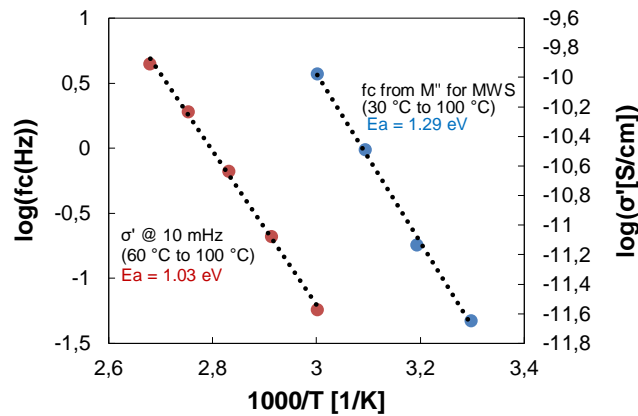


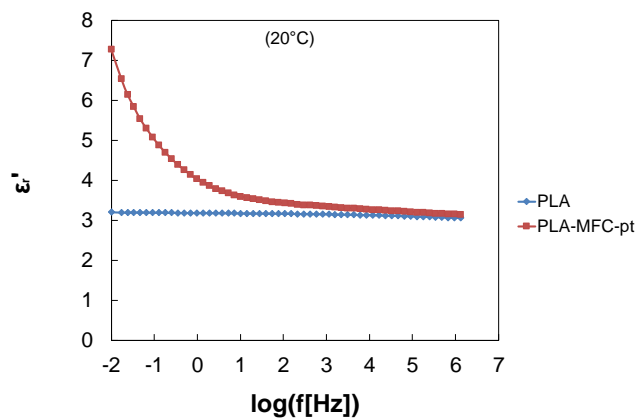
Figure 113. Plot of f_c for MWS polarization from M'' as a function of temperature (primary axis). Plot of σ' at 10 mHz as a function of temperature (secondary axis).

V.9. Comparison of the dielectric properties of PLA and PLA-MFC (post-treated)

PLA-MFC-pt doesn't show the lower temperature β relaxation and the relaxation α could be argued to occur (Figure 111). The T_g corresponding to glass transition occurs in the nanocomposite around 60 °C as confirmed by DSC measurements. On the other hand, PLA show a set of peaks corresponding to α transition.

The MWS polarization peaks due to conduction phenomenon are observed at much higher temperature around 90 °C in PLA (Figure 100) compared to its nanocomposite.

Figure 114 compares the relative permittivity, dissipation factor and AC conductivity spectra of PLA and PLA-MFC-pt at 20 °C for the frequency ranging from 10 mHz to 1.3 MHz.



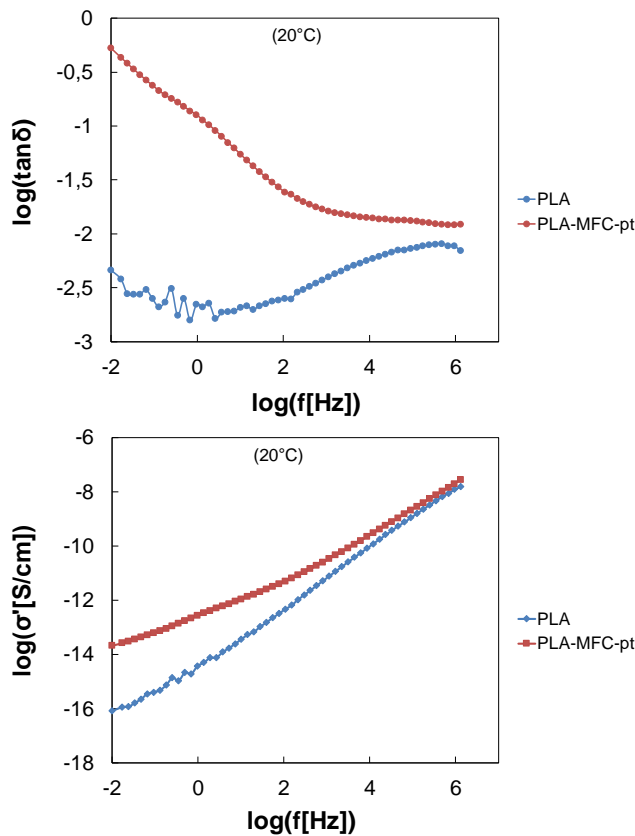


Figure 114. Relative permittivity, dissipation factor and AC conductivity spectra of PLA and PLA-MFC-pt at 20 °C.

The relative permittivity remains almost stable throughout the measured frequency region at 20 °C for PLA. The nanocomposite shows significant increase in relative permittivity at low frequency region which is understood to be due to conduction phenomenon. The level of losses is much higher in the nanocomposite compared to PLA. The level of conductivity is also higher in the nanocomposite compared to PLA by an order of two decades.

With the available data from this study, it is evident that the nanocomposite couldn't show better electrical properties compared to PLA. It has higher level of losses and conductivity. However, as a first attempt, a nanocomposite was successfully prepared, processed and studied for electrical measurements to be compared with PLA.

V.10. Introduction to current measurement

Electrometer is used for measuring current to determine the resistivity of a polymer film. In principle, it applies a voltage across a sample under study and measures the current. Thus, the voltage applied, time for which a voltage is applied and the temperature of measurement are the parameters in the current measurement of a polymer. Once the current is measured, with the measured thickness and the diameter of the measurement electrode of the sample, conductivity or resistivity (volume) is calculated. Figure 115 shows a schematic diagram of an experimental set-up of current measurement.

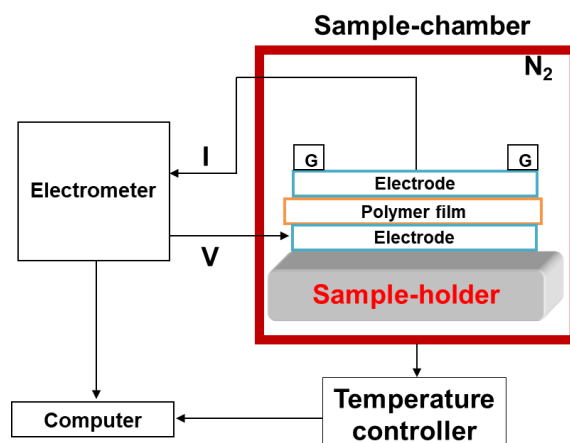


Figure 115. Schematic diagram of the current measurement. ‘G’ represents the guard electrode which encircles the electrode on the top of the sample.

The experimental set-up for the current measurement evolved throughout this work due to the problems related to the malfunctioning of acquisition software, temperature regulation system, sample-cell, sample-chamber or the size of the measurement electrodes itself. In total, five experimental set-ups were used and are discussed in the following section.

V.11. Experimental set-up 1

Characteristics of the experimental set-up 1:

Electrometer: *Keithley 6517B Electrometer/High Resistance Meter* [183];

Sample-chamber: *cylindrical*; Temperature regulation system: *Linkam TMS 94*;

Acquisition software: *Lab made*; Electrodes: *large-sized*; Metalization: *Required*

In this experimental set-up, the electrodes, sample-chamber, heating/cooling methods remain the same as in the experimental set-up 1 of dielectric spectroscopy. The voltage applied across the sample is carried out by an Electrometer instead of *Novocontrol*. Moreover, it is an AC voltage in *DS* while it’s a DC voltage in current measurements. A lab made software was used which forms an interface with both electrometer and temperature control system *Linkam-TMS 94*.

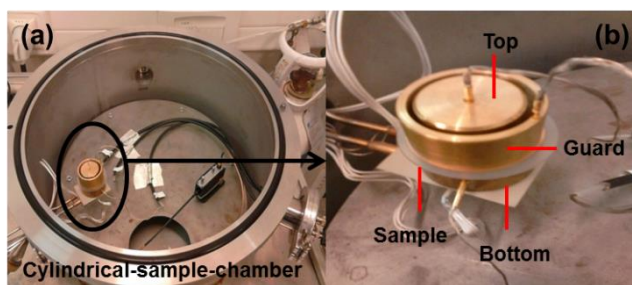


Figure 116. (a) Cylindrical sample-chamber for current measurement; (b) enlarged image of a sample and the electrodes all of which are mounted on a sample holder in the cylindrical sample-chamber.

As discussed earlier in the experimental set-up 1 of dielectric spectroscopy, a significant degree of gradient between the electrodes and between the electrodes and *Linkam TMS 94* exists. All these aspects were discussed earlier in the experimental set-up 1 of dielectric

spectroscopy. Despite the then existing temperature gradient problems, experimental set-up 1 was continued to be used for current measurement to understand and resolve the improper functioning of the lab made software. The result of the current measurement trials showed mismatch in the time for the applied voltage between what was asked in the protocol and that was obtained in the result. Thus, the problems posed by this experimental set-up include mismatch in time (both for the voltage application and to initiate a temperature change), NaN error and temperature gradient. In general, the volume resistivity is calculated as follows:

$$\rho = (A.V)/(t.I)$$

where, A is the effective area of electrode, t is the thickness of a sample, I is the measured conduction current and V is the applied voltage. The area A is fixed for all the samples for the experimental set-up 1. Its value is 8.04 cm^2 with radius, $r = 3.2 \text{ cm}$. This gives the volume resistivity as,

$$\rho = (8.04.V)/(t.I)$$

The conductivity is calculated as the reciprocal of the volume resistivity and it is given by,

$$\sigma = (1/\rho)$$

V.12. Experimental set-up 2

Characteristics of the experimental set-up 2:

Electrometer: *Keithley 6517B Electrometer/High Resistance Meter;*

Sample-chamber: *cryostat;* Temperature regulation system: *TDK Lambda;*

Acquisition software: *Lab made;* Electrodes: *small-sized;* Metalization: *Required*

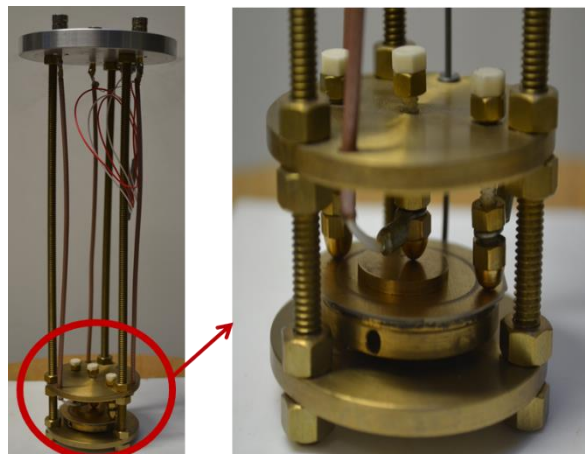


Figure 117. To the left is the image of the sample-cell used for the current measurement in experimental set-up 2. To the right is the enlarged image showing a metallized polymer film placed in between the electrodes in the sample-cell of the experimental set-up 2.

This experimental set-up resembles the experimental set-up 2 of the dielectric spectroscopy. Some of the common features are the sample-chamber (Cryostat), sample electrodes and temperature regulation system (TDK Lambda) which are the same as that used in the

experimental set-up 2 of the dielectric spectroscopy. The sample cell used here is not the same as that used in experimental set-up 2 of dielectric spectroscopy but has apparent similarities in terms of its design. The software remained the same as used in the experimental set-up 1 of the current measurement.

V.13. Experimental set-up 3

Characteristics of the experimental set-up 3:

Electrometer: *Keithley 6517B Electrometer/High Resistance Meter;*

Sample-chamber: *cryostat*; Temperature regulation system: *TDK Lambda;*

Acquisition software: *AMPERE version fb 03.1*; Electrodes: *small-sized*; Metalization: *Required*

This experimental set-up differs from the previous one in the software which is changed to *AMPERE version fb 03.1*.

V.14. Experimental set-up 4

Characteristics of the experimental set-up 4:

Electrometer: *Keithley 6517B Electrometer/High Resistance Meter;*

Sample-chamber: *Model 8009 Resistivity Chamber [184]*; Temperature regulation system: *measurement at ambient temperature*; Acquisition software: *Keithley Model 6524 High Resistance Measurement Software [185]*; Metalization: *Not required*

There are two changes in this experimental set-up compared to the previous one. The software *AMPERE version fb 3.1* is replaced by *Model 6524 High resistance Measurement Software*. The other is the replacement of sample-chamber, sample-cell and electrodes by *Model 8009 Resistivity Chamber*. This instrument comes in a shape of a box that acts as a sample-chamber and it is integrated with sample cell with the electrodes for current measurement. This instrument can operate with peak voltages up to 1000 V and measure volume resistivity in the range of 10^3 to 10^{18} ($\Omega\cdot\text{cm}$). This instrument can be used to perform measurements within the temperature range of -30 °C to 80 °C.

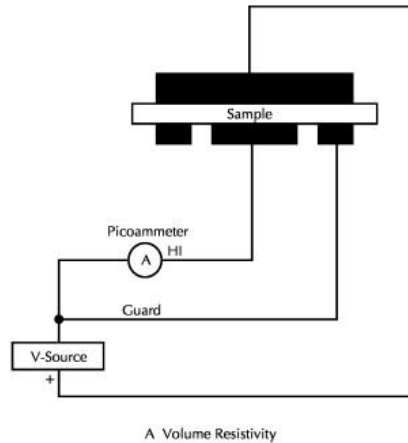


Figure 118. Electrode set up for volume resistivity measurements in Model 8009 Resistivity Chamber. *Courtesy: Keithley Instruments, Inc.[184].*

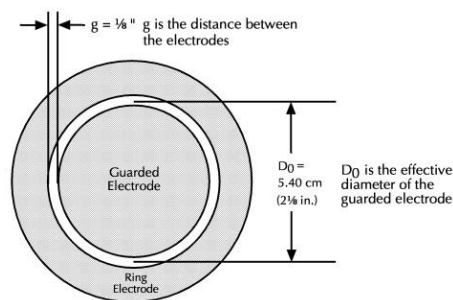


Figure 119. Electrode dimensions showing the effective diameter of the guarded electrode in Model 8009 Resistivity Chamber. *Courtesy: Keithley Instruments, Inc.[184].*

As seen earlier, volume resistivity of a polymer film is calculated as,

$$\rho = (A.V)/(t.I)$$

While using Model 8009 Resistivity Chamber, area A of the electrode is a constant at 22.9 cm^2 . It is obtained using radius r ($= 2.7 \text{ cm}$) of the effective area of the guarded electrode as seen in the Figure 119. There are broadly four test programs embedded in the software which are 6517 Hi-R test, 6517 Hi-R step response, 6517 Hi-R Sweep test and 6517 Hi-R, Temp, and RH [185].

V.15. Experimental set-up 5

Characteristics of the experimental set-up 5:

Electrometer: *Keithley 6517B Electrometer/High Resistance Meter;*

Sample-chamber: *Model 8009 Resistivity Chamber [184];* Temperature regulation system: *Vötsch climatic test chamber (type VC 7018) [187];*

Acquisition software: *AMPERE version fb 03.1;* Metalization: *Not required*



Figure 120. Experimental set-up showing the climatic test chamber with Model 8009 Resistivity Chamber (not seen) inside it.

This set-up is the same as that of previous one but experiments are conducted in controlled conditions inside a Vötsch climatic chamber at desired temperature and relative humidity conditions. The other change in this set-up is the software which is changed to *AMPERE version fb 3.1*.

V.16. Results: Experimental set-up 1 to Experimental set-up 4

The experiments performed with experimental set-up 1 can be broadly classified into two types based on the system of voltage application. These are *Volt_{on/off}* and *Ramp* method. In a *Volt_{on/off}* method (or alternating polarity method), a voltage alternates between zero and an applied voltage V . In case of a *Ramp* method, the applied voltage increases or decreases in time. The experiments performed with *Volt_{on/off}* method shows the mismatch in the time for the asked voltage in the protocol and the result obtained. Thus, the protocol is not executed at the asked time. Figure 121 shows the mismatch in time and Figure 122 shows the measured current for the voltage applied (voltage as appeared in the result).

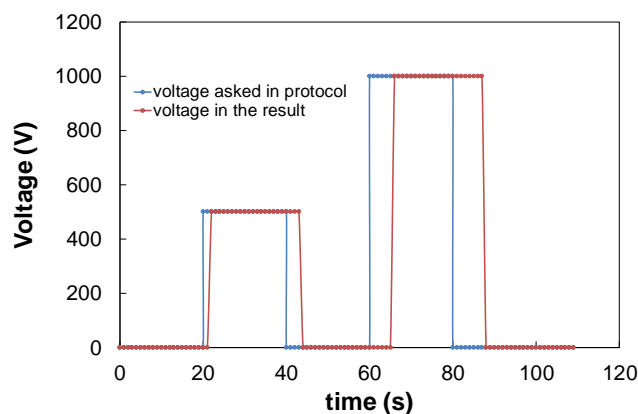


Figure 121. Voltage versus time showing the mismatch. The experiment was conducted at R.T.

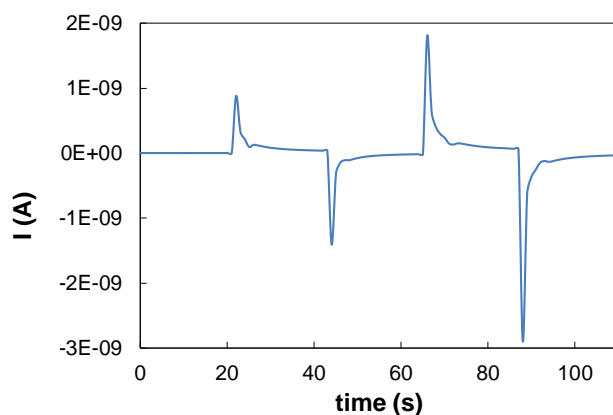


Figure 122. Measured current versus time for the applied voltage (voltage as appeared in the result and not as per the protocol asked).

The problem of mismatch was also consistent in *Ramp* method based measurements.

The experimental set-up 2 consisting of smaller size electrodes, smaller volume sample-chamber and sophisticated heating/cooling systems overcame most of the problems faced in the experimental set-up 1 most importantly the temperature gradient. The problem of mismatch in time of voltage (and temperature) asked and applied was prevalent and infrequent appearance of *NaN* error both of which were ignored. Figure 123 shows the current measured in a PCL film. The measurements were done at 20 °C and -160 °C. Alternating polarity method with voltages alternating between 0 V and alternating V (100 V to 1000 V in steps of 100 V) was used. The *Volt_{on}* and *Volt_{off}* period was set to 60 seconds. At 20 °C, there was no expected increase in the current with increasing voltage until 400 V after which a sudden jump in the level of the current that almost remained constant later. The increase in the current is very low at 20 °C when the voltage increases from 100 V to 1000 V. The overall increase in the current is low when the temperature is raised from -160 to 20 °C.

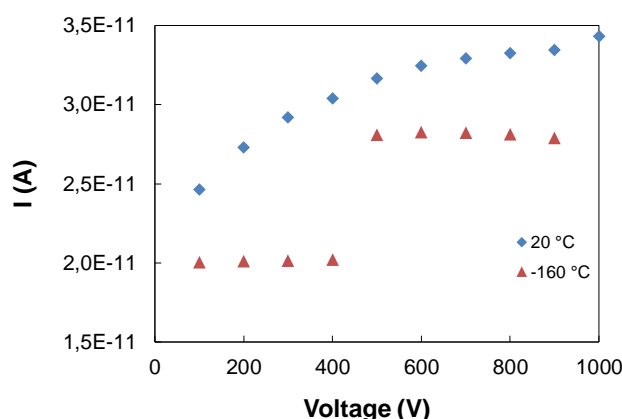


Figure 123. The measured current at 20 °C and -160 °C for the voltages 100 V to 1000 V.

The only exception in the experimental set-up 3 is the replacement of the lab made software by *AMPERE version fb 3.1*. The use of the new software posed no software malfunctioning. The current measurement of PCL was performed for temperatures -160 °C to 20 °C for every 20 °C with identical method of voltage application as described for PCL in the experimental set-up 2. There was almost no increase in the current with increase in voltage for a given

temperature. Also, very low increase in the measured current with increase in temperature. At certain temperatures, the measured currents sometime showed significant increase/decrease in current levels.

It was clear that the sample-cell malfunctioning led to such behavior in both experimental set-up 2 and experimental set-up 3. Plenty of polymer films were prepared, dried and investigated to study the cause of the problem in the sample-cell. The measurements were also performed on PLA films with both the set-up but the observations were consistent as that obtained for PCL. All the results are not presented in this report. With several repeated measurements on these experimental set-ups, it was concluded that the set-up failed to function properly. This was confirmed by the results obtained from the experimental set-up 4.

Keithley Model 6524 High Resistance Measurement software (used in conjunction with Model 8009 Resistivity Test Fixture and Keithley 6517A electrometer) gives four test programs to measure resistivity. Table 17 shows the measured current in PCL.

Table 17. Current measured in PCL.

Voltage (V)	I (A)
1	4×10^{-10}
50	2×10^{-8}
50	2×10^{-8}
50	2×10^{-8}
100	5×10^{-8}

V.17. Results: Experimental set-up 5

The result of the current measurement of PHBV and PCL obtained from this experimental set-up are explained in the following section.

V.17.1. Results: Current measurements of PHBV

a) Effect of temperature: PHBV

Based on the experimental set-up 5, current measurement of PHBV was performed to determine its resistivity at four different temperatures: 20 °C, 30 °C, 40 °C and 50 °C. At each temperature, current was measured during a time t under constant voltage application of voltage V . The measurement was continued for the same duration t under no voltage (0 V) application. The former state where the current is measured under a voltage application V is referred to as $Volt_{on}$ (V_{on}), while the latter where the current is measured at 0 V is referred to as $Volt_{off}$ (V_{off}). These are also known as polarization and depolarization steps respectively. The applied voltage at all temperatures remained 250 V. Figure 124 shows the absorption and desorption currents in PHBV measured at 20 °C.

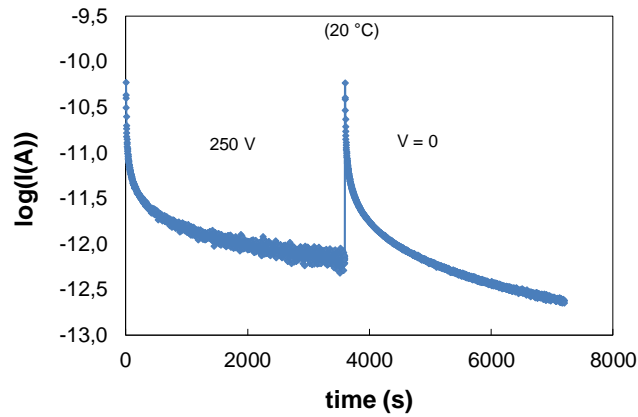


Figure 124. Current in PHBV versus time during an hour of polarization followed by an hour of depolarization step at 20 °C. The applied DC voltage is 250 V.

Table 18 shows the apparent conduction current and apparent conductivity for temperatures 20 °C to 50 °C. The applied voltage at all temperatures remained 250 V. The apparent conduction current is calculated as the average value of the current measured in the last 2000 seconds of an hour of measurement under $V = 250$ volts. Figure 125 shows the apparent conductivity for temperatures 20 °C to 50 °C.

Table 18. Apparent conduction current and apparent conductivity of PHBV.

Temperature (°C)	Duration of (V_{on}) and (V_{off}) in seconds	Average of the current measured in last 2000 seconds (A)	Apparent conductivity (S/m)	Volume resistivity ($\Omega.m$)
20	3600	8.55E-13	8.66E-16	1.2E+15
30	3600	2.87E-12	2.91E-15	3.4E+14
40	3600	9.16E-12	9.27E-15	1E+14
50	3600	2.10E-11	2.13E-14	4.3E+13

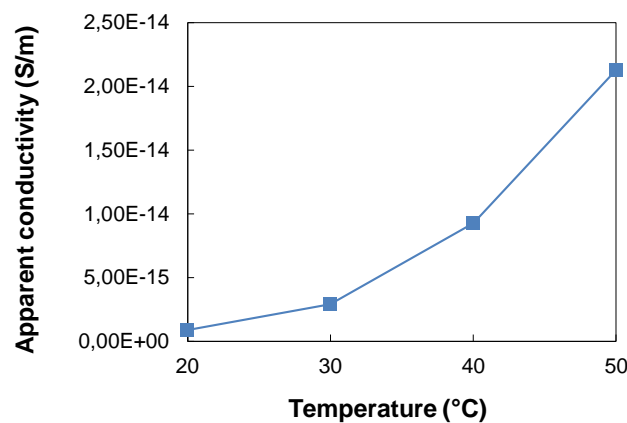


Figure 125. Apparent conductivity of PHBV for temperatures 20 °C to 50 °C.

b) Long duration measurement: PHBV

Only at 20 °C, both short (1 hour) and a relatively longer (7 hours) duration current measurements of PHBV were performed. The short duration current measurement of PHBV

was shown earlier in the Figure 124. Figure 126 shows the long duration current measurement of PHBV during seven hours of polarization and depolarization step respectively at 20 °C.

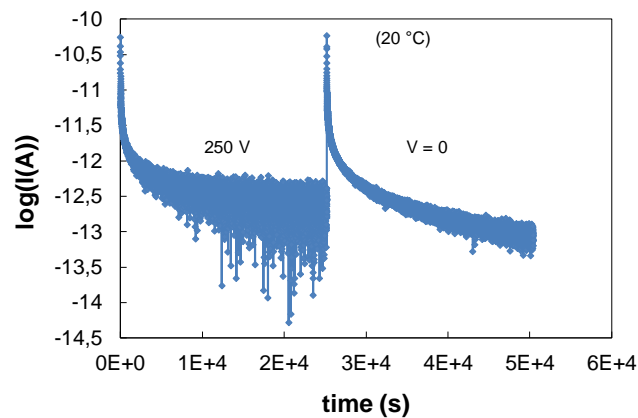


Figure 126. Current in PHBV versus time during 7 hours of polarization followed by 7 hours of depolarization step at 20 °C. The applied DC voltage is 250 V.

Table 19 shows the apparent conduction current and apparent conductivity at 20 °C.

Table 19. Apparent conduction current and apparent conductivity of PHBV at 20 °C.

Temperature (°C)	Duration of (V _{on}) and (V _{off}) in seconds	Average of the current measured in last 2000 seconds	Apparent conductivity (S/m)	Volume resistivity (Ω.m)
20	25200	2,47E-13	2.5E-16	4E+15

c) Effect of post-treatment: PHBV

Based on the same experimental set-up 5, current measurements were performed on a post-treated PHBV. The preparation of the post-treated PHBV film and its degree of crystallinity, melting temperature are described earlier (Chapter 4, Section IV.1.4). Figure 127 shows the absorption and the desorption currents in PHBV measured at 20 °C.

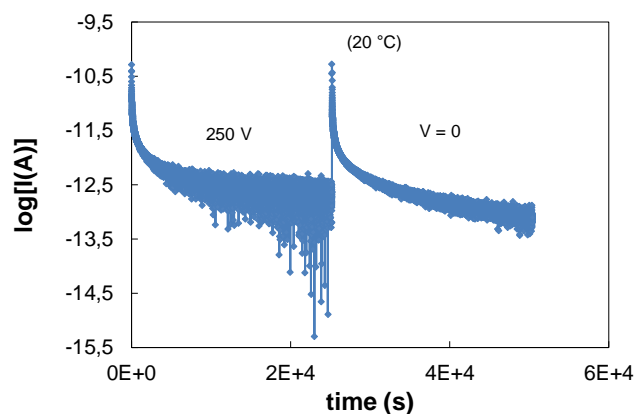


Figure 127. Current measured in post-treated PHBV during seven hours of polarization followed by seven hours of depolarization step at 20 °C. The applied DC voltage is 250 V.

Figure 128 shows the measured current and the apparent conductivity for temperature scale 20 °C to 40 °C for every 10 °C. It must be noted that at 20 °C, current was measured for 7 hours each for both polarization and depolarization step while at 30 °C and 40 °C, the measurements lasted for an hour. For all the temperatures, the reported current values in the Figure 128 represent the average value of the current measured in the last 2000 seconds of measurement. As observed for non-post-treated PHBV, the current measured increases with raise in temperature.

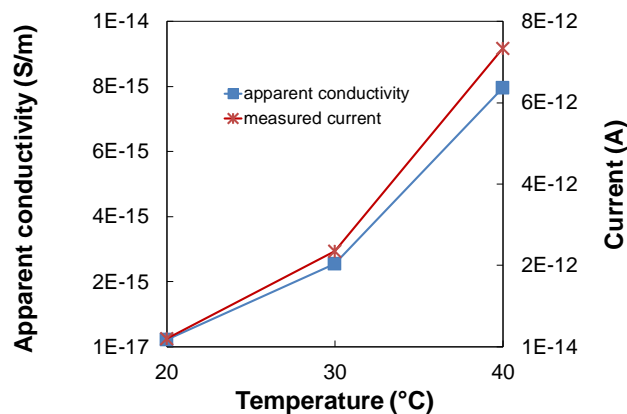


Figure 128. Measured current and apparent conductivity of post-treated PHBV for temperatures 20 °C to 40 °C.

V.17.2. Discussion: Current measurements of PHBV

a) Effect of temperature: PHBV

The increase in current and corresponding conductivity levels with increasing temperature is observed when the temperature raises from 20 °C to 50 °C. Figure 129 shows the superimposed plot of polarization and depolarization currents (Figure 124) of PHBV at 20 °C.

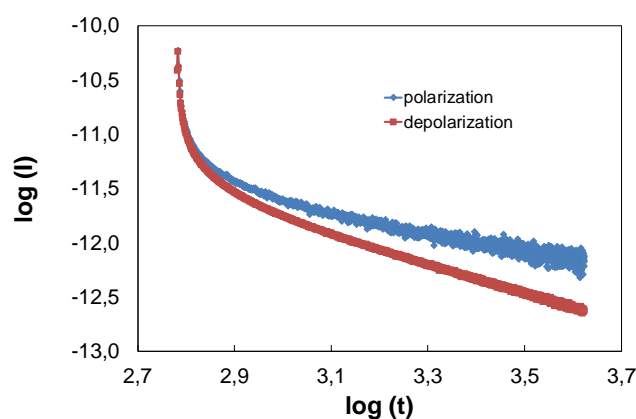


Figure 129. Superimposed graph of polarization and depolarization currents in PHBV at 20 °C.

Figure 130 shows the AC conductivity spectrum of PHBV at 20 °C. The conductivity at 252 mHz at 20 °C is 5.9E-11 (S/m). The calculated conductivity at 20 °C is 8.7E-16 (S/m). In the AC conductivity spectrum, the curve at 20 °C has not yet entered the *flat* region which is an indicative of σ_{dc} behavior. The *flat* region indicative of σ_{dc} is observed for curves beyond 120

°C in PHBV as seen in the Figure 70. At 20 °C, certainly the AC conductivity in *flat* region corresponding to DC behavior would be much lower than 5.9E-11 (S/m). The σ_{dc} may be accessed towards much lower frequency region beyond 252 mHz. The AC conductivity spectrum doesn't provide a DC conductivity at lower frequency end as the curve has not yet entered the *flat* region at 20 °C. Hence, this may contribute to the apparent difference by many orders of magnitude in conductivity between the AC conductivity at the lowest frequency and the calculated DC conductivity in PHBV.

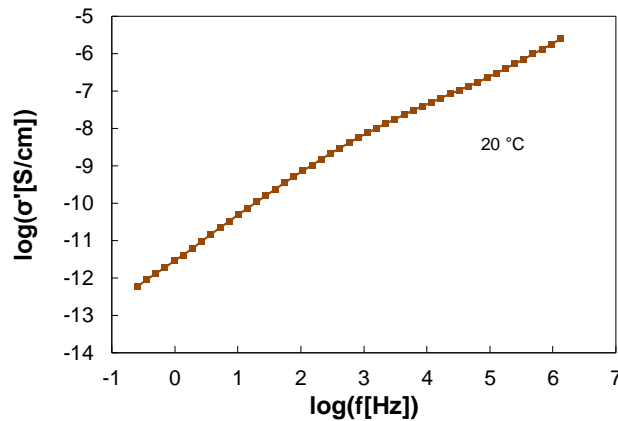


Figure 130. AC conductivity spectrum of PHBV at 20 °C for frequency range of 252 mHz to 1.3 MHz.

b) Comparison of long and short term current measurements in PHBV

PHBV was subjected to both long and short term current measurements. The measured current in the long-term measurement is 3.5 times lesser than the short term current measurement. Measurements longer than 7 hours could possibly lead to even lower level of current.

c) Comparison of current in non-post-treated and post-treated films of PHBV

Both non-post-treated and post-treated PHBV films were dried until a constant weight prior to performing current measurements. Figure 131 shows the measured current at three different temperatures for non-post-treated and post-treated PHBV films.

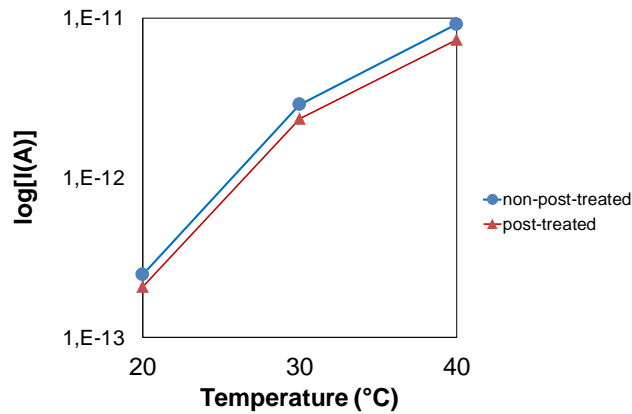


Figure 131. Measured currents at temperatures 20 °C to 40 °C for both non-post-treated and post-treated PHBV films.

On comparing the current levels, the measured current in post-treated film is lower than in non-post-treated film at all temperatures. The percentage of decrease in current levels in post-treated PHBV is given in the Table 20.

Table 20. Percentage decrease of current in post-treated PHBV compared to non-post-treated PHBV.

Temperature (°C)	Percentage decrease
20	16
30	18
40	20

The post-treatment of PHBV shows a positive effect with a significant decrease in level of conductivity. Conductivity in a polymer in its glassy state is lower than a polymer in its rubbery state at the measurement temperature [29]. In this study, both PHBV and post-treated PHBV is in rubbery state at the measurement temperature (20 °C). Hence, this argument may not explain the difference in level of conductivity between PHBV and post-treated PHBV. The other possibility is the difference in degree of crystallinity among the two which is only 2 %. The relatively higher degree of crystallinity in post-treated PHBV compared to non-post-treated PHBV may explain the difference to some extent.

As far as we know, there has been no published report on *DC* conductivity study of PHBV. In this study, we have studied volume resistivity levels of both PHBV and post-treated PHBV at different temperatures.

V.17.3. Result: Current measurement of PCL

Current measurement of PCL at 20 °C with the experimental set-up 5 for a duration of ten hours of polarization and depolarization respectively is shown in the Figure 132.

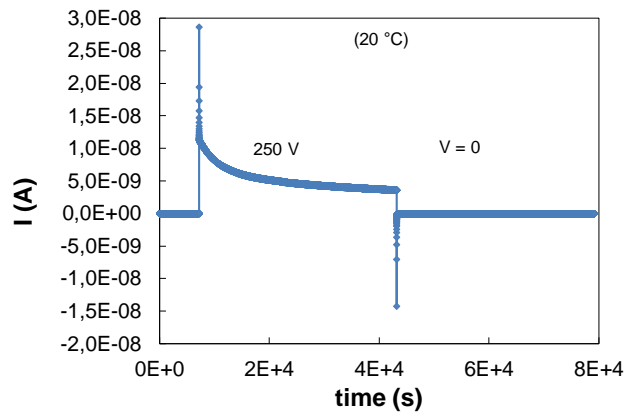


Figure 132. Current in PCL at 20 °C during ten hours of polarization followed by ten hours of depolarization step.

Table 21 shows the measured current which is the average of the current measured during the last 2000 seconds of the measurement and the calculated apparent conductivity.

Table 21. Apparent conduction current and calculated apparent conductivity of PCL at 20 °C.

Temperature (°C)	Duration of (V_{on}) and (V_{off}) in seconds	Average of the current measured in last 2000 seconds	Apparent conductivity (S/m)	Volume resistivity ($\Omega.m$)
20	36000	3,6E-9	5E-12	2E+11

V.17.1. Discussion: Current measurement of PCL

Ohki *et al.* reported two separate reports on the conductivity of PCL to be $8E-11$ (S/m) at room temperature [8], [29]. In one of the studies they mentioned the thickness of the PCL film, while not in the other. In both cases, they have measured the current or apparent conductivity only during 1000 seconds of measurement and the reported value is after 1000 seconds of measurement. In another study reported by Nemoto *et al.*, the conductivity of PCL is reported to be $1.2E-11$ (S/m) at 20 °C after 1200 seconds of measurement since voltage application [30]. The reported values in the literature are an order of magnitude higher. This can be argued to be due to the shorter measurement time of up to 20 minutes. In the present study, the current was measured for 10 hours resulting in much lower current and corresponding apparent conductivity. Figure 133 shows the AC conductivity spectrum of PCL at 20 °C.

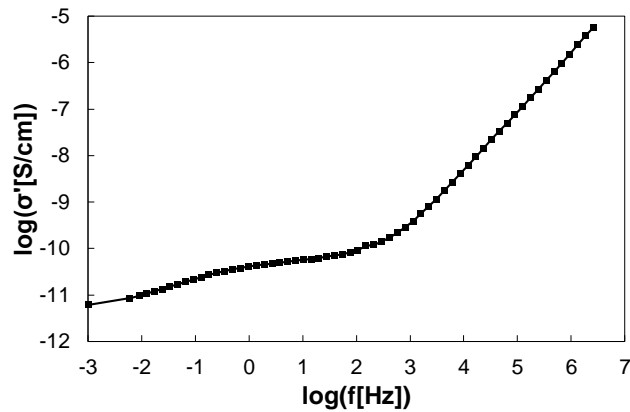


Figure 133. AC conductivity spectrum of PCL at 20 °C for frequency range 1 mHz to 2.6 MHz.

From the AC conductivity spectrum of PCL, the conductivity at the lowest measured frequency (1 mHz) is deduced. The AC conductivity at 1 mHz is two orders of magnitude less than the dc conductivity. It can be seen from the Figure 133 that the AC conductivity has not reached the *flat* region corresponding to the DC behavior. Table 22 shows the conductivity of PCL obtained from this and other reports.

Table 22. Apparent conductivity of PCL at 20 °C from different reports.

Authors	Duration (s)	Temperature (° C)	Electric field (kV/mm)	Thickness (mm)	Conductivity (S/m)
Ohki <i>et al.</i> [29]	1000	RT	25	-	$8 \cdot 10^{-11}$
Ohki <i>et al.</i> [8]	1000	RT	25	0.293	$8 \cdot 10^{-11}$
Nemoto <i>et al.</i> [30]	1200	20	10	0.05	$1.2 \cdot 10^{-11}$
Conductivity (DC)	36000	20	0.31	0.8	$5 \cdot 10^{-12}$
Conductivity (AC)	-	20	-	0.45	$6.1 \cdot 10^{-10}$

V.18. Introduction to electrical breakdown

The polymer films are not metallized for breakdown measurement. Breakdown measurement were performed only on PHBV films of thickness 50 μm obtained from Goodfellow [163]. The polymer films processed in our laboratory were too thick to be used for breakdown measurements. In the domain of electrical breakdown (E_{bd}) study of PHBV, very limited reports have been reported [1], [7], [8]. Moreover, these reports are on impulse breakdown strength of PHBV. As far as our knowledge goes, no report on direct current electric breakdown of PHBV has been communicated. A non-metallized polymer film with dimensions 6 cm * 6 cm is placed in between flat-disc type electrodes in a sample-cell and placed in an oven maintained at 20 °C. The electrodes are made of steel with diameter of top and bottom electrode being 2 cm and 4 cm respectively. A DC voltage ramp of 1 kV/s is applied across the polymer film until the electrical breakdown occurs and the corresponding

breakdown voltage is recorded. A DC voltage up to maximum of 60 kV can be applied across a film with the available voltage source (generator). However, due to limitations imposed by experimental set-up, measurements are limited to a maximum of 30 kV.

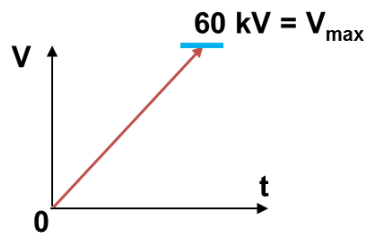


Figure 134. Measurement protocol for breakdown (DC) studies of polymer films.

The DC electrical breakdown values are analyzed by statistical method of Weibull distribution function which is given by the Equation 8,

$$\text{Equation 8. } F(x) = 1 - \exp [-(x-c)/\alpha]^\beta]$$

where, α is the scale parameter, β is the shape parameter, c is the location parameter and x is the breakdown voltage. The scale parameter gives the breakdown strength at which the probability for a breakdown is 63.2 %. On the other hand, the shape parameter describes the distribution range of the electric breakdown field strengths. The location parameter is a value below which the probability of breakdown is zero. This parameter is set to zero leading to Weibull distribution with scale and shape parameters as shown in the Equation 9,

$$\text{Equation 9. } F(x) = 1 - \exp [-(x/\alpha)^\beta]$$

The median rank approximation was used to determine the cumulative distribution function given in the Equation 10,

$$\text{Equation 10. } F(i,n) = [(i-0.3)/(n+0.4)]$$

where, i is the rank or the order of the breakdown strength and n is the total number of samples studied for breakdown.

V.19. Result: Electrical breakdown of PHBV

A total of number of 25 PHBV films were used to study the DC breakdown of PHBV. The thickness of each film was 50 μm . Figure 135 shows the plot of probability against breakdown strength used to calculate both the scale and the shape parameters.

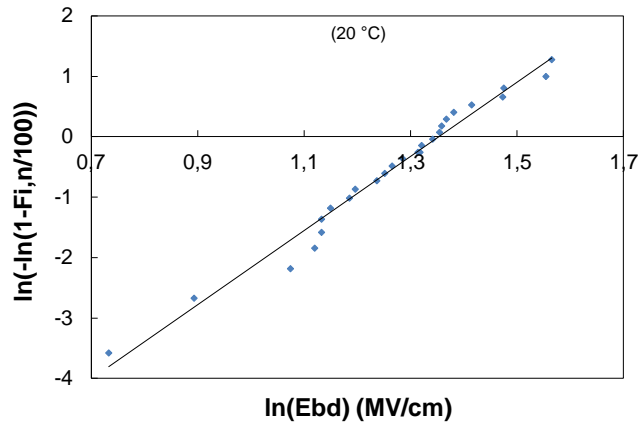


Figure 135. Bi-logarithmic plot of probability against breakdown strength for 25 PHBV films.

The scale parameter was found to be 3.86 MV/cm and the shape parameter equal to 6.3. The average breakdown strength of PHBV for 25 films was found to be 3.75 MV/cm.

V.20. Discussion: Electrical breakdown of PHBV

Figure 136 shows the image of a PHBV film post-breakdown.

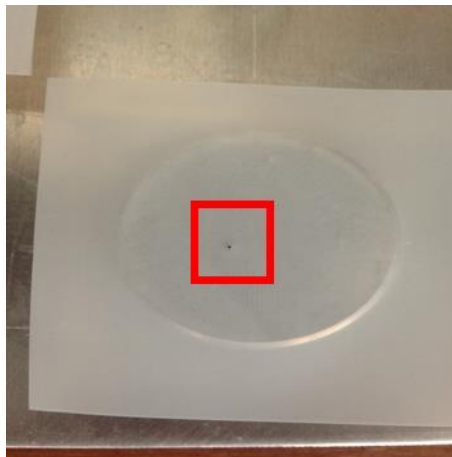


Figure 136. Image of a PHBV film post-breakdown. The spot of the breakdown is visible to the naked eye as a black spot highlighted in the red box in the image.

As far as we know, no communication has been reported on the *DC* breakdown study of PHBV. However, impulse breakdown study of a commercially available PHBV at room temperature has been reported by Ohki *et al.* [1]. They used stainless steel ball electrodes contrary to the present study where we used stainless steel flat electrodes. They reported an impulse breakdown strength of 3.13 MV/cm for a film of thickness 124 μm . However, it is not clear if the reported impulse breakdown strength represents an average value or is reported for a single measurement. This value is in the range of the value obtained for the *DC* breakdown strength of PHBV in this study. Ohki *et al.* suggested that the *DC* breakdown strength of a polymer could be low if its conductivity level is high [1]. They also extended their argument to say that a polymer in rubbery state has lower *DC* breakdown strength compared to a polymer in the glassy state. PHBV has both high conductivity and is above its glass transition temperature, i.e., in rubbery state at the measurement temperature of *DC*

breakdown. Thus, the breakdown is attributed to high conductivity and enhanced molecular motion due to its rubbery state [1]. The *DC* breakdown strength of PHBV is much lesser than the biodegradable polymer PLA which is around 5.7 MV/cm (for a film of 50 μm thick) [7]. The relatively higher *DC* breakdown strength in PLA is argued to be due to its low conductivity and glassy state at the temperature of breakdown measurement [7].

V.21. Summary of the contribution to the field of study

The dielectric spectroscopy experiments conducted on biodegradable polymers in this study covers a wide range of temperature and frequency. This provides complementary data on the dielectric spectra and various relaxation phenomena occurring in a polymer. In the case of PHBV, only a single study communicated by Pratt and Smith spanned such a vast temperature and frequency range [39]. They have reportedly measured dielectric properties beyond the temperature and frequency range of this study on PHBV. However, they provide only contour maps of real permittivity and dissipation factor and do not address the dielectric spectra of different physical quantities. For example, *AC* conductivity has not been addressed. Temperature plots and spectra of modulus are not demonstrated or discussed which in this study focuses on the relaxation phenomena in PHBV. Following Pratt and Smith, there are many reports but none matches the temperature and frequency range of dielectric spectroscopy in this study. Table 23 shows the measured temperature and frequency range of dielectric spectroscopy of PHBV reported in the literature.

Table 23. Dielectric spectroscopy measurement (temperature and frequency) range reported in the literature for PHBV.

Reference	Temperature ($^{\circ}\text{C}$)	Frequency	% of HV content in PHBV
Shanming <i>et al.</i> [37]	40 to 100	1 mHz to 10 MHz	8
Ohki and Hirai [1],[7]	RT	1 Hz to 0.1 MHz	8
Ando <i>et al.</i> [38]	-40 to 30	1 Hz to 100 Hz	25
Pratt and Smith [39]	-180 to 130	0.1 Hz to 3 MHz	24
Fukada and Ando [34]	-150 to 150	10 Hz	17 and 25

The PHBV subjected to the dielectric study by Pratt and Smith contains 24 % of *HV* content. In this study, it is 8 % of *HV* content. Thus, to the best of your knowledge no reports have been found on broad range dielectric spectroscopy of PHBV with 8 % *HV* content. In addition, all their relaxation phenomena and corresponding activation energy are discussed here.

Dissipation factor spectra of PHBV are not so widely discussed in the literature either. Daly *et al.* reported the dissipation factor of aged and rejuvenated PHBV (with 8 % *HV* content) at 30 $^{\circ}\text{C}$ [53]. Pratt and Smith provided contour maps of dissipation factor of PHBV with 24 % *HV* content [39]. In this study, dissipation factor spectra for PHBV (with 8 % *HV* content) is presented for frequency scale 252 mHz to 1.3 MHz for temperatures ranging from -150 $^{\circ}\text{C}$ to 140 $^{\circ}\text{C}$ for every 10 $^{\circ}\text{C}$.

AC conductivity spectra of PHBV has so far not been reported and discussed at and below the room temperature. In this work, AC conductivity at the room temperature was provided. Also, at higher temperatures and lower frequencies, it allows to view the DC conductivity behavior of PHBV at very low measured frequencies. The DC conductivity study of PHBV has not received importance earlier. The DC conductivity level in a PHBV film for different temperatures was reported. A first attempt has been made to understand the influence of morphology of PHBV on its DC conductivity. It is in this regard a post-treated PHBV film was prepared and studied for DC conductivity at and higher than room temperature. Both long and short duration measurements were conducted to understand the behavior of transient current as a function of time. Similarly, DC breakdown strength of PHBV has not been communicated so far. The breakdown experiments were performed and the results were analyzed with a statistical analysis method to calculate the DC breakdown strength of PHBV.

The α relaxation of PHBV obtained from DMTA experiments is compared with its dielectric spectra (Figure 72). The reproducibility of dielectric spectra for PHBV has also been examined. This work provides essential results on the electrical properties of PHBV such as relative permittivity, dissipation factor, conductivity (both AC and DC) and electrical breakdown strength. It also provides the percentage of water uptake in this biodegradable polymer.

Dielectric spectroscopy of PCL was measured for a wide range of temperature and frequency by Wurm *et al.* [70]. They used dielectric spectroscopy as a tool to study the crystallization occurring in PCL by observing dielectric properties, relative permittivity and loss factor. It is Bello *et al.* who conducted dielectric spectroscopy on PCL for a wide range of temperature and frequency to analyze their dielectric spectra. They discussed in detail the relative permittivity and the loss factor spectra and also discussed various relaxation phenomena occurring in PCL and their activation energies [67]. Table 24 shows the few dielectric spectroscopy measurements extending over a wide range of frequency and temperature on PCL reported in the literature.

Table 24. Dielectric spectroscopy measurement (temperature and frequency) range reported in the literature for PCL.

Reference	Temperature (°C) range	Frequency range
Wurm <i>et al.</i> [70]	-150 to 55	10 mHz to 10 MHz
Bello <i>et al.</i> [67]	-140 to 40	5 mHz to 3.2 MHz
Nemoto <i>et al.</i> [30]	20 to 50	10 mHz to 10 kHz
Ohki <i>et al.</i> [29]	RT	0.1 Hz to 0.1 MHz
This study	-160 to 40	12 mHz to 2.6 MHz

Even though various dielectric properties of PCL were widely reported, the dissipation factor and AC conductivity spectra of PCL was ignored. In this study, AC conductivity and dissipation factor spectra of PCL are discussed. Their values at the room temperature are deduced. The DC conductivity of PCL was reported earlier [8], [29], [30]. The duration of measurement is short in those cases. In this work, the current measured in PCL is for ten

hours and the corresponding conductivity is an order lower in magnitude than reported in the literature (Table 22). The percentage of mass uptake in PCL is studied. The α relaxation of PCL obtained from *DMTA* experiments is compared with dielectric spectra (Figure 88). Also, the reproducibility in producing a dielectric spectrum with a same film was examined.

PLA has been one of the most studied biodegradable polymers owing to its electrical properties such as low relative permittivity, low level of conductivity and relatively higher breakdown strength for a biodegradable polymer. Although it has been extensively studied for its electrical properties earlier, here it was studied to verify its different relaxation phenomena and dielectric properties. Despite numerous publications concerning dielectric properties of this polymer, there are very few reports on its dissipation factor and *AC* conductivity studied for a broad range of temperature and frequency. Xu *et al.* reportedly studied the *AC* conductivity of PLA for temperatures 80 °C to 140 °C [94]. Celli and Scandola discussed dissipation factor plot of temperature as a part of their study on physical ageing in PLA [45]. In this study, such missing aspects were covered. The percentage of mass uptake in PLA is measured.

PLA based nanocomposite reported in this study is first of its kind to have been prepared, processed and explored for their thermal and dielectric properties.

V.22. Comparison between the biodegradable polymers and conventional polymers

Conventional polymers PET, PE and thermosets such as epoxy resin which are widely used in applications such as capacitor, cables and electrical insulation systems are chosen for comparison of their dielectric properties with the biodegradable polymers. The main dielectric properties concerning applications in capacitors are relative permittivity and breakdown strength. These properties are compared among the biodegradable polymers and the conventional polymer PET. Table 25 shows the dielectric properties of the studied biodegradable polymers and PET.

Table 25. Comparison of dielectric properties of the biodegradable polymers and PET.

Dielectric property	PHBV	PETS	PLA	PET
ϵ_r' (50 Hz; RT)	3.6	3.06 [1]	3.2	3.4 [186]
ϵ_r' (1 kHz; RT)	3.3	3.04 [7]	3.2	3.2 [187]
$\tan\delta$ (50 Hz; RT)	0.032	-	0.0024	0.002 [186]
$\tan\delta$ (1 kHz; RT)	0.037	-	0.004	0.005 [187]
σ_{dc} (RT) (S/m)	2.5E-16	6E-15 [7]	1E-15 [29]	1E-16 [188]
E_{bd} (MV/cm) (RT)	3.86	4.23 [7]	5.66 [7]	5.94 [160]

PHBV has higher relative permittivity than PET. However, in terms of breakdown strength, PHBV has lower breakdown strength than PET and shows much higher level of losses. The structure of PETS resembles PET which differs by an ethylene-succinate group in it. The chemical structures of PET and PETS are shown in the Figure 137.

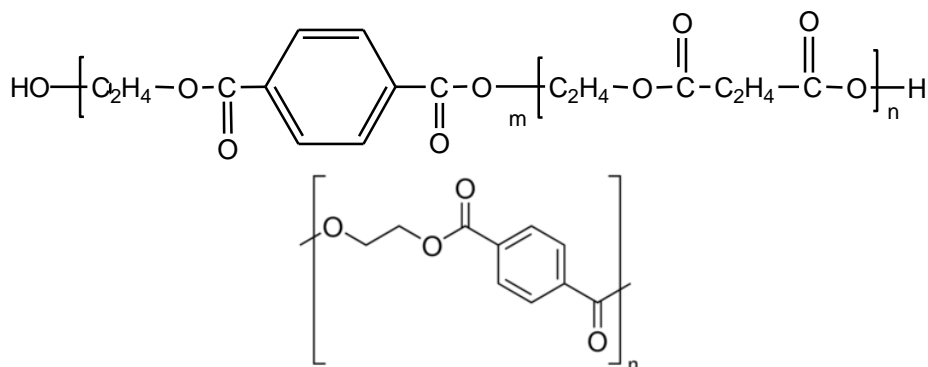


Figure 137. To the above is the structure of PETS and to the below is the structure of PET [189].

The dielectric constant of PETS is closer to PET. The breakdown strength is lesser than PET. Table 26 shows the thermal properties of PETS and PET.

Table 26. Comparison of thermal properties of PETS and PET.

Polymer	PETS	PET
T _g (°C)	50 [1]	78
T _m (°C)	210 [1]	258

Both PET and PETS are polyesters and thermoplastics and on comparing their dielectric and thermal properties, PETS could challenge PET where the existing difference could be accepted depending on the application used.

PLA has a dielectric constant and dissipation factor equivalent to PET. Although the conductivity and breakdown strength are better in PET, the difference may be marginal depending on the application used. Capacitor applications usually demand thin films and it was seen earlier that PLA can be processed into thin films (Table 7). PLA offers different processing methods such as extrusion and compression molding to obtain films. However, the difference in melting temperature between PLA and PET is much more than the difference between PETS and PET as seen in the Table 27.

Table 27. Comparison of thermal properties of PLA and PET.

Polymer	PLA	PET
T _g (°C)	62	78
T _m (°C)	155	258

For use in application such as electrical cables, the polymer should have low level of losses. Its thermal properties must be adequate to the requirements of the application. Factors such as ageing also play a key role here. Table 28 compares the dielectric properties of biodegradable polymers with conventional polymer PE.

Table 28. Comparison of dielectric properties of the biodegradable polymers and PE.

Polymer	PHBV	PETS	PLA	PE
ϵ_r' (50 Hz; RT)	3.6	3.06 [1]	3.2	2.3 [158]
ϵ_r' (1 kHz; RT)	3.3	3.04 [7]	3.2	2.3 [13]
$\tan\delta$ (50 Hz; RT)	0.032	-	0.0024	0.0002 [158]
$\tan\delta$ (1 kHz; RT)	0.037	-	0.004	0.002 [13]
σ_{dc} (RT) (S/m)	2.5E-16	6E-15 [7]	1E-15 [29]	6E-15 [7]
E_{bd} (MV/cm) (RT)	3.86	4.23 [7]	5.66 [7]	4.79 [7]

PHBV has much higher level of losses compared to PE. In perspective of processing, PHBV even though can be extruded still poses thermal limitations while processing. The polymer may undergo thermal degradation around 20 °C above its melting temperature. This could also lead to decrease in its molecular weight. Thus, PHBV allows a narrow window of processing. The second factor is its poor ageing property [53].

The conductivity in PETS is of the same order as that of PE and the breakdown strength though lower is still closer to PE. Table 29 compares the thermal properties of PLA, PETS and PE.

Table 29. Comparison of thermal properties of PLA, PETS and PE.

Polymer	PLA	PETS	PE
T_g (°C)	62	50 [1]	-30 [1]
T_m (°C)	155	210 [1]	110 [1]

Both PLA and PETS are polar and yet show conductivity either equivalent or lower than PE. This is because PE is in rubbery state in room temperature while PETS is in glassy state until 50 °C. This has been argued to justify the low conductivity and high breakdown strength in both PETS and PLA [1].

PLA shows interesting electrical properties in terms of conductivity and breakdown strength. The breakdown strength in PLA is higher than in PE. PLA like PE can be extruded into cables [141]. Though low level of losses would be favorable in cable applications, PE has lower level of losses compared to PLA. The other disadvantage in PLA compared to PE is the high degree of moisture permeability as reported by Shinyama and Fujita [13]. PLA shows a larger moisture permeability of 250 g/m² compared to 24 g/m² in PE in a day's time [13]. Today, several forms of PE are available depending on its molecular weight and physical properties. LDPE and HDPE are two types of PE which are both thermoplastics and differ in toughness owing to their physical properties. A thermoset cross-linked variant of polyethylene known as XLPE find various applications in electrical cables. A comparison of PLA and XLPE has been reported by Nakagawa *et al.* [60] and the result is presented in the Table 30.

Table 30. Comparison of dielectric properties of the biodegradable polymer PLA and cross-linked XLPE.

Polymer	PLA	XLPE
ϵ_r' (50 Hz; RT)	3	2.4
$\tan\delta$ (50 Hz; RT)	0.022	0.018
Volume resistivity (Ω/m) (RT)	49×10^{14}	46×10^{14}

In the same study, Nakagawa *et al.* showed that the impulse breakdown strength of PLA is 1.3 times of XLPE [60]. Despite PLA exhibiting such interesting electrical properties compared to PE or XLPE, their use in cables could be argued for many reasons such as water permeability. PLA insulated cable [141] shows whitening in the bending tests unlike XLPE which is reported to withstand small radius bending tests [190]. PLA poses the potential to replace PE in applications where thermal and electrical criteria are within the reach of PLA.

Table 31 summarizes the electrical properties of the biodegradable polymers and epoxy resin. It may not be appropriate to compare the electrical properties of biodegradable polymers with a material such as epoxy resin which is one of the most widely used material in electrical insulation. Secondly, it is a thermoset unlike the biodegradable polymers which are thermoplastics. Epoxy resin can be molded with least defects unlike thermoplastic biodegradable polymers.

Table 31. Dielectric properties of the biodegradable polymers and epoxy resin.

Polymer	PHBV	PETS	PLA	epoxy resin
ϵ_r' (50 Hz; RT)	3.6	3.06 [1]	3.2	4.64*, < 3.5+ [157]
ϵ_r' (1 kHz; RT)	3.3	3.04 [7]	3.2	4.45*, < 3.5+ [157]
$\tan\delta$ (50 Hz; RT)	0.032	-	0.0024	0.0336 [191]
$\tan\delta$ (1 kHz; RT)	0.037	-	0.004	0.029 [154]
σ_{dc} (RT) (S/m)	2.5E-16	6E-15 [7]	1E-15 [29]	5E-14 [192]
E_{bd} (MV/cm) (RT)	3.86	4.23 [7]	5.66 [7]	4.4 [193]

*these values are reported for epoxy resin with amine as a curing agent; +these values are reported for epoxy resin with acid anhydride as a curing agent

In fact, besides dielectric and thermal properties, other factors also play a key role in finding an application for a polymer such as adhesion, resistance to chemicals, hardness etc. These properties should be considered for each specific targeted application. It must be noted that the properties of these biodegradable polymers may be improved either considering their formulation or by addition of specific fillers or additives.

Conclusions and perspectives

A review work on the electrical and the thermal properties on ten biodegradable polymers is presented. Their electrical and thermal properties were examined and compared with conventional polymers. The review concluded poly(lactic acid) is the most studied biodegradable polymer. Both PLA and PETS challenge the electrical properties of conventional polymers. PETS could compete with PET and PE in relative permittivity, *DC* conductivity and thermal properties but it couldn't be a part of this study due to lack of suppliers. Biodegradable polymers have higher level of conductivities except PLA: its conductivity is closer to the conductivity of LDPE. In general, PLA has also a good dielectric strength when compared with classical polymers.

Suitable films for electrical measurements could be obtained for PHBV, PCL, PLA, PP and PLA-MFC. The successful method of obtaining films suitable for electrical measurements was slow cooling (annealing) of the polymer melt under pressure in the hot-press. The films were neither formed nor suitable for electrical measurements if the mold was dismantled earlier. Besides, quenching of polymer-melt did not yield suitable films. Solvent casting method of processing couldn't produce films meeting the criteria of electrical measurements.

A novel PLA based nanocomposite was prepared and their processing conditions were optimized.

PHBV and PLA, though polyesters too, are more hydrophilic than conventional PET. Conversely, under the conditions studied, their water uptake is not far from the one of many other polymers and materials used in electrical insulation.

In case of PLA-MFC nanocomposite, the sample dried at 60 °C showed a cold-crystallization peak which is absent in PLA-MFC dried at 90 °C. The drying temperature influenced the morphology of a polymer. The post-treatment of PLA-MFC resulted in the absence of cold-crystallization. The post-treatment of PHBV changed their polymer morphology with an increase in their degree of crystallinity.

The functioning of the dielectric spectroscopy and the current measurement experimental set-ups, sample cells built during the thesis were tested and validated.

Broadband dielectric spectroscopy demonstrated various relaxation phenomena occurring in each of the biodegradable polymers studied. These relaxation phenomena were α transition usually attributed to glass transition, local mode (β , γ) and relaxation due to interfacial (*MWS*) polarization. Both PHBV and PLA showed α , β and relaxation due to *MWS* polarization contrary to PCL, which showed all the four relaxation phenomena. Merging of peaks of local mode of β and γ occurs in PCL. PLA-MFC shows α relaxation and relaxation due to *MWS* polarization.

The current measurements of post- and non-post-treated PHBV showed a positive effect of post-treatment with an increase in volume resistivity. The measurements performed in this study shows volume resistivity of PHBV is higher than PLA or LDPE at room temperature. PCL has lower volume resistivity than PLA at room temperature.

PHBV has a promising low relative permittivity and high volume resistivity. However, it has poor aging property and narrow processing window. PCL has poor electrical and thermal properties and cannot be used for electrical engineering applications without further improvements. The PLA based nanocomposite that was prepared, processed and characterized in our study offered low volume resistivity and high level of losses. It doesn't appear to be an interesting material in this state. PLA is convincing enough to challenge PET in some applications, provided the thermal properties are improved and water uptake levels are reduced or where the polymer is acceptable for a desired application.

Only hot-processing apparatus were used to process films in this study. With a perspective to produce better quality, homogenous and thinner films and with an industrial viewpoint, different types of processing methods such as molding and extrusion could be tried. This work has been dedicated to water uptake studies, thermal and electrical properties of polymers. From application point of view, studies on ageing and mechanical strength of these polymers could be interesting.

The experimental results confirm that PLA is the promising biodegradable polymer in the context of dielectrics. As reported in the literature, PLA insulated cable has been processed and studied for electrical properties and bending tests. Research activity should focus in the direction of improving the thermal and mechanical properties of PLA. In the aspect of installation of a PLA cable at ambient temperature, the addition of plasticizers to lower its glass transition temperature should be investigated. Considering the literature survey, PETS whose thermal properties are excellent compared to PLA, is promising too. Further research on PETS to study the level of losses (dissipation factor), relaxation phenomena, ability to be processed into thin films and water uptake should be conducted. The level of current in PETS and PLA should be investigated at different temperatures above the room temperature. As reported, biodegradable polymers are not easily available in the market. The option of preparing these polymers in the laboratory must be encouraged in the future studies.

References

- [1] Y. Ohki and N. Hirai, "Dielectric Properties of Biodegradable Polymers," in *IEEE Conference on Electrical Insulation and Dielectric Phenomena*, 2006, pp. 668–671.
- [2] Y. Maeno *et al.*, "Dipolar polarization and depolarization currents in biodegradable polymers," in *Proceedings of 2005 International Symposium on Electrical Insulating Materials*, 2005, vol. 2, pp. 417–420.
- [3] S. Hikosaka, H. Ishikawa, and Y. Ohki, "Effects of Crystallinity on Thermally Stimulated Current and Complex Permittivity of Poly(L-lactide)," in *Annual Report Conference on Electrical Insulation and Dielectric Phenomena*, 2008, pp. 497–500.
- [4] Y. Maeno *et al.*, "Effect of glass transition on conduction current in biodegradable poly-L-lactic acid," in *The 17th Annual Meeting of the IEEE Lasers and Electro-Optics Society, LEOS.*, 2004, pp. 49–52.
- [5] F. Kato, S. Omori, M. Matsushita, and Y. Ohki, "Effect of Crystallinity on Electrical Conduction Characteristics of Poly-L-lactic Acid," in *IEEE Conference on Electrical Insulation and Dielectric Phenomena*, 2006, pp. 15–18.
- [6] M. Matsushita *et al.*, "Effects of glass transition on the dielectric breakdown and electrical conduction in several biodegradable polymers," in *Proceedings of 2005 International Symposium on Electrical Insulating Materials*, 2005, vol. 2, pp. 413–416.
- [7] Y. Ohki and N. Hirai, "Electrical Conduction and Breakdown Properties of Several Biodegradable Polymers," *IEEE Trans. Dielectr. Electr. Insul.*, vol. 14, no. 6, pp. 1559–1566, Dec. 2007.
- [8] Y. Ohki, N. Hirai, N. Fuse, T. Tanaka, M. Kothoh, and S. Okabe, "Search for adequate biodegradable polymer as an eco-friendly electrical insulating material," *Proc. Int. Symp. EcoTopia Sci.*, 2007.
- [9] F. Kato and Y. Ohki, "Electrical conduction and dielectric relaxation in polyethylene terephthalate succinate," *Electr. Eng. Japan*, vol. 170, no. 4, pp. 1–8, Mar. 2010.
- [10] H. Ishikawa, S. Omori, and Y. Ohki, "Dielectric Properties of Polybutylene Succinate and Polybutylene Succinate Adipate," in *IEEE International Conference on Solid Dielectrics*, 2007, pp. 635–638.
- [11] H. Ishikawa and Y. Ohki, "Temperature Dependence of Complex Permittivity in Biodegradable Polybutylene Succinate," *IEEJ Trans. Fundam. Mater.*, vol. 128, no. 10, pp. 647–651, Oct. 2008.
- [12] N. Hirai *et al.*, "Dielectric properties of biodegradable polylactic acid and starch ester," in *Proceedings of the 2004 IEEE International Conference on Solid Dielectrics*, 2004, vol. 1, pp. 87–89.
- [13] K. Shinyama and S. Fujita, "Study on the electrical properties of a biodegradable plastic," in *Proceedings of the 7th International Conference on Properties and Applications of Dielectric Materials (Cat. No.03CH37417)*, 2003, vol. 2, pp. 707–710.
- [14] K. Shinyama and S. Fujita, "Mechanical and electrical properties of biodegradable plastics," in *Proceedings of 2005 International Symposium on Electrical Insulating Materials*, 2005, vol. 3, pp. 775–779.
- [15] "Polypropylene capacitor has up to 4.7 μ F capacitance." [Online]. Available:

-
- <http://www.globalsources.com/gsol/I/Polypropylene-capacitor/a/9000000126982.htm>. [Accessed: 18-Apr-2017].
- [16] “Comparison Of Cable Insulating Materials | EEP.” [Online]. Available: <http://electrical-engineering-portal.com/comparison-of-cable-insulating-materials>. [Accessed: 18-Apr-2017].
- [17] “Medium Voltage Insulators, Post-Insulator - GIPRO Insulators Austria.” [Online]. Available: <http://www.gipro.com/en/insulators/medium-voltage-insulators.php>. [Accessed: 18-Apr-2017].
- [18] T. Kijchavengkul and R. Auras, “Compostability of polymers,” *Polym. Int.*, vol. 57, no. 6, pp. 793–804, Jun. 2008.
- [19] G. Kale, T. Kijchavengkul, R. Auras, M. Rubino, S. E. Selke, and S. P. Singh, “Compostability of bioplastic packaging materials: an overview,” *Macromol. Biosci.*, vol. 7, no. 3, pp. 255–77, Mar. 2007.
- [20] N. Yoshie *et al.*, “Effect of low molecular weight additives on enzymatic degradation of poly(3-hydroxybutyrate),” *Polymer (Guildf.)*, vol. 41, no. 9, pp. 3227–3234, Apr. 2000.
- [21] Y. Ando and E. Fukada, “Piezoelectric properties and molecular motion of poly(β -hydroxybutyrate) films,” *J. Polym. Sci. Polym. Phys. Ed.*, vol. 22, no. 10, pp. 1821–1834, Oct. 1984.
- [22] T. A. Hanafy, K. Elbanna, S. El-Sayed, and A. Hassen, “Dielectric relaxation analysis of biopolymer poly(3-hydroxybutyrate),” *J. Appl. Polym. Sci.*, vol. 121, no. 6, pp. 3306–3313, Sep. 2011.
- [23] G. R. Saad, A. A. Mansour, and A. H. Hamed, “Dielectric investigation of cold crystallization of poly(3-hydroxybutyrate),” *Polymer (Guildf.)*, vol. 38, no. 16, pp. 4091–4096, Aug. 1997.
- [24] G. J. Pratt and M. J. A. Smith, “Dielectric relaxation spectroscopy of a poly- β -hydroxybutyrate homopolymer,” *Eur. Polym. J.*, vol. 33, no. 6, pp. 857–861, Jun. 1997.
- [25] “Sustainable Process, Product and Systems Design,” 2007. [Online]. Available: http://www.tnw.tudelft.nl/fileadmin/Faculteit/TNW/Studeren/Postgraduates/Process_and_Equipment_Design/DIDEA/Outside_Delft_Courses/doc/OSPT_Sust_Design_course_2nd_time.pdf. [Accessed: 18-Mar-2015].
- [26] D. K. Platt, *Biodegradable Polymers: Market Report*. iSmithers Rapra Publishing, 2006.
- [27] “Alibaba.” [Online]. Available: <http://www.alibaba.com/>. [Accessed: 18-Mar-2015].
- [28] “Plasticker.” [Online]. Available: <http://plasticker.de/>. [Accessed: 18-Mar-2015].
- [29] N. Hirai, H. Ishikawa, and Y. Ohki, “Electrical conduction properties of several biodegradable polymers,” in *Conference on Electrical Insulation and Dielectric Phenomena*, 2007, pp. 592–595.
- [30] Y. Nemoto, F. Kato, N. Hirai, Y. Ohki, S. Kaneko, and S. Okabe, “Effects of blending various biodegradable polymer plasticizers on the conduction current and AC breakdown strength in starch ester,” in *Proceedings of the International Symposium on Electrical Insulating Materials*, 2008, pp. 542–545.
- [31] O. Gallot-Lavallee and L. Heux, “Dielectric spectroscopy on a PHBV bio-polymer,” in

-
- 2013 Annual Report Conference on Electrical Insulation and Dielectric Phenomena, 2013, pp. 559–562.
- [32] E. E. Shafee, “The influence of semicrystalline morphology on the dielectric relaxation properties of poly(3-hydroxybutyrate),” *Eur. Polym. J.*, vol. 37, no. 8, pp. 1677–1684, Aug. 2001.
- [33] I. Šics, V. Tupureina, M. Kalniņš, T. A. Ezquerro, and F. J. Baltá-Calleja, “Dielectric relaxation of poly-(β -hydroxybutyrate) relating to microstructure,” *J. Macromol. Sci. Part B Phys.*, Aug. 2006.
- [34] E. Fukada and Y. Ando, “Piezoelectric properties of poly- β -hydroxybutyrate and copolymers of β -hydroxybutyrate and β -hydroxyvalerate,” *Int. J. Biol. Macromol.*, vol. 8, no. 6, pp. 361–366, Dec. 1986.
- [35] A. Bergmann and A. Owen, “Dielectric relaxation spectroscopy of poly[(R)-3-hydroxybutyrate](PHB) during crystallization,” *Polym. Int.*, vol. 53, no. 7, pp. 863–868, Jul. 2004.
- [36] G. J. Pratt and M. J. A. Smith, “Dielectric spectroscopy of some ‘biopol’ polymers,” in *Proceedings of 1995 IEEE 5th International Conference on Conduction and Breakdown in Solid Dielectrics*, 1995, pp. 28–32.
- [37] S. Ke, H. Huang, L. Ren, and Y. Wang, “Nearly constant dielectric loss behavior in poly(3-hydroxybutyrate-co-3-hydroxyvalerate) biodegradable polyester,” *J. Appl. Phys.*, vol. 105, no. 9, p. 96103, May 2009.
- [38] Y. Ando, M. Minato, K. Nishida, and E. Fukada, “Primary piezoelectric relaxation in a copolymer of β -hydroxybutyrate and β -hydroxyvalerate,” *IEEE Trans. Electr. Insul.*, vol. E1-21, no. 3, pp. 505–510, 1986.
- [39] G. J. Pratt and M. J. A. Smith, “Dielectric spectroscopy of a commercial polyhydroxybutyratehydroxyvalerate copolymer,” in *Proceedings of 1994 4th International Conference on Properties and Applications of Dielectric Materials*, 1994, vol. 1, pp. 231–234.
- [40] I. Šics, T. A. Ezquerro, A. Nogales, F. J. Baltá-Calleja, M. Kalniņš, and V. Tupureina, “On the Relationship between Crystalline Structure and Amorphous Phase Dynamics during Isothermal Crystallization of Bacterial Poly(3-hydroxybutyrate-co-3-hydroxyvalerate) Copolymers,” *Biomacromolecules*, vol. 2, no. 2, pp. 581–587, Jun. 2001.
- [41] M. Hernández, “On the high temperature TSDC peak in poly(ϵ -caprolactone),” *Polymer (Guildf.)*, vol. 41, no. 19, pp. 7223–7230, Sep. 2000.
- [42] H.-J. Tai, “Dielectric spectroscopy of poly(butylene succinate) films,” *Polymer (Guildf.)*, vol. 48, no. 15, pp. 4558–4566, Jul. 2007.
- [43] H.-J. Tai, “Interfacial polarization phenomenon in the recrystallization of poly(butylene succinate),” *Polymer (Guildf.)*, vol. 49, no. 9, pp. 2328–2333, Apr. 2008.
- [44] H.-J. Tai, “Dielectric spectroscopy of poly(butylene succinate-co-butylene adipate) films,” *Polym. Eng. Sci.*, vol. 51, no. 2, pp. 386–390, Feb. 2011.
- [45] A. Celli and M. Scandola, “Thermal properties and physical ageing of poly (l-lactic acid),” *Polymer (Guildf.)*, vol. 33, no. 13, pp. 2699–2703, Jan. 1992.
- [46] A. R. Brás, P. Malik, M. Dionísio, and J. F. Mano, “Influence of Crystallinity in Molecular Motions of Poly(l-lactic acid) Investigated by Dielectric Relaxation

- Spectroscopy,” *Macromolecules*, vol. 41, no. 17, pp. 6419–6430, Sep. 2008.
- [47] A. R. Brás, M. T. Viciosa, Y. Wang, M. Dionísio, and J. F. Mano, “Crystallization of Poly(L-lactic acid) Probed with Dielectric Relaxation Spectroscopy,” *Macromolecules*, vol. 39, no. 19, pp. 6513–6520, Sep. 2006.
- [48] M. Dionísio, M. T. Viciosa, Y. Wang, and J. F. Mano, “Glass Transition Dynamics of Poly(L-lactic acid) during Isothermal Crystallisation Monitored by Real-Time Dielectric Relaxation Spectroscopy Measurements,” *Macromol. Rapid Commun.*, vol. 26, no. 17, pp. 1423–1427, Sep. 2005.
- [49] A. R. Brás, M. T. Viciosa, M. Dionísio, and J. F. Mano, “Water effect in the thermal and molecular dynamics behavior of poly(L-lactic acid),” *J. Therm. Anal. Calorim.*, vol. 88, no. 2, pp. 425–429, May 2007.
- [50] N. Matsugasaki, K. Shinyama, and S. Fujita, “Dielectric breakdown and mechanical properties of polylactic acid of different spherulite sizes,” *IEEJ Trans. Electr. Electron. Eng.*, vol. 8, no. S1, pp. S106–S107, Sep. 2013.
- [51] P. K. C. Pillai, B. K. Gupta, and S. Chandrasekhar, “Thermally stimulated discharge current studies in cellulose acetate,” *J. Electrostat.*, vol. 9, no. 4, pp. 315–316, Jun. 1981.
- [52] H. S. S. Jois and D. K. Bhat, “Miscibility, water uptake, ion exchange capacity, conductivity and dielectric studies of poly(methyl methacrylate) and cellulose acetate blends,” *J. Appl. Polym. Sci.*, vol. 130, no. 5, pp. 3074–3081, Dec. 2013.
- [53] J. H. Daly, D. Hayward, J. J. Liggat, and A. R. Mackintosh, “Ageing and rejuvenation of Biopol™, [poly (3-hydroxybutyrate-co-3-hydroxyvalerate)] copolymers: A dielectric study,” *J. Mater. Sci.*, vol. 39, no. 3, pp. 925–931, Feb. 2004.
- [54] S. A. Madbouly, A. A. Mansour, and N. Y. Abdou, “Crystallization kinetics of PHB/PVAc blends using time resolved dielectric spectroscopy,” *Eur. Polym. J.*, vol. 43, no. 9, pp. 3933–3942, Sep. 2007.
- [55] E. E. Shafee, “Investigation of the phase structure of poly(3-hydroxybutyrate)/poly(vinyl acetate) blends by dielectric relaxation spectroscopy,” *Eur. Polym. J.*, vol. 37, no. 3, pp. 451–458, Mar. 2001.
- [56] E. Ten, D. F. Bahr, B. Li, L. Jiang, and M. P. Wolcott, “Effects of Cellulose Nanowhiskers on Mechanical, Dielectric, and Rheological Properties of Poly(3-hydroxybutyrate-co-3-hydroxyvalerate)/Cellulose Nanowhisker Composites,” *Ind. Eng. Chem. Res.*, vol. 51, no. 7, pp. 2941–2951, Feb. 2012.
- [57] T. H. M. Abou-Aiad, K. N. Abd-El-Nour, I. K. Hakim, and M. S. El-Sabee, “Dielectric Relaxation and Spectroscopic Investigation of Polyhydroxybutyrate PHB Blended with Polyvinyl Acetate PVAc and Poly(Vinylacetate-Co-vinyl Alcohol) PACA,” *Polym. Plast. Technol. Eng.*, vol. 46, no. 1, pp. 1–6, Jan. 2007.
- [58] A. A. Mansour, G. R. Saad, and A. H. Hamed, “II. Dielectric investigation of cold crystallization of poly(3-hydroxybutyrate) and poly(3-hydroxybutyrate-co-3-hydroxyvalerate),” *Polymer (Guildf.)*, vol. 40, no. 19, pp. 5377–5391, Sep. 1999.
- [59] G. Ceccorulli and M. Scandola, “Thermal and dielectric properties of blends of polymethylmethacrylate and atactic poly-3-hydroxybutyrate,” *J. Macromol. Sci. Part A*, vol. 36, no. 2, pp. 327–337, Feb. 2007.
- [60] T. Nakagawa, T. Nakiri, R. Hosoya, and Y. Tajitsu, “Electrical Properties of Biodegradable Polylactic Acid Film,” *IEEE Trans. Ind. Appl.*, vol. 40, no. 4, pp. 1020–

-
- 1024, Jul. 2004.
- [61] S. Omori, M. Matsushita, and Y. Ohki, "Comparison of Dielectric Properties among Various Poly(lactide) Films," in *IEEE 8th International Conference on Properties and Applications of Dielectric Materials*, 2006, pp. 936–939.
- [62] F. Kato, M. Matsushita, S. Omori, and Y. Ohki, "Effect of Endothermic Reaction Associated with Glass Transition on the Breakdown Strength of Biodegradable Polymer Films," in *IEEE Conference on Electrical Insulation and Dielectric Phenomena*, 2006, pp. 241–244.
- [63] T. Nakagawa, T. Nakiri, R. Hosoya, and Y. Tajitsu, "Electrical properties of biodegradable polylactic acid film," in *Proceedings of the 7th International Conference on Properties and Applications of Dielectric Materials (Cat. No.03CH37417)*, 2003, vol. 2, pp. 499–502.
- [64] Y. Ohki, Y. Maeno, T. Tanaka, M. Kohtoh, and S. Okabe, "Thermally stimulated polarization and depolarization currents in polyethylene terephthalate succinate," in *Annual Report Conference on Electrical Insulation and Dielectric Phenomena*, 2005, pp. 503–506.
- [65] J. Ren and K. Adachi, "Dielectric Relaxation in Blends of Amorphous Poly(dl -lactic acid) and Semicrystalline Poly(l -lactic acid)," *Macromolecules*, vol. 36, no. 14, pp. 5180–5186, Jul. 2003.
- [66] S. Napolitano and M. Wübbenhorst, "Monitoring the cold crystallization of poly(3-hydroxy butyrate) via dielectric spectroscopy," *J. Non. Cryst. Solids*, vol. 353, no. 47–51, pp. 4357–4361, Dec. 2007.
- [67] A. Bello, E. Laredo, and M. Grimau, "Comparison of analysis of dielectric spectra of PCL in the ϵ^* and the M^* formalism," *J. Non. Cryst. Solids*, vol. 353, no. 47–51, pp. 4283–4287, Dec. 2007.
- [68] G. Kortaberria, C. Marieta, A. Jimeno, P. Arruti, and I. Mondragon, "Crystallization of poly(l-lactid acid) monitored by dielectric relaxation spectroscopy and atomic force microscopy," *J. Microsc.*, vol. 224, no. 3, pp. 277–289, Dec. 2006.
- [69] A. K. Sharma and C. Ramu, "Dielectric properties of solution grown cellulose acetate thin films," *Mater. Lett.*, vol. 11, no. 3–4, pp. 128–132, May 1991.
- [70] A. Wurm, R. Soliman, and C. Schick, "Early stages of polymer crystallization—a dielectric study," *Polymer (Guildf.)*, vol. 44, no. 24, pp. 7467–7476, Nov. 2003.
- [71] N. Fuse *et al.*, "Partial discharge degradation of several biodegradable polymers," *Electr. Eng. Japan*, vol. 168, no. 2, pp. 1–10, Jul. 2009.
- [72] K. Miyata, S. Fujita, Y. Ohki, and T. Tanaka, "Comparison of partial discharge resistance among several biodegradable polymers," *IEEE Trans. Dielectr. Electr. Insul.*, vol. 14, no. 6, pp. 1474–1476, Dec. 2007.
- [73] Y. Ohki, N. Fuse, S. Hikosaka, Y. Takemura, M. Mizuno, and K. Fukunaga, "Complex permittivity spectra of several insulating polymers at electrical and THz frequencies," in *IEEE Conference on Electrical Insulation and Dielectric Phenomena*, 2009, pp. 7–10.
- [74] M. Mierzwa, G. Floudas, J. Dorgan, D. Knauss, and J. Wegner, "Local and global dynamics of polylactides.," *J. Non. Cryst. Solids*, vol. 307–310, pp. 296–303, Sep. 2002.
- [75] J. Mijović and J.-W. Sy, "Molecular Dynamics during Crystallization of Poly(l -lactic

- acid) As Studied by Broad-Band Dielectric Relaxation Spectroscopy,” *Macromolecules*, vol. 35, no. 16, pp. 6370–6376, Jul. 2002.
- [76] W. Urbaniak-Domagala, “Electrical properties of polylactides,” *J. Electrostat.*, vol. 71, no. 3, pp. 456–461, Jun. 2013.
- [77] T. Ochiai and E. Fukada, “Electromechanical Properties of Poly-L-Lactic Acid,” *Jpn. J. Appl. Phys.*, vol. 37, no. Part 1, No. 6A, pp. 3374–3376, Jun. 1998.
- [78] F. Henry, L. C. Costa, and M. Devassine, “The evolution of poly(lactic acid) degradability by dielectric spectroscopy measurements,” *Eur. Polym. J.*, vol. 41, no. 9, pp. 2122–2126, Sep. 2005.
- [79] M. M. Abdel Moteleb, G. R. Saad, and R. I. Nessim, “The effects of preheating on the dielectric relaxation, and of temperature on the ‘static’ dielectric constant, of cellulose acetate fibers,” *Polym. Degrad. Stab.*, vol. 36, no. 3, pp. 217–224, Jan. 1992.
- [80] M. Dawy and A. -A. M. A. Nada, “IR and Dielectric Analysis of Cellulose and Its Derivatives,” *Polym. Plast. Technol. Eng.*, vol. 42, no. 4, pp. 643–658, Jan. 2003.
- [81] D. J. Crofton and R. A. Pethrick, “Dielectric studies of cellulose and its derivatives: 2. Effects of pressure and temperature on relaxation behaviour,” *Polymer (Guildf.)*, vol. 23, no. 11, pp. 1609–1614, Oct. 1982.
- [82] E. Borzabadi, A. S. Vaughan, and A. G. Bailey, “Electrostatic surface potential decay on cellulose acetate,” in *2003 Annual Report Conference on Electrical Insulation and Dielectric Phenomena*, 2003, pp. 193–196.
- [83] I. Šics *et al.*, “Simultaneous measurements of small angle x-ray scattering, wide angle x-ray scattering, and dielectric spectroscopy during crystallization of polymers,” *Rev. Sci. Instrum.*, vol. 71, no. 4, p. 1733, Apr. 2000.
- [84] A. Wurm, A. A. Minakov, and C. Schick, “Combining X-ray scattering with dielectric and calorimetric experiments for monitoring polymer crystallization,” *Eur. Polym. J.*, vol. 45, no. 11, pp. 3282–3291, Nov. 2009.
- [85] A. Wurm, R. Soliman, J. G. P. Goossens, W. Bras, and C. Schick, “Evidence of pre-crystalline-order in super-cooled polymer melts revealed from simultaneous dielectric spectroscopy and SAXS,” *J. Non. Cryst. Solids*, vol. 351, no. 33–36, pp. 2773–2779, Sep. 2005.
- [86] V. Veeravazhuthi, S. K. Narayandass, and D. Mangalaraj, “Dielectric behaviour of pure and nickel-doped cellulose acetate films,” *Polym. Int.*, vol. 45, no. 4, pp. 383–388, Apr. 1998.
- [87] R. Barker and C. Thomas, “Glass transition and ionic conductivity in cellulose acetate,” *J. Appl. Phys.*, vol. 35, no. 1, pp. 87–94, 1964.
- [88] M. Sousa *et al.*, “Dynamical characterization of a cellulose acetate polysaccharide,” *J. Phys. Chem. B*, vol. 114, no. 34, pp. 10939–53, Sep. 2010.
- [89] M. M. Abdel Moteleb, “Low frequency dielectric response of some cellulose derivatives,” *Cellul. Chem. Technol.*, vol. 28, no. 1, pp. 3–9, 1994.
- [90] G. R. Saad, M. G. Botros, and R. I. Nessim, “Dielectric study of acetylated cotton cellulose and saponified cellulose acetate,” *Die Angew. Makromol. Chemie*, vol. 197, no. 1, pp. 23–39, May 1992.
- [91] A. E. Kotp and M. T. Ahmed, “Dielectric and Electric Modulus of Poly(3-hydroxybutyrate) Semi-crystalline Polymer,” *Int. J. Polym. Mater.*, vol. 57, no. 12, pp.

- 1075–1082, Oct. 2008.
- [92] C. Chiteme, D. McLachlan, and G. Sauti, “ac and dc percolative conductivity of magnetite-cellulose acetate composites,” *Phys. Rev. B*, vol. 75, no. 9, p. 94202, Mar. 2007.
- [93] K. Shinyama and S. Fujita, “The effects of plasticizer on the mechanical and electrical characteristics of PLA,” in *International Symposium on Electrical Insulating Materials (ISEIM 2008)*, 2008, pp. 267–270.
- [94] P. Xu, H. G. Gui, S. Z. Yang, Y. S. Ding, and Q. Hao, “Dielectric and conductivity properties of poly(L-lactide) and poly(L-lactide)/ionic liquid blends,” *Macromol. Res.*, vol. 22, no. 3, pp. 304–309, Dec. 2013.
- [95] D. Newman, E. Laredo, A. Bello, A. Grillo, J. L. Feijoo, and A. J. Müller, “Molecular Mobilities in Biodegradable Poly(dl -lactide)/Poly(ϵ -caprolactone) Blends,” *Macromolecules*, vol. 42, no. 14, pp. 5219–5225, Jul. 2009.
- [96] Y. Ohki and K. Miyata, “Effects of Temperature and Crystallinity on Partial Discharge Resistance of Poly-L-lactic Acid,” *IEEJ Trans. Electr. Electron. Eng.*, vol. 5, no. 3, pp. 323–327, May 2010.
- [97] K. Shinyama and S. Fujita, “Fundamental study on electrical properties of biodegradable plastics,” in *Proceedings of the Fourth International Conference on Materials for Resources*, 2001, pp. 284–287.
- [98] L. Hartshorn and E. Rushton, “The dielectric properties of cellulose acetate,” *J. Inst. Electr. Eng.*, vol. 83, no. 501, pp. 315–332, Sep. 1938.
- [99] H. G. Shinouda and A. A. Hanna, “Dielectric and infrared study of some cellulose derivatives,” *J. Appl. Polym. Sci.*, vol. 21, no. 6, pp. 1479–1488, Jun. 1977.
- [100] J. K. Upadhyay, P. K. Khare, and A. Verma, “Thermally Stimulated Discharge Currents in Cellulose Acetate,” *Indian J. Phys. A Proc. Indian Assoc. Cultiv. Sci. A*, vol. 73, no. 2, pp. 183–194, 1999.
- [101] R. W. Seymour, S. Weinhold, and S. K. Haynes, “Mechanical and dielectric relaxation in cellulose esters,” *J. Macromol. Sci. Part B*, vol. 16, no. 3, pp. 337–353, Aug. 2006.
- [102] T. H. M. Abou-Aiad, “Morphology and Dielectric Properties of Polyhydroxybutyrate (PHB)/Poly(methylmethacrylate)(PMMA) Blends with Some Antimicrobial Applications,” *Polym. Plast. Technol. Eng.*, vol. 46, no. 4, pp. 435–439, Mar. 2007.
- [103] S. A. Madbouly, A. A. Mansour, and N. Y. Abdou, “Molecular dynamics of amorphous/crystalline polymer blends studied by broadband dielectric spectroscopy,” *Eur. Polym. J.*, vol. 43, no. 5, pp. 1892–1904, May 2007.
- [104] Shafee E.El., “Dielectric relaxation study of atactic poly(epichlorohydrin)/poly(3-hydroxybutyrate) blends,” *Eur. Polym. J.*, vol. 38, no. 3, pp. 413–421, Mar. 2002.
- [105] T. H. Abou-Aiad, M. Z. El-Sabee, K. N. Abd-El-Nour, G. R. Saad, E.-S. A. El-Sayed, and E. A. Gaafar, “Miscibility and the specific interaction of polyhydroxybutyrate blended with polyvinylacetate and poly(vinyl acetate-co-vinyl alcohol) with some biological applications,” *J. Appl. Polym. Sci.*, vol. 86, no. 9, pp. 2363–2374, Nov. 2002.
- [106] J. A. Malmonge, L. F. Malmonge, G. C. Fuzari, S. M. Malmonge, and W. K. Sakamoto, “Piezo and dielectric properties of PHB-PZT composite,” *Polym. Compos.*, vol. 30, no. 9, pp. 1333–1337, Sep. 2009.

-
- [107] R. Crétois, L. Delbreilh, E. Dargent, N. Follain, L. Lebrun, and J. M. Saiter, "Dielectric relaxations in polyhydroxyalkanoates/organoclay nanocomposites," *Eur. Polym. J.*, vol. 49, no. 11, pp. 3434–3444, Nov. 2013.
- [108] S. M. Aguilar, J. D. Shea, M. A. Al-Joumayly, B. D. Van Veen, N. Behdad, and S. C. Hagness, "Dielectric characterization of PCL-based thermoplastic materials for microwave diagnostic and therapeutic applications.," *IEEE Trans. Biomed. Eng.*, vol. 59, no. 3, pp. 627–33, Mar. 2012.
- [109] H. J. Woo, S. R. Majid, and A. K. Arof, "Conduction and thermal properties of a proton conducting polymer electrolyte based on poly (ϵ -caprolactone)," *Solid State Ionics*, vol. 199–200, pp. 14–20, Sep. 2011.
- [110] A. Wurm *et al.*, "Crystallization of poly(ϵ -caprolactone)/MWCNT composites: A combined SAXS/WAXS, electrical and thermal conductivity study," *Polymer (Guildf)*, vol. 55, no. 9, pp. 2220–2232, Apr. 2014.
- [111] R. Sabater i Serra, J. L. Escobar Ivirico, J. M. Meseguer Dueñas, A. Andrio Balado, J. L. Gómez Ribelles, and M. Salmerón Sánchez, "Dielectric relaxation spectrum of poly (ϵ -caprolactone) networks hydrophilized by copolymerization with 2-hydroxyethyl acrylate.," *Eur. Phys. J. E. Soft Matter*, vol. 22, no. 4, pp. 293–302, Apr. 2007.
- [112] Y. Zhang *et al.*, "Influence of Crystallization on Molecular Dynamics of the Amorphous Phase in Poly(ϵ -caprolactone) and Poly(ϵ -caprolactone)/LiClO₄ Complexes Investigated by Dielectric Relaxation Spectroscopy," *J. Polym. Res.*, vol. 20, no. 12, p. 312, Nov. 2013.
- [113] L. May-Hernández, F. Hernández-Sánchez, J. L. Gomez-Ribelles, and R. Sabater-i Serra, "Segmented poly(urethane-urea) elastomers based on polycaprolactone: Structure and properties," *J. Appl. Polym. Sci.*, vol. 119, no. 4, pp. 2093–2104, Feb. 2011.
- [114] B. Kuttich, C. Lederle, and B. Stühn, "Water dependence of the dielectric β -relaxation in poly(ϵ -caprolactone).," *J. Chem. Phys.*, vol. 139, no. 24, p. 244907, Dec. 2013.
- [115] R. Sabater i Serra, J. L. Escobar Ivirico, J. M. Meseguer Dueñas, A. A. Balado, J. L. Gómez Ribelles, and M. Salmerón Sánchez, "Segmental dynamics in poly(ϵ -caprolactone)/poly(L-lactide) copolymer networks," *J. Polym. Sci. Part B Polym. Phys.*, vol. 47, no. 2, pp. 183–193, Jan. 2009.
- [116] V. V. Meriakri, D. S. Kalenov, M. P. Parkhomenko, S. Zhou, and N. A. Fedoseev, "Dielectric Properties of Biocompatible and Biodegradable Polycaprolone and Polylactide and Their Nanocomposites in the Millimeter Wave Band," *American Journal of Materials Science*, vol. 2, no. 6. Scientific & Academic Publishing, pp. 171–175, 2012.
- [117] L. Yu, S. Ke, Y. Zhang, B. Shen, A. Zhang, and H. Huang, "Dielectric relaxations of high-k poly(butylene succinate) based all-organic nanocomposite films for capacitor applications," *J. Mater. Res.*, vol. 26, no. 19, pp. 2493–2502, Sep. 2011.
- [118] L. Yu *et al.*, "Green dielectric materials composed of natural graphite minerals and biodegradable polymer," *RSC Adv.*, vol. 2, no. 23, pp. 8793–8796, Sep. 2012.
- [119] F. B. Ali and R. Mohan, "Thermal, mechanical, and rheological properties of biodegradable polybutylene succinate/carbon nanotubes nanocomposites," *Polym. Compos.*, pp. 1309–1314, 2009.

-
- [120] K. Shinyama, T. Oi, and S. Fujita, "Dielectric relaxation phenomena of polylactic acid with β -crystalline chitin," *Int. J. Polym. Sci.*, vol. 389491, 2012.
- [121] Y. Matsumiya, T. Inoue, T. Iwashige, and H. Watanabe, "Dielectric Relaxation of Polymer/Carbon Dioxide Systems," *Macromolecules*, vol. 42, no. 13, pp. 4712–4718, Jul. 2009.
- [122] K. Shinyama, T. Oi, and S. Fujita, "Electrical properties of polylactic acid with nucleating agent added," *Electr. Eng. Japan*, vol. 180, no. 3, pp. 25–31, Aug. 2012.
- [123] J. K. Jeszka, L. Pietrzak, M. Pluta, and G. Boiteux, "Dielectric properties of polylactides and their nanocomposites with montmorillonite," *J. Non. Cryst. Solids*, vol. 356, no. 11–17, pp. 818–821, Apr. 2010.
- [124] V. Kumar, N. K. Sharma, and R. Kumar, "Dielectric, mechanical, and thermal properties of bamboo-polylactic acid bionanocomposites," *J. Reinf. Plast. Compos.*, vol. 32, no. 1, pp. 42–51, Oct. 2012.
- [125] T. Oi, K. Shinyama, and S. Fujita, "Dielectric breakdown properties of polylactic acid with β -crystalline chitin," *IEEJ Trans. Electr. Electron. Eng.*, vol. 6, no. 3, pp. 287–288, May 2011.
- [126] Y. Cao, D. Zhu, T. Ngai, L. Qin, C. Wu, and J. Shen, "Dielectric investigations on how Mg salt is dispersed in and released from polylactic acid," *Chinese J. Polym. Sci.*, vol. 32, no. 4, pp. 497–508, Mar. 2014.
- [127] M. Pluta, J. K. Jeszka, and G. Boiteux, "Polylactide/montmorillonite nanocomposites: Structure, dielectric, viscoelastic and thermal properties," *Eur. Polym. J.*, vol. 43, no. 7, pp. 2819–2835, Jul. 2007.
- [128] S. J. Doyle and R. A. Pethrick, "Dielectric relaxation studies of heterogeneously substituted cellulose acetate and its plasticization by dibutyl phthalate," *Polym. Int.*, vol. 27, no. 4, pp. 321–331, 1992.
- [129] S. Ramesh, R. Shanti, and E. Morris, "Discussion on the influence of DES content in CA-based polymer electrolytes," *J. Mater. Sci.*, vol. 47, no. 4, pp. 1787–1793, Sep. 2011.
- [130] N. I. Harun, R. M. Ali, A. M. M. Ali, and M. Z. A. Yahya, "Dielectric behaviour of cellulose acetate-based polymer electrolytes," *Ionics (Kiel)*, vol. 18, no. 6, pp. 599–606, Dec. 2011.
- [131] Y. R. V. Naidu and A. K. Sharma, "Dielectric relaxation in iodine doped cellulose acetate films," *Ferroelectrics*, vol. 159, no. 1, pp. 275–280, Sep. 1994.
- [132] D. J. Crofton and R. A. Pethrick, "Dielectric studies of cellulose and its derivatives: 3. Glycerol in cellulose acetate," *Polymer (Guildf)*, vol. 23, no. 11, pp. 1615–1618, Oct. 1982.
- [133] P. K. Khare, P. L. Jain, and R. K. Pandey, "Effect of doping on TSD relaxation in cellulose acetate films," *Bull. Mater. Sci.*, vol. 23, no. 6, pp. 529–532, Jan. 2000.
- [134] P. K. C. Pillai, B. K. Gupta, and M. Goel, "Polarization studies by the TSC technique on a blend of cellulose acetate and polyvinyl acetate," *J. Polym. Sci. Polym. Phys. Ed.*, vol. 19, no. 9, pp. 1461–1470, Sep. 1981.
- [135] G. Reshmi, P. Mohankumar, and M. Malathi, "Preparation, characterization and dielectric studies on carbonyl iron/cellulose acetate hydrogen phthalate core/shell nanoparticles for drug delivery applications," *Int. J. Pharm.*, vol. 365, no. 1–2, pp. 131–135, Jan. 2009.

-
- [136] V. Rao, P. V. Ashokan, and J. V. Amar, "Studies on dielectric relaxation and ac conductivity of cellulose acetate hydrogen phthalate-poly (vinyl pyrrolidone) blend," *J. Appl. Polym. Sci.*, vol. 86, no. 7, pp. 1702–1708, Nov. 2002.
- [137] V. Rao, P. V. Ashokan, and M. H. Shridhar, "Studies on the compatibility and specific interaction in cellulose acetate hydrogen phthalate (CAP) and poly methyl methacrylate (PMMA) blend," *Polymer (Guildf.)*, vol. 40, no. 25, pp. 7167–7171, Dec. 1999.
- [138] V. Rao, P. V. Ashokan, and M. H. Shridhar, "Studies of dielectric relaxation and a.c. conductivity in cellulose acetate hydrogen phthalate–poly(methyl methacrylate) blends," *Mater. Sci. Eng. A*, vol. 281, no. 1–2, pp. 213–220, Apr. 2000.
- [139] A. K. Sharma and C. Ramu, "Dielectric behaviour of iron-doped cellulose acetate films," *Polym. Int.*, vol. 29, no. 3, pp. 213–217, 1992.
- [140] T. Oi, K. Shinyama, and S. Fujita, "Electrical Properties of Heat-Treated Poly-Lactic Acid," *IEEEJ Trans. Fundam. Mater.*, vol. 131, no. 5, pp. 395–400, 2011.
- [141] T. Nakiri, Y. Kawachi, M. Honda, K. Imoto, T. Yamakita, and Y. Tajitsu, "Development of Electric Wire Using Biodegradable Polymer," *IEEE Trans. Ind. Appl.*, vol. 43, no. 4, pp. 1069–1074, 2007.
- [142] R. Chambers, J. H. Daly, D. Hayward, and J. J. Liggat, "The effect of processing on the properties of poly(3-hydroxybutyrate-co-3-hydroxyvalerate) copolymers," *J. Mater. Sci.*, vol. 36, no. 15, pp. 3785–3792, 2001.
- [143] R. E. Barker and C. R. Thomas, "Effects of Moisture and High Electric Fields on Conductivity in Alkali-Halide-Doped Cellulose Acetate," *J. Appl. Phys.*, vol. 35, no. 11, p. 3203, Jul. 1964.
- [144] K. E. Prindle, "Insulating material," US2173726 A, 1939.
- [145] T. Kirkpatrick William, "Insulation liner for motor core slots," US2495010 A, 1950.
- [146] H. Hayami, K. Moriuchi, and S. Ebina, "Electrically insulated cable and arrangement for connecting the cable," US6064002 A, 2000.
- [147] "Wikipedia." [Online]. Available: <https://en.wikipedia.org/>. [Accessed: 31-Mar-2015].
- [148] F. Kremer and A. Schönals, *Broadband Dielectric Spectroscopy*. Berlin, Heidelberg: Springer Berlin Heidelberg, 2003.
- [149] "Alpha-A High Resolution Dielectric, Conductivity, Impedance and Gain Phase Modular Measurement System," 2009.
- [150] A. Schönals, "Dielectric spectroscopy on the dynamics of amorphous polymeric systems." 1998.
- [151] A. Schönals, "Broadband Dielectric Spectroscopy and its Relationship to Other Spectroscopic Techniques," in *6 th International Conference on Broadband Dielectric Spectroscopy and its Applications*, 2010.
- [152] D. K. Das Gupta and R. S. Brockley, "A study of 'absorption currents' in low-density polyethylene," *J. Phys. D. Appl. Phys.*, vol. 11, no. 6, pp. 955–962, Apr. 1978.
- [153] M. Cheolhong, "Temperature Dependence of Dielectric Breakdown in Polymers," The Pennsylvania State University, 2008.
- [154] S. Singha and M. Thomas, "Dielectric properties of epoxy nanocomposites," *IEEE Trans. Dielectr. Electr. Insul.*, vol. 15, no. 1, pp. 12–23, 2008.

-
- [155] K. Nishimura and M. Shibayama, "Technical Report of Aichi Industrial Technology Institute," 2005.
- [156] T. C. Mike Chung, "Functionalization of Polypropylene with High Dielectric Properties: Applications in Electric Energy Storage," *Green Sustain. Chem.*, vol. 2, no. 2, pp. 29–37, May 2012.
- [157] N. Tagami *et al.*, "Dielectric properties of epoxy/clay nanocomposites - effects of curing agent and clay dispersion method," *IEEE Trans. Dielectr. Electr. Insul.*, vol. 15, no. 1, pp. 24–32, 2008.
- [158] R. N. Clarke, "Kaye&Laby, Tables of Physical and Chemical Constants." [Online]. Available: http://www.kayelaby.npl.co.uk/general_physics/2_6/2_6_5.html. [Accessed: 03-Sep-2015].
- [159] H. Li *et al.*, "Electric Field and Temperature Dependence of Electrical Conductivity in Biaxially Oriented Polypropylene Films," *IEEE Trans. Plasma Sci.*, vol. 42, no. 11, pp. 3585–3591, Nov. 2014.
- [160] T. R. Jow and P. J. Cygan, "Investigation of dielectric breakdown of polyvinylidene fluoride using AC and DC methods," in *Conference Record of the 1992 IEEE International Symposium on Electrical Insulation*, 1992, pp. 181–184.
- [161] O. Myllymäki *et al.*, "Mechanical and Permeability Properties of Biodegradable Extruded Starch/ polycaprolactone Films," *Packag. Technol. Sci.*, vol. 11, pp. 265–274, 1998.
- [162] Grafen Chemical Industries Co., "General properties Polylactic Acid PLA-05."
- [163] "Good fellow." [Online]. Available: <http://www.goodfellow.com/fr/>. [Accessed: 24-Jun-2015].
- [164] N. Guigo, K. Mazeau, J.-L. Putaux, and L. Heux, "Surface modification of cellulose microfibrils by periodate oxidation and subsequent reductive amination with benzylamine: a topochemical study," *Cellulose*, vol. 21, no. 6, pp. 4119–4133, Dec. 2014.
- [165] N. Ljungberg, J.-Y. Cavaillé, and L. Heux, "Nanocomposites of isotactic polypropylene reinforced with rod-like cellulose whiskers," *Polymer (Guildf.)*, vol. 47, no. 18, pp. 6285–6292, Aug. 2006.
- [166] J.-S. Yoon, H.-W. Jung, M.-N. Kim, and E.-S. Park, "Diffusion coefficient and equilibrium solubility of water molecules in biodegradable polymers," *J. Appl. Polym. Sci.*, vol. 77, no. 8, pp. 1716–1722, Aug. 2000.
- [167] F. A. Long and L. J. Thompson, "Diffusion of water vapor in polymers," *J. Polym. Sci.*, vol. 15, no. 80, pp. 413–426, Feb. 1955.
- [168] E.-A. McGonigle, J. H. Daly, Stephen D. Jenkins, J. J. Liggat, and R. A. Pethrick, "Influence of Physical Aging on the Molecular Motion and Structural Relaxation in Poly(ethylene terephthalate) and Related Polyesters," vol. 33, pp. 480–489, 2000.
- [169] Q. Huan *et al.*, "Markedly improving mechanical properties for isotactic polypropylene with large-size spherulites by pressure-induced flow processing," *Polymer (Guildf.)*, vol. 54, no. 3, pp. 1177–1183, 2013.
- [170] E. BRUN, "Vieillissement hygrothermique d'un composite résine époxyde silice et impact sur sa rigidité diélectrique," 2009.
- [171] Y. Doi, *Microbial polyesters*. VCH, 1990.

-
- [172] F. Biddlestone, A. Harris, J. N. Hay, and T. Hammond, "The Physical Ageing of Amorphous Poly(hydroxybutyrate)," *Polym. Int.*, vol. 39, no. 3, pp. 221–229, Mar. 1996.
- [173] G. J. M. de Koning and P. J. Lemstra, "Crystallization phenomena in bacterial poly[(R)-3-hydroxybutyrate]: 2. Embrittlement and rejuvenation," *Polymer (Guildf.)*, vol. 34, no. 19, pp. 4089–4094, Jan. 1993.
- [174] N. Grassie, E. J. Murray, and P. A. Holmes, "The thermal degradation of poly(-(d)- β -hydroxybutyric acid): Part 1—Identification and quantitative analysis of products," *Polym. Degrad. Stab.*, vol. 6, no. 1, pp. 47–61, Jan. 1984.
- [175] A. Nogales, T. A. Ezquerro, J. M. García, and F. J. Baltá-Calleja, "Structure-dynamics relationships of the α -relaxation in flexible copolyesters during crystallization as revealed by real-time methods," *J. Polym. Sci. Part B Polym. Phys.*, vol. 37, no. 1, pp. 37–49, Jan. 1999.
- [176] M. Grimau, E. Laredo, M. C. Pérez Y., and A. Bello, "Study of dielectric relaxation modes in poly(ϵ -caprolactone): Molecular weight, water sorption, and merging effects," *J. Chem. Phys.*, vol. 114, no. 14, pp. 6417–6425, Apr. 2001.
- [177] B. Alp, S. Cesur, and D. Balkose, "Crystallization Control of Polycaprolactone (PCL) with Inorganic and Organic Additives," *aidic.it*.
- [178] J. Vanderschueren, M. Ladang, and J. Heuschen, "Thermally Stimulated Depolarization of Phase-Separated Polymer Systems," *Macromolecules*, vol. 13, no. 4, pp. 973–977, Jul. 1980.
- [179] G. P. Johari, "Viscous Liquids and the Glass Transition. II. Secondary Relaxations in Glasses of Rigid Molecules," *J. Chem. Phys.*, vol. 53, no. 6, p. 2372, Sep. 1970.
- [180] F. Garwe, A. Schönhals, H. Lockwenz, M. Beiner, K. Schröter, and E. Donth, "Influence of Cooperative α Dynamics on Local β Relaxation during the Development of the Dynamic Glass Transition in Poly(n-alkyl methacrylate)s," *Macromolecules*, vol. 29, no. 1, pp. 247–253, Jan. 1996.
- [181] N. Delpouve, L. Delbreilh, G. Stoclet, A. Saiter, and E. Dargent, "Structural Dependence of the Molecular Mobility in the Amorphous Fractions of Polylactide," *Macromolecules*, vol. 47, no. 15, pp. 5186–5197, Aug. 2014.
- [182] F. Roman, P. Colomer, Y. Calventus, and J. M. Hutchinson, "Study of the Molecular Dynamics of Multiarm Star Polymers with a Poly(ethyleneimine) Core and Poly(lactide) Multiarms," *Materials (Basel)*, vol. 10, 2017.
- [183] "Electrometer/ High Resistance Meter." [Online]. Available: <http://www.tek.com/keithley-low-level-sensitive-and-specialty-instruments/keithley-high-resistance-low-current-electrom>. [Accessed: 26-Oct-2016].
- [184] "Model 8009 Resistivity Test Fixture/Model 8009 Resistivity Chamber." [Online]. Available: <http://www.tek.com/landing-page/keithley-accessories>. [Accessed: 26-Oct-2016].
- [185] "Model 6524 High Resistance Measurement Software User's Manual," 1999.
- [186] "PLASTIC PRODUCTS, INC." [Online]. Available: <http://www.plastic-products.com/part12.htm>. [Accessed: 14-May-2017].
- [187] "TDK Film Capacitors General Technical Information."
- [188] C. Park, T. Kaneko, M. Hara, and M. Akazaki, "Effects of Mechanical Stresses on the

-
- Dielectric Breakdown Strengths of PET and FRP,” *IEEE Trans. Electr. Insul.*, vol. EI-17, no. 3, pp. 234–240, Jun. 1982.
- [189] “Sigma-Aldrich.” [Online]. Available: <http://www.sigmaaldrich.com/>. [Accessed: 01-Apr-2015].
- [190] “XLPE Insulated Power Cables.”
- [191] I. Plesa, F. Ciuprina, and P. V. Notingher, “Dielectric Spectroscopy of Epoxy Resin with and without Inorganic Nanofillers,” *Journal of Advanced Research in Physics*, vol. 1, no. 1. 2010.
- [192] J. Katayama, Y. Ohki, N. Fuse, M. Kozako, and T. Tanaka, “Effects of Nanofiller Materials on the Dielectric Properties of Epoxy Nanocomposites,” *IEEE Trans. Dielectr. Electr. Insul.*, vol. 20, no. 1, pp. 157–165, 2013.
- [193] M. Kurimoto, D. Kusaba, H. Suzuki, Y. Murakami, and M. Nagao, “DC dielectric breakdown characteristics of mesoporous-alumina/epoxy composite,” in *Proceedings of 2011 International Symposium on Electrical Insulating Materials*, 2011, pp. 165–168.

Annexes

Range of frequencies studied in the dielectric spectroscopy

The temperature plot of relative permittivity, loss factor, dissipation factor and modulus are measured for set of frequencies. The highest and the lowest frequency at which the dielectric spectroscopy measurements were made may vary for a biodegradable polymer in this study. However, all the intermediate frequencies remained the same. Table 32 shows the list of the frequencies at which the dielectric spectroscopy measurements were performed.

Table 32. List of frequencies.

f [Hz]
2.60E+06
1.86E+06
1.33E+06
9.49E+05
6.78E+05
4.84E+05
3.46E+05
2.47E+05
1.76E+05
1.26E+05
9.00E+04
6.43E+04
4.59E+04
3.28E+04
2.34E+04
1.67E+04
1.20E+04
8.54E+03
6.10E+03
4.36E+03
3.11E+03
2.22E+03
1.59E+03
1.13E+03
8.10E+02
5.78E+02
4.13E+02
2.95E+02
2.11E+02
1.51E+02
1.08E+02
7.68E+01
5.49E+01
3.92E+01
2.80E+01

2.00E+01
1.43E+01
1.02E+01
7.29E+00
5.21E+00
3.72E+00
2.66E+00
1.90E+00
1.36E+00
9.68E-01
6.91E-01
4.94E-01
3.53E-01
2.52E-01
1.80E-01
1.29E-01
9.18E-02
6.56E-02
4.68E-02
3.35E-02
2.39E-02
1.71E-02
1.22E-02
9.00E-03
6.00E-03
1.00E-03

Résumé de la thèse en français

Introduction générale de la thèse

L'utilisation extensive des combustibles fossiles, l'augmentation considérable de la pollution et l'émission de gaz à effet de serre dans l'atmosphère posent un défi majeur au monde actuel. La prise de conscience croissante de cette menace a amené la société et les entreprises à travers le monde à s'orienter vers des approches plus vertes. En effet, elles sont aujourd'hui de plus en plus nombreuses à être engagées dans des activités de recherche pour produire de façon plus respectueuse de l'environnement ou pour davantage prendre en compte l'environnement dans leur fonctionnement et leurs consommations.

Le déclin des ressources en combustibles fossiles et les difficultés de recyclage des résidus de consommation incitent à avoir recours aux polymères biodégradables. En plus de cela, l'organisation internationale de normalisation (ISO 26000) et d'autres directives et réglementations européennes telles que *REACH* (Enregistrement, évaluation, autorisation et restriction des substances chimiques, 2007), *DEEE* (déchets d'équipements électriques et électroniques) et *RoHS* (Restriction of Hazardous Substances, 2002) fournissent des normes et des directives pour les entreprises pour une approche respectueuse de l'environnement. Ces contextes ont été la force motrice pour rechercher des alternatives.

Dans le domaine du génie électrique, de nombreux polymères conventionnels tels que le polyéthylène (PE), le polychlorure de vinyle (PVC), le polypropylène (PP), le polyéthylène téréphtalate (PET), le poly(sulfure de phénylène) (PPS), le fluorure de polyvinylidène (PVDF), le polyamide (PA), le polycarbonate (PC) et les thermodurcissables (résine époxy) trouvent des applications dans des systèmes d'isolation électrique tels que les condensateurs, les câbles, etc. Ces polymères sont issus du pétrole, peu respectueux de l'environnement et la plupart d'entre eux ne sont pas biodégradables. Dans certains cas, le recyclage est difficile et par conséquent, ils s'accumulent dans l'environnement.

Dans le but de remettre en question et de remplacer ces produits conventionnels partiellement ou complètement par des produits biodégradables, ce travail de thèse explore les propriétés diélectriques de matériaux polymères biodégradables et/ou biosourcés.

Dans ce premier chapitre, une étude détaillée sur l'état actuel des travaux de recherche sur les polymères biodégradables dans le domaine du génie électrique est réalisée. Ceci a été fait sur la base du recensement des publications sur les propriétés diélectriques des polymères biodégradables à ce jour. Les propriétés thermiques d'un certain nombre de polymères biodégradables et classiques sont rapportés et comparés. D'une manière similaire, les propriétés électriques telles que la permittivité, le facteur de pertes, la conductivité et la tenue diélectrique sont rapportées et comparées. Ce premier chapitre est présenté comme un travail de restitution de l'état de l'art. Sur la base de ce travail et de divers autres paramètres, plusieurs polymères biodégradables et polymères classiques ont été choisis pour être préparés

et/ou traités et pour explorer leurs propriétés thermiques et diélectriques et leur niveau d'absorption eau.

Les résultats expérimentaux et analytiques de l'étude comprennent des mesures de spectroscopie diélectrique effectuées pour une large gamme de température et de fréquence sur différents polymères biodégradables. La résistivité volumique à différentes températures et les études de tenue diélectrique à température ambiante sont présentées. Les résultats des analyses thermiques et des études d'absorption d'eau des polymères sont interprétés.

Dans le deuxième chapitre intitulé *Polymer-film-processing*, les polymères traités en laboratoire ainsi que leurs conditions de traitement sont mentionnés. Les conditions dans lesquelles différents échantillons ont été séchés et conditionné pour différentes techniques de caractérisation sont également élaborées.

Dans le troisième chapitre, les micrographies optiques et l'absorption d'eau dans les polymères sont présentés et discutés. Dans le quatrième chapitre, les résultats de la calorimétrie différentielle à balayage et de l'analyse mécanique dynamique sont présentés et mentionnés.

Dans le cinquième chapitre, l'installation expérimentale de la spectroscopie diélectrique, la mesure de courant et de claquage électrique sont montrées. Les résultats expérimentaux obtenus à partir des mesures de spectroscopie diélectrique réalisées pour une large gamme de température et de fréquence pour différents polymères et matériaux composites sont interprétés. Les résultats des mesures de résistivité volumique à différentes températures et des mesures de claquage électrique à température ambiante sont également interprétés. La comparaison des propriétés thermiques et électriques des polymères biodégradables et conventionnels est effectuée à la fin de ce chapitre.

Ce chapitre est suivi des *Conclusion et perspectives*.

Conclusions et perspectives de la thèse

Une synthèse des travaux sur les propriétés électriques et thermiques est présentée sur dix polymères biodégradables. Leurs propriétés électriques et thermiques ont été examinées et comparées avec celles de polymères classiques. La revue a conclu que le PLA, poly (acide lactique), est le polymère biodégradable le plus étudié. PLA et PETS ont des propriétés électriques proches de celles de polymères conventionnels utilisés dans l'isolation électrique. Le PETS pourrait concurrencer le PET et le PE en termes de permittivité relative, de conductivité *DC* et de propriétés thermiques, mais n'a pas pu être étudié faute de fournisseurs. Les polymères biodégradables ont des conductivités plus élevées, sauf le PLA: sa conductivité est proche de celle du LDPE. Le PLA a également une bonne rigidité diélectrique par rapport aux polymères classiques.

Des films adaptés aux mesures électriques ont été obtenus pour les polymères PHBV, PCL, PLA, PP et PLA-MFC. La méthode consiste en un refroidissement lent de la masse fondue de polymère sous pression dans la presse à chaud. Les films ne sont ni formés ni adaptés aux mesures électriques si le moule est démonté trop tôt. De plus, la trempe de polymère fondue ne produit pas de films adaptés. L'utilisation d'une méthode de coulée avec un solvant n'a pas non plus permis de produire de films pour répondre aux critères de mesure électrique.

Un nouveau nanocomposite à base de PLA a été préparé et ses conditions de traitement ont été optimisées.

Le PHBV et PLA sont plus hydrophiles que le PET conventionnel. À l'inverse, dans les conditions étudiées, leur absorption d'eau n'est pas loin de la celle de nombreux autres polymères et matériaux utilisés dans l'isolation électrique.

Dans le cas du nanocomposite PLA-MFC, l'échantillon séché à 60 ° C a montré un pic de cristallisation à froid qui est absent du PLA-MFC séché à 90 ° C. La température de séchage a influencé la morphologie du polymère. Le post-traitement du PLA-MFC a entraîné l'absence de cristallisation à froid. Le post-traitement de PHBV a changé leur morphologie polymère avec une augmentation de leur degré de cristallinité.

Le fonctionnement de la spectroscopie diélectrique et des appareils de mesure de courant, cellules d'échantillons construites au cours de la thèse ont été testés et validés.

La spectroscopie diélectrique dans une large gamme de fréquence et de température a démontré différents phénomènes de relaxation dans chacun des polymères biodégradables étudiés. Ces phénomènes de relaxation sont la relaxation due à la transition vitreuse (α), celles dues aux modes locaux (β , γ) et la relaxation due à la polarisation interfaciale (MWS). Le PHBV et le PLA ont montré les relaxations α , β et la relaxation due à la polarisation MWS contrairement au PCL, qui a montré les quatre phénomènes de relaxation. La fusion des pics des modes locaux de β et γ se produit dans le PCL. Le PLA-MFC montre une relaxation α et la relaxation due à la polarisation MWS.

Nos mesures avec le PHBV traité et non traité ont montré un effet positif du post-traitement avec une augmentation du niveau de résistivité volumique. Les mesures effectuées dans cette étude montrent une résistivité à volume de PHBV, qui est plus élevée que celle de PLA ou PE à température ambiante. PCL a une faible résistivité volumique que le PLA à température ambiante.

Le PHBV a une faible permittivité relative et une résistivité volumique élevée. Cependant, il a une tenue au vieillissement médiocre et une fenêtre thermique de préparation étroite. Le PCL a de mauvaises propriétés électriques et thermiques et ne peut pas être utilisé pour des applications d'ingénierie électrique sans n'y apporter des améliorations. Le nanocomposite à base de PLA préparé, traité et caractérisé dans notre étude a présenté une faible résistivité volumique et un niveau élevé de pertes. Il ne peut pas être considéré comme un matériau intéressant dans son état actuel. Le PLA serait potentiellement un substitut du PET dans certaines applications, à condition que les propriétés thermiques soient améliorées et que les niveaux d'absorption d'eau soient réduits, ou acceptables selon les applications visées.

Seuls les appareils de traitement à chaud ont été utilisés pour fabriquer des films dans cette étude. Dans la perspective industrielle de produire des films de meilleure qualité, homogènes et minces, différents types de méthodes de traitement tels que le moulage et l'extrusion pourraient être essayés. Ce travail a été consacré aux études d'absorption de l'eau, aux propriétés thermiques et électriques des polymères. Du point de vue de l'application, les études sur vieillissement et la résistance mécanique de ces polymères pourraient être intéressantes.

Les résultats expérimentaux confirment que le PLA est un polymère biodégradable prometteur pour l'isolation électrique. Comme indiqué dans la littérature, le câble isolé PLA a été réalisé et les propriétés électriques et de tenue en flexion ont été étudiées. L'activité de recherche devrait se concentrer dans le sens de l'amélioration des propriétés thermiques et mécaniques de PLA. En ce qui concerne l'installation d'un câble PLA à température ambiante, il convient d'étudier l'ajout de plastifiants pour abaisser sa température de transition vitreuse. Compte tenu de la revue de la littérature, le PETS, dont les propriétés thermiques sont meilleures par rapport au PLA, est également prometteur. D'autres recherches sur les PETS pour étudier le niveau des pertes (facteur de dissipation), les phénomènes de relaxation, la capacité à être transformée en films minces et l'absorption d'eau devraient être menées. Les niveaux de courant dans le PETS et le PLA doivent également être étudiés à différentes températures supérieures à la température ambiante. Comme indiqué dans la littérature, les polymères biodégradables ne sont pas facilement disponibles sur le marché. La possibilité de préparer ces polymères en laboratoire doit être encouragée dans les études futures.